Advances In RTM Manufacturing Of Metal-FRP Hybrids By Self-Sealing And In-Mold Cleaning Techniques

zur Erlangung des akademischen Grades DOKTOR DER INGENIEURWISSENSCHAFTEN (Dr.-Ing.) der Fakultät für Maschinenbau
der Universität Paderborn

genehmigte
DISSERTATION

von
Deviprasad Chalicheemalapalli Jayasankar, M. Sc.
aus Tirupati

Tag des Kolloquiums:	30. August 2023
Referent:	Prof. Dr. rer. nat. Thomas Tröster
Korreferent:	Prof. Dr. rer. nat. Volker Schöppner

Abstract

The importance of fiber-reinforced plastics for lightweight construction applications is steadily increasing due to their outstanding weight-specific property values. However, a decisive disadvantage of these composite materials has so far been the high material and process costs, which is why fiber-reinforced plastics are almost exclusively used in small to medium-sized series. Optimization of manufacturing methods is of great importance to reduce the production cost. In this study, two concepts are proposed that can optimize vacuum assisted light resin transfer molding (VA-LRTM) further, leading to a possibility of fully automatic process. Conventional VA-LRTM methods are used to produce complex fiber-reinforced plastics (FRP) and hybrid components. Traditional molds used to produce components via VA-LRTM are sealed using polymer materials to prevent the leakage of matrix system. The seals undergo tremendous amounts of thermal, chemical, and mechanical loadings. Thus, sealings must be replaced in short intervals. In the current study, a concept where sealing is achieved by accelerating the curing of matrix system itself with the help of heating elements and catalysts resulting in a self-sealing approach is proposed. Another concern is mold surface contamination during component production. To address this, a modified automatic cleaning technique based on ultrasonic cleaning was proposed which can be integrated into the production line with minimum modification. Both the proposed concepts were validated and optimized using experiments, simulations, and analytical approaches by producing metal-FRP hybrid shafts.

Zusammenfassung

Die Bedeutung von faserverstärkten Kunststoffen für Leichtbauanwendungen nimmt aufgrund ihrer hervorragenden gewichtsspezifischen Eigenschaftswerte stetig zu. Ein entscheidender Nachteil dieser Verbundwerkstoffe sind jedoch bisher die hohen Material- und Prozesskosten, weshalb faserverstärkte Kunststoffe fast ausschließlich in kleinen bis mittleren Serien eingesetzt werden. Um die Produktionskosten zu senken, ist die Optimierung der Herstellungsverfahren von großer Bedeutung. In dieser Studie werden zwei Konzepte vorgeschlagen, die das vakuumunterstützte leichte Resin Transfer Molding (VA-LRTM) weiter optimieren können, so dass ein vollautomatischer Prozess möglich wird. Herkömmliche VA-LRTM-Verfahren werden zur Herstellung komplexer faserverstärkter Kunststoffe (FVK) und Hybridbauteile eingesetzt. Herkömmliche Formen, die zur Herstellung von Bauteilen mittels VA-LRTM verwendet werden, sind mit Polymermaterialien abgedichtet, um ein Austreten des Matrixsystems zu verhindern. Die Dichtungen sind einer enormen thermischen, chemischen und mechanischen Belastung ausgesetzt. Die Dichtung mussen daher in kurzen Abstanden ausgetauscht werden. In der aktuellen Studie wird ein Konzept vorgeschlagen, bei dem die Abdichtung durch Beschleunigung der Aushärtung des Matrixsystems selbst mit Hilfe von Heizelementen und Katalysatoren erreicht wird, was zu einem selbstdichtenden Ansatz führt. Ein weiteres Problem ist die Verunreinigung der Formoberfläche während der Bauteilproduktion. Um dieses Problem zu lösen, wurde eine modifizierte automatische Reinigungstechnik auf der Grundlage der Ultraschallreinigung vorgeschlagen, die mit minimalen Änderungen in die Produktionslinie integriert werden kann. Beide vorgeschlagenen Konzepte wurden anhand von Experimenten, Simulationen und analytischen Ansätzen durch die Herstellung von Metall-FRP-Hybridwellen validiert und optimiert.

Prior Publications

Deviprasad C. J, T. Stallmeister, Z. Wang, T. Tröster; Manufacturing of hybrid components by VARTM-Process using new sealing technique developed. In: Hybrid 2020

Table of Contents

1 Introduction

1.1 Background

Over the past few years, resource efficiency and CO_2-reduction are getting more important in industrial production, for example in the automotive sector as the number of vehicles on road are increasing steadily [1] [2]. Figure 1-1 shows the statistical data of passenger cars produced from 1988-2020. In order to regulate increased emission of CO_2, the Europe Commission introduced European Green deal in 2019 with a primary goal of significant reduction of CO_2 by 50% until 2030 in comparison with 1990 emission levels [3] [4]. With this new regulation, automotive industries are exploring the methods to produce weight-reduced components (lightweight) without sacrificing its mechanical properties as safety of the occupant in case of crash is also an important requirement [5]. Weight reduction in automotive leads to lower energy consumption, for example lowering weight by 100 kg for a petrol-driven car reduces the CO_2 emissions by as much as 8 g/km [6] [7]. The most widely used materials to reduce weight for automotive components are high strength steels and aluminum alloys, but they are limited to stability issues as the thickness reaches threshold value [8].

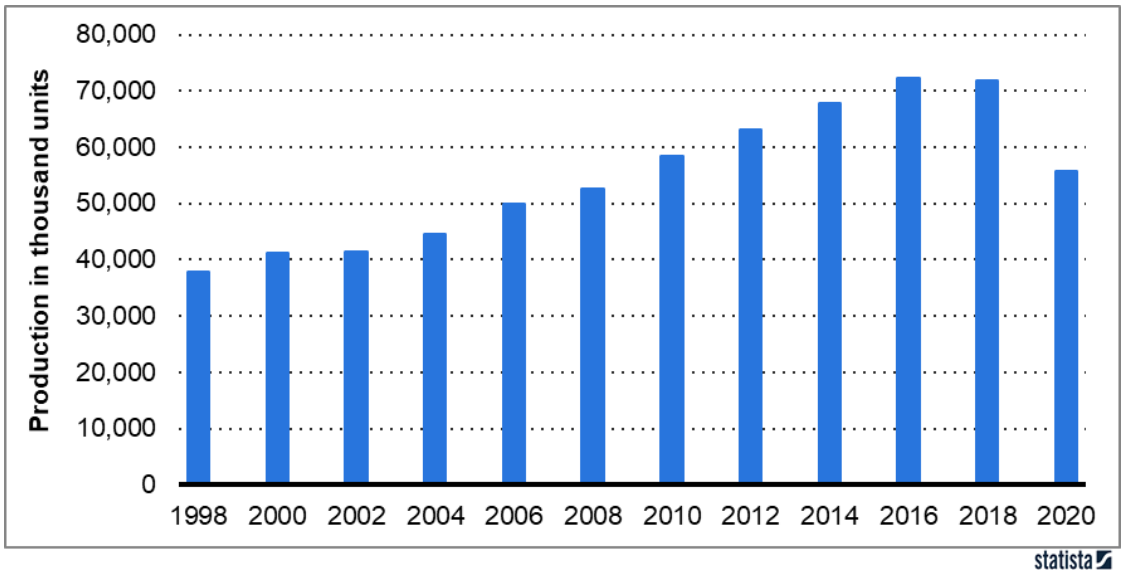

Figure 1-1: Statistical data for production of passenger cars from 1998 – 2020. The fall in 2020 is mainly due to coronavirus pandemic [2].

Fiber reinforced plastics (FRP) are alternative materials that are restricted to sports cars, aerospace, etc. as they are expensive due to the high production cycle time and material cost [9]. However, a trade-off between low mass and acceptable cost can be achieved by hybrid lightweight design that uses the expensive FRP just in highly stressed areas [10] [11]. The hybrid components are light in weight compared to the metal components without sacrificing its mechanical properties along with being cheaper when compared to components made entirely out of FRP [12]. Initially, joining was the main type of manufacturing approach used in industry where metal and FRP are manufactured separately and joined using special techniques such as adhesive bonding, riveting, welding, etc. [13] [14] [15]. This approach requires a longer cycle,

higher cost and added mass when bolts and rivets are used. The use of bolts and rivets also result in thermal damage and crack creations in FRP that reduces their mechanical properties and makes it difficult to predict failure [15]. The other widely used technique for FRP-Metal Hybrids is forming where the production cycle can be as short as one single step [16] [17]. In forming, the metal and FRP are bonded in the early stage to form laminates by pressing techniques and then undergo different forming manufacturing techniques based on application and materials [18]. However, both the techniques have their own advantages and disadvantages depending on the component to be produced and more potential for optimization [18]. Injection molding is a joining process that has potential for further optimization to produce FRP-metal hybrid products in a single step [19]. In general, the performance of manufacturing process in injection molding depends highly on the design of molds that are used for manufacturing components [20] [21]. The molds undergo various stages in their lifecycle that requires extensive labor as they are yet to be fully automated [21]. The main stages in mold lifecycle are,

1 Mold Design [19] [21] [22] [23]
2 Mold Manufacturing [21] [22]
3 Mold Assembly [22]
4 Component Production [21] [24] [25]
5 Mold Maintenance [26] [27]
6 Mold Cleaning [26] [27]

The lifecycle of molds are getting more optimized as automated techniques are introduced in various stages with the implementation of Industry 4.0 [28] [29] [30]. Resin transfer molding (RTM), a classification of injection molding is a widely used process for producing A2 surface quality in automotive industries [31] [32]. RTM is used mainly for producing fiber reinforced plastics where the viscosity of plastic is much lower as it needs to impregnate the fibers when compared to traditional injection modeling [32] [33]. Examples of application of RTM in series production can be found in a few structures of BMW's i3 and i8. RTM is a promising manufacturing technique that can be optimized for producing FRP-metal hybrids [12] [34]. However, this process is expensive and labor intensive as they are yet to be fully automated. To make the process more economical, new techniques that can be implemented at various stages of production cycle are investigated both in experimental and in simulation approaches [35] [36] [37] [38] [39] [40]. One of the most researched areas in RTM is focused on the influence of parameters such as injection pressure, injection temperature, mold temperature, injection methods etc., on the final product quality [41] [42] [43] [44]. Selection of materials in RTM process is another major researched topic, as different materials require different set of parameters and approaches [18] [45] [46]. Improving the performance of the RTM injection machine for example, increasing the number of parameters that can be controlled is another well-researched area [28] [29]. However, there is little to no research recorded/published on maintenance stages such as replacement of the sealing materials and cleaning of the mold that are cost effective. Both these areas have potential for optimization leading to a more economically-efficient-automatic process. The current work addresses the maintenance stage in the production line of RTM process that is manually intense but has the potential for automation with the help of new Self-sealing and cleaning technique.

1.2 Objective

The main objective of the current work is to optimize the production cycle of vacuum assisted light resin transfer molding (VA-LRTM) that may potentially lead to a fully automated production line. Traditional molds of VA-LRTM are sealed using polymer materials to prevent the leakage of matrix system as they have lower viscosity. The seals undergo tremendous amount of thermal, chemical, and mechanical loadings, which requires a constant monitoring during production cycles as they need to be replaced immediately to prevent leakage that can lead to demolding and component quality issues leading to higher maintenance. Such an issue leads to production downtime as the seals should be replaced which leads to material wastage. The current work introduces a cost and time efficient sealing concept for manufacturing both FRP and hybrid components replacing conventional polymer seals. The sealing is achieved by accelerating the curing of matrix system itself with the help of heating elements and catalysts resulting in a self-sealing technique/approach.

Another major issue in the RTM process is mold contamination caused by various factors such as improper application of mold sealer and leakage occurred due to sealing failure. These factors influence the final quality of the produced products that are normally classified as A2 surface finish. The cleaning process of mold is labor intense as they are yet to be automated. Most widely used cleaning method for mold is ultrasonic cleaning method, which is considered in the current work for optimization. In traditional ultrasonic cleaning method, the mold is removed from press and immersed into a tank that contains the cleaning solution which is acidic in nature. Before immersing the mold, all electric elements should be removed and they should be installed again before production, making it more time consuming. Also, cleaning the entire mold is not required as the mold contains many sub-components/sub-assemblies, which will never come in contact with matrix system. Matrix system is normally injected directly into the mold cavity where the fibers are placed for production stage. The mold cavity sub-components are typically made from stainless steel or mold steel that are corrosive resistance, where the contaminations are prone to occur over the production cycles. The other sub-components of the mold such as screws, pushpins, inserts, etc., are typically not contaminated as they never encounter the matrix system in a well-designed tool making it unnecessary for them to be made from corrosive resistance materials as it increases the cost and complexity of production. These sub-components of the mold should be removed as the cleaning solution is acidic in nature which accelerates the corrosive process and installed back before production similar to electrical elements.

The current work introduces an In-mold cleaning concept based on ultrasonic cleaning method that does not require moving the mold from press or removing electric and corrosive elements from the mold and is compatible with new self-sealing. To validate the concept, a special mold is designed based on both Self-sealing and In-mold concept that produces metal-FRP hybrid cylindrical shaft demonstrator that has the same cross-section as driveshaft of an automotives. Parameter study was conducted on metal-FRP hybrids cylindrical shaft using traditional production method that was mechanically tested. The results from traditional production were used as reference to compare with Self-sealing. Figure 1-2 shows the typical production stages involved in an Intrinsic Resin Transfer Molding (RTM) process on which the current work is concentrated.

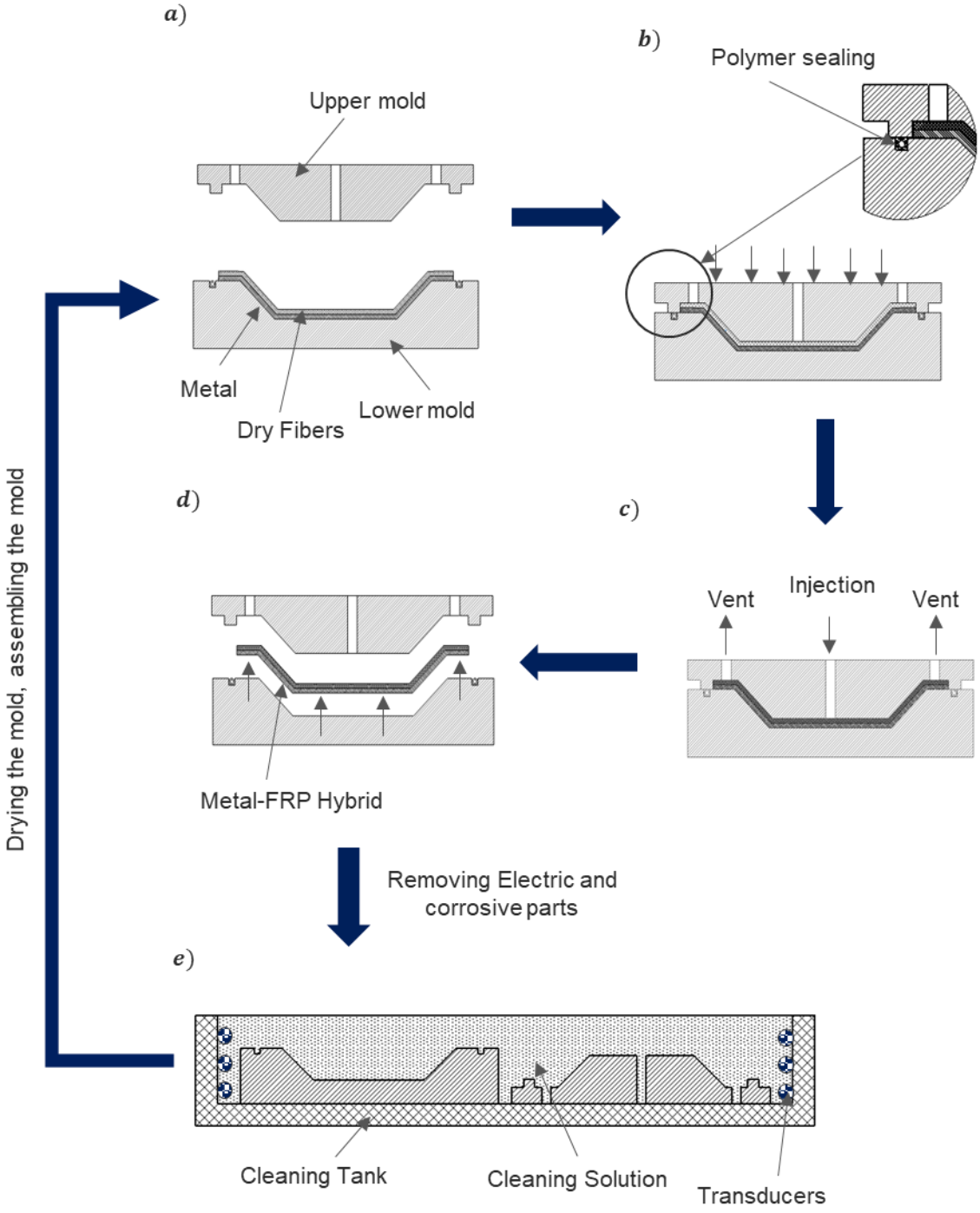

Figure 1-2: Block diagram showing the process cycle of Intrinsic Resin Transfer Molding (RTM) a) Placement of fiber and metal in a mold; b) Adding the polymer sealing around the mold counter, followed by closing the mold; c) Injecting the Matrix system into the fiber; d) Demolding the produced Hybrid structure and e) Moving the mold to a cleaning unit after removing all the electric and corrosive parts, and the mold is dried, mold sealing is applied and assembled back, which is now ready for the next production phase.

1.3 Thesis Outline

Current study is divided into 6 chapters based on the milestones. Basic introduction, followed by a strong motivation for the current work has been addressed in chapter 1. Chapter 2 provides detailed literature study on various topics that are necessary for fulfilling the motivation of the current work, few of them are listed below.

- Hybrid manufacturing structures, production methods and materials
- Scope for RTM optimization
- Importance of process optimization
- Ultrasonic cleaning

Various manufacturing methods for hybrid structures are studied in chapter 2. Chapter 2 also addresses various materials that can be used for hybrid manufacturing process and selecting appropriate interface layer between metal and FRP. Various mechanical test procedures that can be used to characterize the hybrid structure are addressed in chapter 3. Chapter 4 introduces the concepts and its working principle to overcome the challenges addressed in chapter 2. Chapter 5 deals with analytical approach for the concept and basic guidelines for designing the mold based on demonstrator geometry. Finite element methods are used for validating the mold design for steady state thermal analysis. The process of manufacturing mold followed by its assembly is also described in chapter 5. Chapter 6 describes the process study carried out in the current work, which involves selecting the process parameter and the interface layer between metal and CFRP. Chapter 6 also explains the method followed to validate the Self-sealing process and optimize it further using AM printed cooling channel. In chapter 6, In-mold cleaning concept was also validated successfully using the mold that produces hybrid shafts.

2 State of the Art

2.1 Hybrid Structures

Hybrid manufacturing techniques have gained importance because of their ability to manufacture lightweight structures with tailored properties. The main concept of the hybrid manufacturing technique is using multiple materials to make structures that compensates each other's weakness without scarifying their original properties making it a superior component that cannot be manufactured out of one material [31] [45]. Metal-FRP hybrid structures are emerging combination because of their desirable unique characteristics such as higher strength to weight ratio, fatigue performance, corrosion resistance, vibration damping, etc. [18] [45]. FRP-metal hybrid structures were first introduced for aerospace fuselage structures to replace the aluminum alloys for further weight reduction. Metal-FRP hybrids found its application in various parts of the car body due to its lightweight property. A potential application of metal-FRP hybrid structures in automotive sector is for crashworthiness system [47]. Normally, FRP alone cannot be used for crashworthiness as their failure mode is characterized as brittle when loading takes places in fiber direction because of their unstable interlaminar layers during dynamic conditions. However, the failure behavior of the complete structure can be modified to a ductile failure by integrating metals to its structure so that it makes use of plastic deformation phase of metals [47]. The combination of metal-FRP hybrids vary depending on the applications, such as it can either be a laminate structure or a sandwich structure [31] [45]. Figure 2-1 shows few combinations between FRP and metals that are widely investigated. Sandwich structures consist of two metal sheets bonded to an FRP between them. Locally FRP reinforced metals consist of CFRP just at a highly stress concentrated areas to balance out the material cost. Metal inserts are usually placed prior to the curing of FRP that avoids the hole drilling process of FRP structure and ensures that the fiber continuity in FRP is not damaged. Table 1 shows advantages of metal-FRP hybrids structure properties along with their approaching methods.

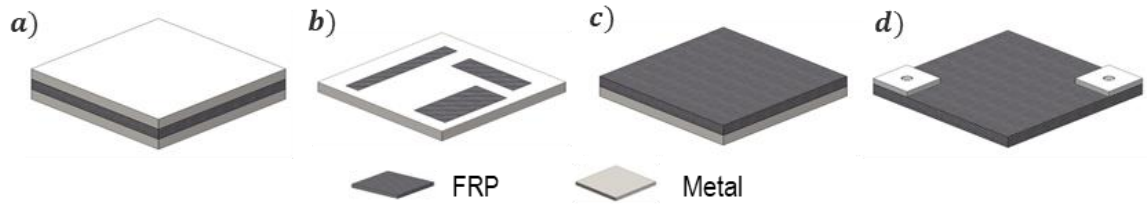

Figure 2-1: Metal-FRP hybrid combination configuration a) Sandwich structure; b) Locally FRP reinforced metal; c) Laminate structure and d) FRP with metallic inserts.

A combination of Sandwich structure and Laminate structure were first used in fuselages of aircrafts for weight reduction. In 1978, first hybrid structure was fabricated by bonding unidirectional aramid fibers to aluminum alloy that was named Aramid Reinforced Aluminum Laminate (ARALL) [48] [49]. ARALL consists of alternating thin aluminum alloy layers of 0.3 mm thickness and uniaxial or biaxial aramid fiber prepreg of 0.22 mm thickness with fiber content of 50 % by weight. In comparison with aluminum alloy, ARALL exhibits higher strength, better fatigue, and impact performance. ARALL structure was integrated into lower wing skin panels of the former Fokker 27 aircraft and cargo doors of the Boeing C-17 [50].

Table 1: Advantages of FRP-metal-hybrid structures [18] [45] .

Properties	Strategies
High fatigue	High fatigue resistance can be achieved by the intact bridging fibers in the wake of the crack, which restrain crack opening resulting in a better fatigue characteristic
High strength	Both metal alloys and fibers used for making hybrids have higher strength than their individual resulting in high strength structure.
High Impact resistance	In comparison with composites, the damage tolerance behavior of FML can be compared to conventional aluminum alloys, only at higher impact energy levels.
High energy absorption	A significant energy absorption through localized fiber fracture and shear failure in the metal piles makes it a suitable candidate when loaded in fiber direction
Low density	In combination of epoxy-based polymer matrix and low-density aluminum sheets, metal-FRP hybrids structures are a weight saving structural in comparison
Lower material degradation	FMLs have an excellent moisture and corrosion resistance, FMLs degradation because of environmental aspects is significantly lower as compared to either metallic structures, or composite structures
Fire resistance	The high melting point of the fibers in FML (for instance, glass fibers in GLARE laminates can withstand 1100 °C and carbon fiber in CARALL can withstand 2500 °C) prevents penetration of fire to the inner layers. When compared with the melting point of monolithic aluminum alloy which is 650 °C, FML makes the perfect substitute for aircraft fuselage that ensures enough time to passengers for evacuating the aircraft safely in case of fire events.

Later, glass fibers replaced the aramid fibers resulting in a new hybrid structure named Glass Reinforced aluminum laminates (GLARE). GLARE exhibited improved formability, better fracture toughness, and compression resistance than ARALL, making it more attractive and replacing most of the aluminum in the upper fuselage panels and leading edges of A380 resulting in a weight reduction of 784 kg [51]. GLARE was modified further by using aluminum–lithium alloy instead of just aluminum alloy that exhibited better damage tolerance and thermal fatigue than the previous versions [52]. Table 2 shows the various commercially available ARALL´s and GLARE´S. Carbon fiber reinforced aluminum laminate (CARALL) was the result from combination of carbon fiber and aluminum alloy. With carbon fibers having superior properties than both aramid and glass fibers made it an immediate alternative. However, CARALL could not be used in humid environment as it tends to accelerate the galvanic corrosion in aluminum alloy because

of large electric potential difference between carbon and aluminum [53]. To overcome this issue, Titanium-graphite (TiGr) laminate was introduced consisting of titanium alloy sheet bonded to graphite-reinforced polymer. TiGr possesses higher specific strength in comparison with ARALL and GLARE that can be applied to high-temperature environments [18] [54]. TiGr laminate has been installed to the wings and fuselage skins of the Boeing 787 and the hatches of the V-22 engine [55]. Figure 2-2 shows the location of composites in Airbus 380 and Boeing 787 aircrafts.

Table 2: Summary of commercially available Hybrid Laminates.

Laminates	Aluminum Alloy	Aluminum Thickness / mm	FRP Thickness / mm	FRP direction / °	Characteristics
ARALL - 1	7075-T6	0.3	0.22	0/0	Fatigue, strength
ARALL - 2	2024-T3	0.3	0.22	0/0	Fatigue, formability
ARALL - 3	7475-T76	0.3	0.22	0/0	Fatigue, strength, exfoliation
ARALL - 4	2024-T8	0.3	0.22	0/0	Fatigue, elevated temperature
GLARE - 1	7475-T61	0.3-0.4	0.266	0/0	Fatigue, strength, yield stress
GLARE - 2	2024-T3	0.2-0.5	0.266	0/0,90/90	Fatigue, strength
GLARE - 3	2024-T3	0.2-0.5	0.266	0/90	Fatigue, impact
GLARE - 4	2024-T3	0.2-0.5	0.266	0/90/0, 90/0/90	Fatigue, strength in 0/90 direction
GLARE - 5	2024-T3	0.2-0.5	0.266	0/90/90/0	Impact
GLARE - 6	2024-T3	0.2-0.5	0.266	±45, ∓45	Shear, off-axis properties

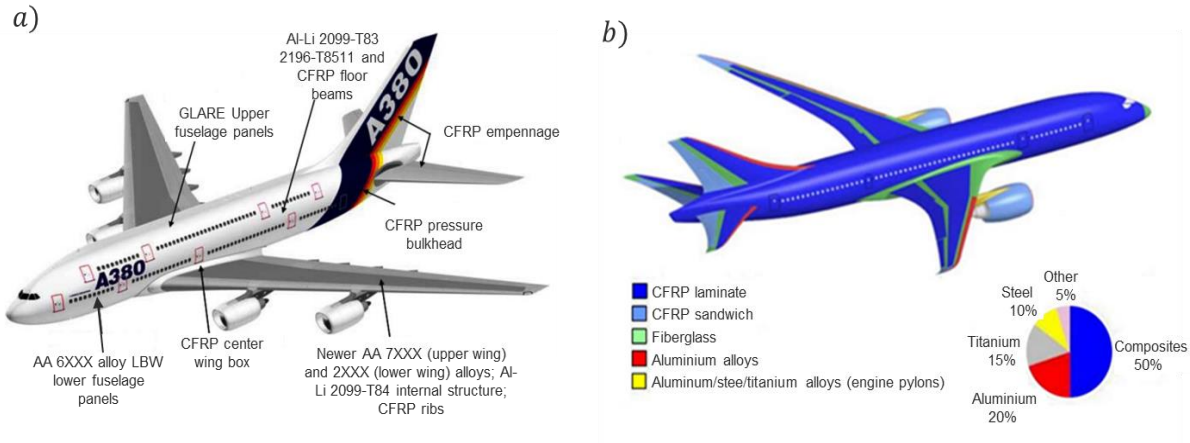

Figure 2-2: Material distribution in a) Airbus 380 and b) Boeing 787 [53].

Successful application of metal-FRP hybrids across various structures of aircrafts made it a potential candidate in automotive sector for weight reduction and better stability [18]. Benteler group developed a front bumper made of GFRP-aluminum-hybrid that weighed 45% less and can withstand 11% more loads without additional cost in comparison to Aluminum bumper [54].

Porsche developed a hybrid structure out of GFRP in a honeycomb structure with high strength steel bonded by adhesive for A-pillar of 911 Cabriolet [55]. This structure was superior to its previously used high strength steel structure in terms of strength but also achieved a weight reduction of 5 kg. In 2015, BMW 7 series developed a concept of “carbon core”, applying metal-FRP hybrid components to various structures such as roof beam, B pillar, C pillar, threshold beam, and central channel as shown in Figure 2-3a resulting in a weight reduction of 130 kg [56]. Hexcel produced sub frame with combination of carbon fibers and aluminum as shown in Figure 2-3b. The produced sub frame had an improved NVH performance was lighter in weight [18]. Mitsubishi Rayon along with Enkei Corporation developed a hybrid wheel combining a forged aluminum wheel with CFRP as shown in Figure 2-3c. The produced hybrid wheel was not only a lightweight structure but also reduced the tire noise and vibrations [18].

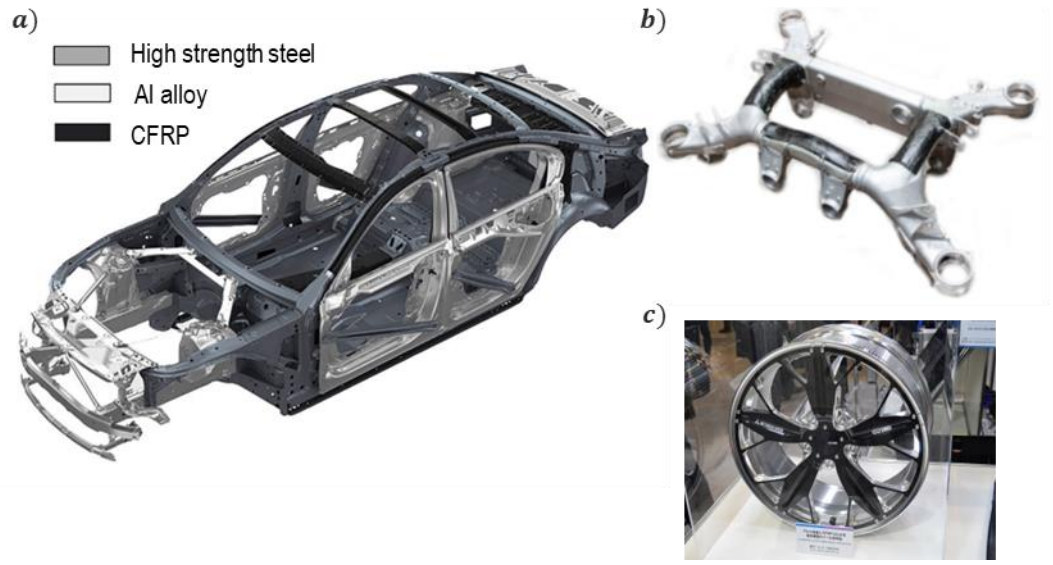

Figure 2-3: a) BWM 7 series car body; b) Hexcel sub-frame and c) Mitsubishi Rayon and Enkei Corporation Wheel.

Due to high stiffness and better energy absorption, another potential application of FRP-metal hybrids in automotive sector is crash management. The combination of Aluminum and CFRP in a square hollow cross section resulted an improvement of 38% and 30% in specific energy absorbed and crush force efficiency respectively in comparison with Al6063T5 [57]. In a different study, the combination of aluminum and carbon fibers in a round hollow cross section was investigated to produce a drive shaft. It was reported that with combination of Aluminum and carbon fibers, the weight of drive shaft could be reduced to 75% and increase the torque to 160% in comparison with steel drive shaft [58]. The other potential application of aluminum and carbon fibers is hydrogen storage cylinders. The hybrid hydrogen storage cylinder was capable of storing more hydrogen and at the same time, the weight was reduced by 50% compared to the monolithic metal storage cylinder with the same volume [59]. With all the advantages and application mentioned, it is challenging to fabricate metal-FRP-hybrids because of their individual physicochemical properties, especially the large difference in Coefficient of Thermal Expansion (CTE).

2.2 Materials

In general, a metal-FRP hybrid structure consists of at least four different materials with completely different properties. In this section, materials that are used or reported as a potential application for hybrids are discussed. The functionality of each material is listed in Table 3. It should be noted that in some cases the metal sheets are coated with adhesive substrate introducing new materials that were classified under surface treatment category.

Table 3: Functionality of the material used in Metal-FRP Hybrid structure.

Category	Examples of Materials	Functionality
Matrix	Polyester, Vinyl ester, Epoxy, Phenolic, Polyamides, polyethylene, etc.	Matrix ductility is to bind the fibers and transfer the loads between fibers. In case of hybrids, it also binds the metal part to the FRP
Reinforcement	Glass fibers, Carbon fibers, Aramid fibers, etc.	Reinforcement is for load carrier
Additives	Colorants, Flame retardant, Binders, UV stabiliser, etc.	Increase the functionality of the CFRP and change its properties depending on the requirements.
Catalyst	1, 4 - diazabicyclo [2. 2. 2] octane, Dibutyltin dilaurate, Dimethyltin carboxylate, etc.	Catalysts were used to accelerate the rate of a chemical reaction by reducing the activation energy.
Metal	Aluminum alloys, Steel alloys, Titanium alloys etc.	Additional stiffness and better load carrier

2.2.1 Matrix System

The matrix system selected should match both the process and use requirements such as mechanical properties, environmental resistance, costs, storage, safety, etc. Preferred properties of a matrix system for a process are low viscosity and good wettability. In general, matrix systems are classified based on their nature and number of components used. There are two types of matrix systems based on number of components used namely, one-part matrix system and two-part matrix system. As the name suggested, in a one-part matrix system both the base compound and curing agent are pre-mixed and stored. They are directly injected or applied on to the fibers and cured. The main advantage of a one-part matrix system is ease of processing as there is no mixing stage that results in formation of air pockets. However, the disadvantage is it requires heat for curing and should be stored in special units where the temperature is below 0 °C. In the two-part matrix system, base compound and curing agent are stored separately and only mixed right before the production process. In some cases, the mixing takes place just before contacting the fiber via mixing heads. The main advantage of the two-part matrix system is that it cures at room temperature without any necessity of additional temperature, and they can be stored in room

conditions without any complications. However, it does have disadvantages such as measuring problems and blending issues during mixing stage, which is an additional stage, shorter work time, etc. Based on the nature of matrix, they are classified into thermoplastics and thermosets. Both thermosets and thermoplastics are available in one-part and two-part systems based on requirements.

2.2.1.1 Thermoplastics

Thermoplastic resins are polymers linked by intermolecular interactions or van der Waals forces, forming a linear or branched molecular structure as shown in Figure 2-4. This linear or branched molecular structure can only provide a relatively small restriction for the motion of molecular chains, which makes the thermoplastics formable under temperature [124]. Some of the examples of thermoplastic polymers are polyamide (PA), polypropylene (PP), polyethylene (PE), poly phenylene sulfide (PPS) etc. They have good reversible thermal, mechanical, and rheological properties and are compatible with fibers such as glass, carbon, or aramid, etc. For a better understanding, mechanical and physical properties of most used thermoplastics without fibers are listed in Table 4

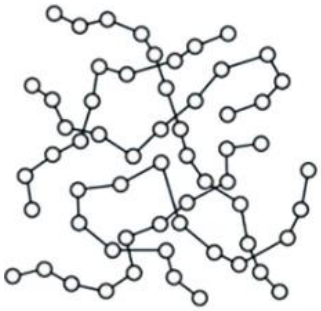

Figure 2-4: Molecular structures of thermoplastic resins [124].

Table 4: Physical and mechanical properties of typical thermoplastic polymers (without fibers) used in structural applications [125].

Thermoplastic polymer	Tensile modulus / GPa	Tensile strength / MPa	Melting point / °C	Density / g cm^{-3}
Polypropylene (PP)	1.50 -1.75	28 - 39	134 - 165	0.98 – 0.91
Polyethylene (PE)	0.15	10 - 18	104 - 113	0.918 – 0.919
Polyurethane (PU)	0.028 - 0.72	5 - 28	220 - 230	1.15 – 1.25
Polyamide (PA)	0.7 - 3.3	40 - 86	211 - 265	1.03 – 1.16
Poly ether ether ketone (PEEK)	3.1 - 8.3	90 - 110	340 - 344	1.3 – 1.44

It can be noted that the melting points of thermoplastic range from 100 – 350 °C making its way into wide applications. PP is the most widely used thermoplastic as it has the lowest density among all thermoplastics whereas PEEK has better tensile modulus. Structure of PP is shown in Figure 2-5. PP is a commodity polymer which is impervious to most solvents and chemicals [125]. PP is suitable for simple fabrication techniques because of its relatively low melting point making it a perfectly suitable matrix for both short and long fibers in injection, extrusion, and compression molding techniques.

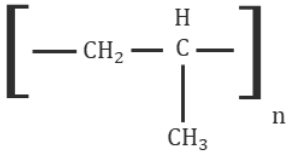

Figure 2-5: Structure of Polypropylene (PP).

2.2.1.2 Thermosets

In the current study, thermoset based epoxy resin was selected as they can also be used as an adhesive between FRP and metal along with being a matrix system. Another major requirement in the current study is heat resistance which eliminates all thermoplastic resins. RTM process was used where pressure can be as high as 15 bar making it a necessity to use binders. Epoxy is available in both liquid and powder form that can be used as binder. The major property of epoxy is that it acts as a thermoplastic before adding the curing compound making it a perfectly suitable candidate for binder role. By using epoxy, the number of materials used can be drastically reduced as it acts as binder, matrix, and adhesive in the current case.

Generally, thermoset resins are polymers joined together by chemical bonds, forming a highly cross-linked molecular structure as shown in Figure 2-6. This cross-linked structure can greatly restrict the motion of molecular chains, which makes them unfit for reuse once they are cured [124]. Table 5 lists few of thermoset polymers that are used in FRP. The advantages of thermoset polymers are heat resistance, higher mechanical stability in comparison with thermoplastics, strong durable chemical bonds, etc. However, it does come with a few disadvantages such as handling inconveniences, brittleness, non-recyclable, inability to form once cured, etc.

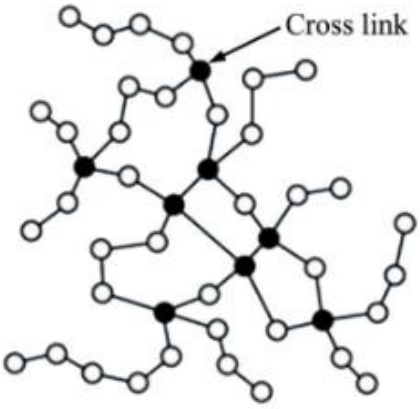

Figure 2-6: Molecular structures of thermoset resins [124].

Table 5: Physical and mechanical properties of typical thermoset polymers (without fibers) used in structural applications [127] [128].

Thermoset polymer	Tensile modulus / GPa	Tensile strength / MPa	Density / g cm^{-3}
Epoxy	3 - 6	35 - 100	1.1 – 1.4
Vinyl ester	3.1 – 3.8	69 - 83	1.2 – 1.4
Polyester	2.0 – 4.5	40 – 90	1.2 – 1.5
Urea Formaldehyde	9	65	1.55
Phenol formaldehyde	8.3	50	1.4

It can be noted from Table 4 and Table 5, the density of both thermoset and thermoplastic are almost same with difference in their mechanical properties. In general, thermosets don't have any melting point as after a certain temperature, they just disintegrate rather than changing to liquid stage. From Table 5, Epoxy resin, Vinyl, Phenol formaldehyde are most widely used resins that have many grades depending on their application, which is discussed further. Epoxy is not only used as matrix system in FRP but also as a coating and adhesives agent for metal and FRP. The main advantage of epoxy is it cures quickly at wide temperatures from 5 °C to 150 °C. In general, epoxy is classified into three types namely cycloaliphatic epoxies, epoxidized oil epoxies and glycidated epoxies. The most commonly available epoxy is based on glycidation of bisphenol A with epichlorohydrin as shown in Figure 2-7. Epoxy is cured using hardener that functions by means of either anionic or cationic homopolymerization or co–reactants such as amines, acids, anhydrides, phenol, etc. [129]. The advantages of epoxy resin are minimum shrinkage and high chemical resistance. At the same time, epoxy resin has few drawbacks such as low elasticity, low stiffness, and high cost.

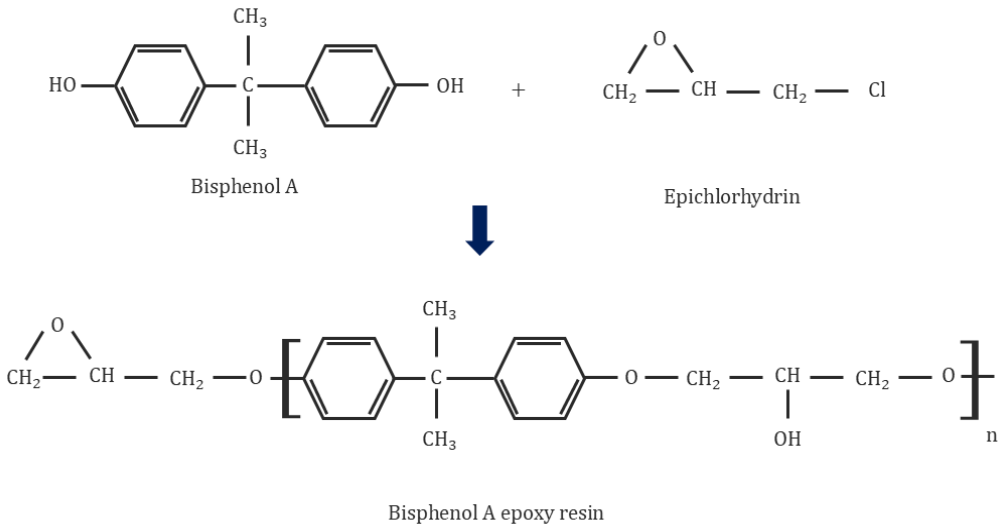

Figure 2-7: Bisphenol-A epoxy curing reaction mechanism [127].

2.2.2 Fibers

Most used fibers in FRP are glass, carbon, Kevlar, and aramid. Table 6 shows the mechanical and physical property of fibers used in FRP structures. Fibers are available in different formats such as continuous, discontinuous, particles, fabric, or waver, etc. Out of all fibers, carbon and glass fibers are most widely used because of their high tensile modulus which is studied further. In general, Carbon fibers are produced via carbonizing precursor fibers or synthesized directly from a hydrocarbon gas, such as methane. Carbon fibers made by carbonizing precursor fibers are categorized according to the type of precursor fibers used, such as PAN-based, pitch-based, and rayon-based carbon fibers. Based on properties, Carbon fibers are divided into four types namely ultrahigh modulus, high modulus, ultrahigh strength and high strength carbon fibers. In the current study, high strength carbon fibers are used which had a tensile strength of 4.2 GPa.

Table 6: Physical and mechanical properties of fiber used in FRP applications [132].

Fibers	**Tensile modulus / GPa**	**Tensile strength / GPa**	**Compressive strength / GPa**	**Density / g cm^{-3}**
Boron	415	3.5	5.9	2.5 – 2.6
SiC (Nicaolon)	200	2.8	3.1	2.6
E-glass	70	1.5 – 2.5	-	2.5
S-Glass	90	4.5	> 1.1	2.46
Carbon P 100 (Pitch based)	725	2.2	0.48	2.15
Carbon M60J (PAN based)	585	3.8 – 6.5	1.67	1.94
Aramid (Kevlar 49)	125	3.5	0.39 – 0.48	1.45
Poly (p-phenylene benzobisthiazole) (PBZT)	325	4.1	0.26 – 0.41	1.58
poly (p-phenylenebenzobisoxazole) (PBZO)	360	5.7	0.2 – 0.4	1.58
PE (Spectra 1000)	172	3	0.17	1
Nylon	6	1	0.1	1.14
Textile PET	12	1.2	0.09	1.39

The diameter of fibers typically ranges from 9 to 17 µm. They are combined to form a yarn which is an important factor in composite industry. Yarn size is measured in number of filament count. Some of yarn types that are common are 1K, 2K, 4K, 6k, etc., with typical layer thickness in the range of 0.12 – 1 mm. There are special yarns with larger thickness, but they are specially made to order due to the cost and requirements. Another important factor is the direction of the fibers because of their anisotropic nature. Most common type is unidirectional where the fibers are aligned in one direction. The main advantage of unidirectional is said to be anisotropic in nature when combined with matrix. Next variant is a bi-directional fiber orientation where the fibers are in two directions normally 90° apart with possibility of different properties. The fibers are further classified based on their weaving patterns as they play a very important role in matrix flow and strength of the structure produced as shown in Figure 2-8. For example, plain weave is the most common weave pattern consisting of a 1 x 1 fibers produced by a weft strand going over and then under each alternating warp strand. This weave has the highest frequency of over and under passes that are very stable. The overall structure will be less pliable and harder to use as a composite that has complex shapes and 3D features but works very well for flat surfaces.

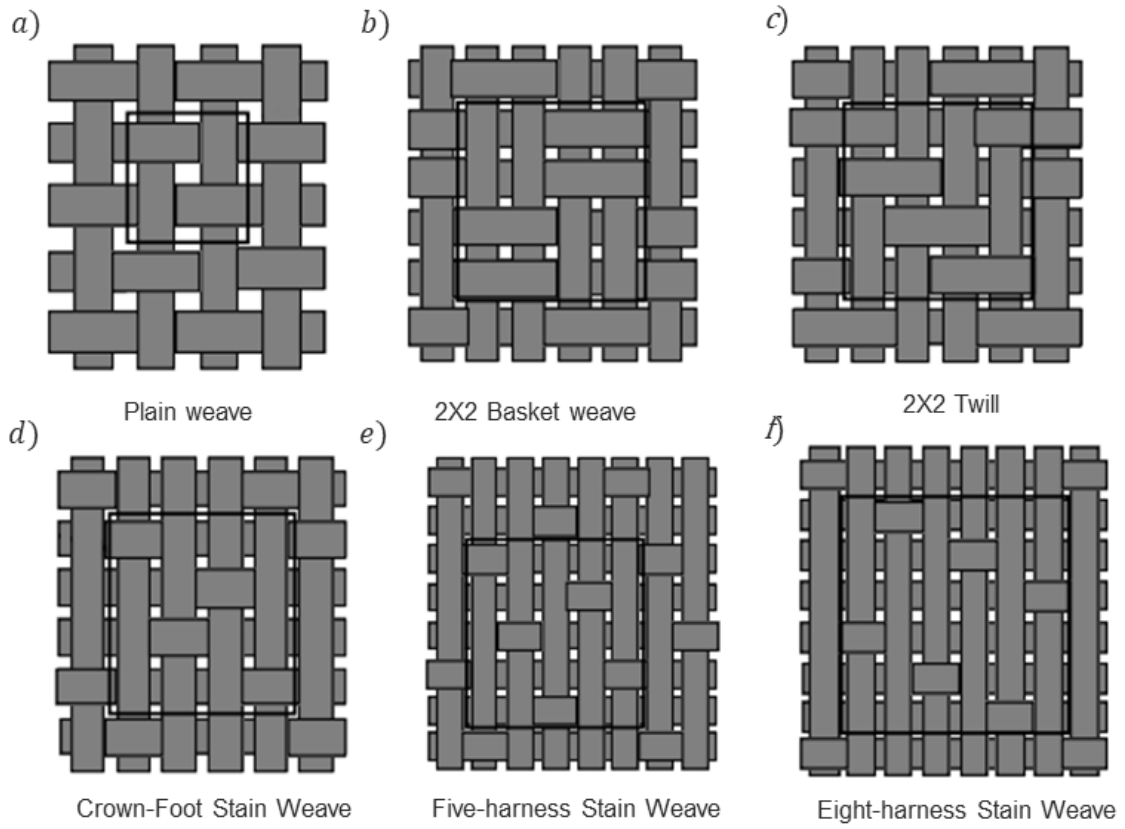

Figure 2-8: Commonly used 2D weave patterns [133].

Filament winding is another technique for preparing carbon fibers for cylindrical cross sections. In general, it is an automated method for axisymmetric geometries that can weave fibers in a desired angle. In the current study, fiber aligned in 45 ° in a 1X1 twill pattern by winding techniques is used to validate the concept.

2.2.3 Additives

In general, polymers matrix can be modified based on the process with the help of additives. During the matrix injection process, some of the fiber properties can diminish where additives can help to stabilize or enhance properties that were lost during processing. With the blend of additives, matrix system can be made safer, cleaner, tougher, and more colorful. A process called compounding helps to melt blending matrix with additives that changes the physical, thermal, electrical, or aesthetic characteristics of the matrix based on requirements. Using additives provides many benefits such as increased safety, reducing production cost, increase longevity, enhanced appearance, water resistance, surface smoothness, etc. One of main characteristics of additives is to become part of polymer matrix without any drawbacks. Below are some of the most used additive applications [134].

- Colorants: Used to add color,
- Antimicrobial: Used to control the build-up of bacteria, fungi, and algae on the surface of food-related applications or high-contact consumer products,
- Antistatic: Used to decrease the static electricity conduction and are often used in sensitive electronics and industrial goods,
- UV Stabilizers: Used for the protection of the resin's mechanical properties by absorbing selective UV rays (less degradation),
- Plasticizers: Used to make resins softer, more flexible, and pliable (modification of viscosity),
- Flame retardants: Used to make products resistant to combustion or eliminate its tendency to burn,
- Optical brighteners: Used to improve whiteness.

In some cases, the matrix system is mixed with shredded fibers such as glass or carbon or metal particles to increase the mechanical strength. In this case, the particle size of the additive plays a very vital role as they should be compatible with other material used. Fillers are other type of additives that can be classified separately which are used to reduce the cost of the composite without reducing their mechanical properties. Fillers are often referred to as extenders that can also improve fire and smoke performance by reducing organic content in composite laminates. Also, filled resins shrink less than unfilled resins, thereby improving the dimensional control of molded parts. Use of inorganic fillers such as Calcium carbonate, Kaolin, Alumina trihydrate, Calcium sulfate, etc. are getting more prominent in industries.

Binder is a variant of additives that are used for fiber alignments. The main characteristic of binder is that it should be compatible with the matrix system and cure along with it. Compatibility essentially rests with an understanding of both the resin's and the binder's Chemistry and must be considered on a case-by-case basis. Binders may be liquid or solid at the injection temperature. In case, if the binders are liquid at the injection temperature they may wick into the tows of fibers. If the binder is solid at the injection temperature, but still soluble, the same effects can occur. Hot stage microscopic test is carried out to see the functionality of binder with resin [32]. In the present study, epoxy-based powder binder additive is used for aligning the fiber before injection phase that is compatible with matrix system and aids during curing.

2.2.4 Catalysts

The main function of catalyst is to accelerate the curing of the matrix system. Catalysts are also referred to as initiator or accelerator as they can also be used to initiate or accelerate the curing based on application. It should be noted that normal catalyst, accelerated based catalyst and initiator-based catalyst are recommended not to be used together as they result in violent decomposition of the peroxide with the risk of fire and explosion [135]. There are a few exceptions where they are used together in case of them being in same group. In general, catalysts used are invariably based on organic peroxides. They are chemically unstable that can decompose explosively in the pure form. They are mostly supplied as solutions, dispersions or pastes in a plasticizer or as a powder mixed with an inert filler to stabilize them [135]. Most catalysts are used between 1% and 4% based on the resin weight. Use of catalyst also reduces the pot life of the matrix system that should be carefully studied before application as some production processes need specific time before pot life. Pot life is defined as the amount of time it takes for the product viscosity to double, or quadruple for lower viscosity products (<1000 cPs). Pot life test is carried out at room temperature (23 ℃), whereas the gel time test is carried out at elevated temperatures for the same method. However, a wide range of catalysts are available with desired pot-life. There are special catalysts that can lengthen the pot-life without altering gel and cure times so that demolding is not affected. This can be achieved by using inhibitors to the matrix system. Functionality of inhibitors ranges from increasing the pot-life, gel time and cure time, etc.

The most used accelerator-catalysts are based on either cobalt soap or tertiary amine. Other types of accelerator-catalyst such as quaternary ammonium compounds, vanadium, tin, and zirconium salts are used in special cases. Typically, organic peroxide such as methylethylketone peroxide (MEKP) is used for room temperature cured processes, or benzoyl peroxide for heat-cured molding. When triggered by heat or used in conjunction with a promoter such as cobalt naphthenate, peroxides convert to a reactive state exhibiting free radicals causing the unsaturated resin to react forming cross-link and become solid. Some additives such as TBC (tertiary butyl catechol) are used to slow the rate of reaction and are called inhibitors [136]. It is of great importance to select the catalyst that is compatible with the matrix system.

In the current study, the following accelerate based catalysts were selected as candidates for epoxy-based matrix system to accelerate the curing.

- DABCO (1, 4 - diazabicyclo [2. 2. 2] octane),
- DBTL (Dibutyltindilaurate),
- UL-28 (Dimethyltin carboxylate).

DABCO also known as triethylenediamine (TEDA) is a bicyclic organic compound based on amine group that is compatible with both epoxy and polyurethane matrix system. DABCO is available in powdered form. DBTL is a catalyst for solvent-based two-component matrix system. DBTL improves the curing systems favoring the isocyanate/polyol reaction over other side reactions such as isocyanate/water and enhancing the properties such as scratch resistance, hardness, and mechanical, etc. This catalyst is compatible for polyurethanes, silicone resins, RTV silicone resins, epoxy, etc. UL-28 is mainly used for two-part urethane resins but is also compatible with

epoxy resin. UL-28 are typically available in solvent form making it easy for mixing with matrix system.

Before using the above-mentioned catalyst with the matrix system for production, a Differential scanning calorimetry (DSC) was performed to know the influence factor as recommended from the supplier. DSC is a thermal analysis test used to measure the amount of heat flow into or out of the sample with respect to temperature or time under controlled conditions. DSC results provide information of samples such as glass transition temperature, melting, crystallization, specific heat capacity, cure process, etc. The samples can be a made from wide variety of materials such as polymers, plastics, composites, laminates, chemicals etc. Figure 2-9 shows a typical DSC test result of the sample in heat flow VS temperature curve graph.

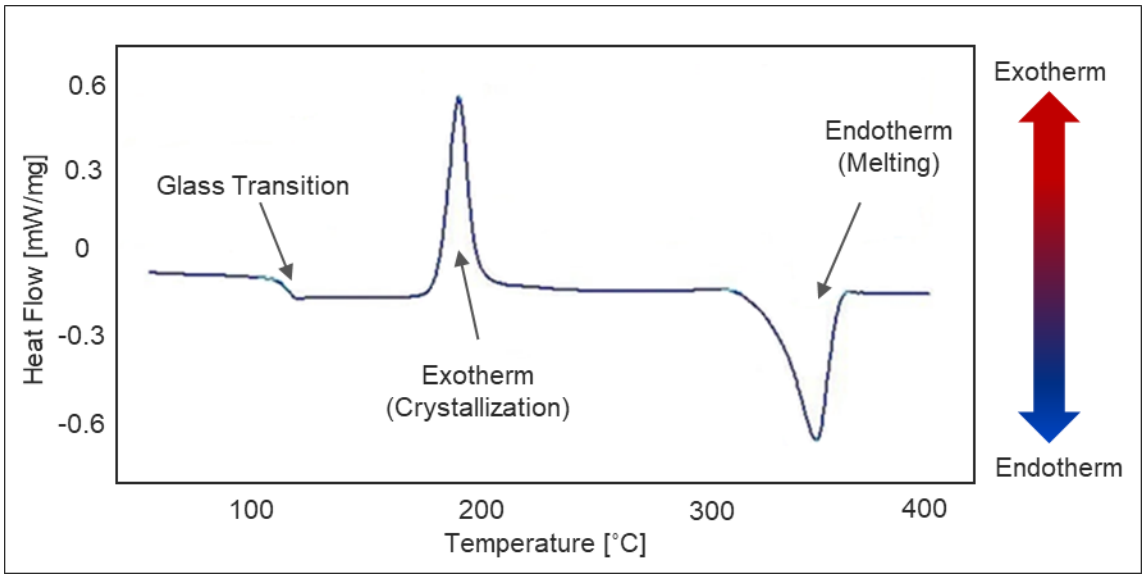

Figure 2-9: Typical DSC profile of PET showing Heat flow of the sample with respect to temperature [70].

Generally, DSC instrument contains a heating block with a sensor that detects the difference in temperature between the sample cell and a reference cell. Once the sample cell is loaded, both the cells are heated in synchronization at a predetermined rate according to the American Society for Testing and Materials (ASTM) standards. If the sample cell requires more energy to maintain the increase in temperature in comparison with the reference cell shows an endotherm peak as shown in Figure 2-9. Similarly, if the sample cell requires less energy in comparison with the reference cell, an exothermic peak can be observed as seen in Figure 2-9. Generally, endothermic peak refers to melting and exothermic refers to crystallization or curing of the mixed product. Nevertheless, there are different tests that provide various information's of the samples via DSC instrument according to ASTM, out of which ASTM E 798-06 was performed in current work to study the rate of curing of the selected resin with respect to the above-mentioned catalysts.

2.2.5 Metals

Metals play a vital role in metal-FRP hybrids as they are the main materials that distribute the stresses in the structure. In general, metals have better bearing strength and impact resistance than FRP due to their plasticity nature. Table 7 lists various metals' physical and mechanical properties that are used or can be used in metal-FRP hybrids.

Table 7: Physical and mechanical properties of few metals used in FRP applications.

Metals	Tensile modulus / GPa	Tensile strength / MPa	Density / g cm^{-3}
Mild Steel alloy	210	360	7.85
Titanium alloy	115	220	4.5
Aluminum alloy	70	275	2.66
Magnesium alloy	45	260	1.74

In the current study, E235+C (cold rolled) steel tubes with tensile strength of ~ 490 MPa are used to manufacture metal-FRP hybrids. E235 steel is also referred to as EN 1.0308 steel which is a non-alloy carbon steel grade. Table 8 shows the chemical composition of the E235 based on EN 10296 standard. The letter E indicates that the steel tube is machined, whereas the numbers that follow the letter E give the information of its minimum tensile modulus in N/mm^2 (MPa). The letter C at the end of the 235 gives the information about the method it was manufactured, in current case its cold drawn via hard process. Cold drawing refers to drawing at room temperature for obtaining specific properties and nature of the steel alloys, normally better than pure drawing. During cold drawing, the steel alloys are not only stretched in longitudinal direction but also in lateral direction as shown in Figure 2-10. After the cold drawing process, the tensile strength of the material can be increased up to 90%, but the plasticity is significantly reduced. Table 9 shows the range of properties for E235 steel tubes manufactured via various techniques.

Table 8: Chemical composition of E235 /1.0308 (EN 10296-1-2003) [70].

C%	Si %	Mn %	P %	S %
0.17 max	0.35 max	1.20 max	0.025 max	0.25 max

E235+C are mainly used where high-precision tubes with superior mechanical properties are required. One of the key characteristics of E235+C is their high dimensional accuracy for both inside and outside diameters. In addition to high dimensional accuracy, these tubes have extremely limited wall thickness tolerances. This ensures that the tubes have consistent wall thickness throughout their length, making them suitable for applications where precision is critical. Another advantage of E235+C is its reduced eccentricity, which means that the tube's centerline

is positioned closer to the outer surface improving the tubes roundness [71]. These advantages make E235+C an ideal fit for the current study where both concentricity and precious play a very important role. Also, E235+C is already a widely used material in automotive industry for various other applications such as transmission shafts, fuel injection pipes, piston pins, steering systems, shock absorbers and tubes for power steering systems, etc.

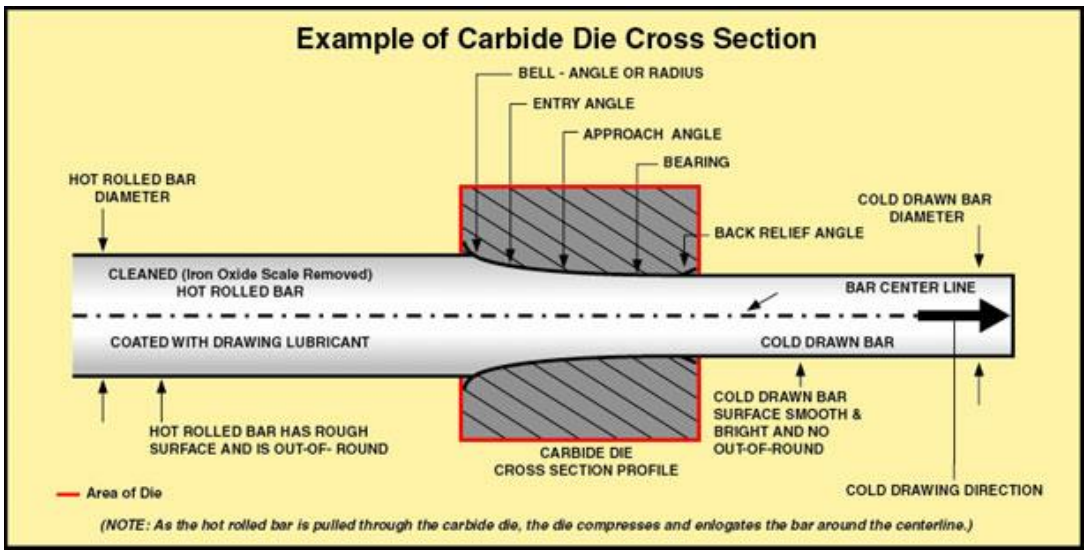

Figure 2-10: illustration of the cold drawing process [72].

Table 9: Mechanical properties of E235 /1.0308 under various preparation conditions [70].

Preparing Conditions	Tensile strength / MPa	Elongation / %
+C (Cold drawn / hard)	480 min	6 min
+LC (Cold drawn / soft)	420 min	10 min
+SR (Cold drawn and stress relieved)	420 min	16 min
+A (Soft annealed)	315 min	25 min
+N (Normalized)	340 - 480	25 min

2.3 Surface Treatment Influence in Metal-FRP Hybrids

The interface plays a major role in metal-FRP hybrids as they are key elements in transferring loads between metal and FRP that have direct influence on the component's mechanical properties. Modifying a suitable polymer to increase the bonding strength between metal and FRP is highly challenging and costly because the physicochemical properties of the two materials are quite different [18]. However, mechanical interlocking based on modified metal surface can be achieved very easily and efficiently. In general, the surface of the metal is altered via different surface treatment based on requirement prior to bonding with FRP. The surface treatment can be as simple as using the sandpaper manually and as precious as using laser technique which is automatic. Surface treatment methods for metal-FRP hybrids can be classified into three categories namely mechanical, chemical, and energy methods as shown in Table 10.

Table 10: Comparison of surface treatments for interfacial bonding of metal-FRP hybrid components [18].

Category	Surface treatment	Nature of treatment	Bonding strength	Characteristics
Mechanical methods	Abrasion	Cleaning, roughening	Low	Simple, low efficiency
	Grit blasting	Cleaning, roughening	Adequate	High efficiency and controllable roughness, workpiece deformation
Chemical methods	Solvent wipe	Cleaning	Low	Simple, low efficiency
	Etching	Cleaning	Adequate	Simple, high efficiency, environmental pollution, difficulty in reagent preparation
	Coupling agent	Coupling and oxidation	High	Moderate effectiveness, environmental pollution, difficulty in reagent preparation
	Anodize	Oxidation	Adequate	High efficiency, environmental pollution, difficulty in reagent preparation
Energy methods	Laser	Roughening, cleaning, and activation	High	High efficiency, easy automation, surface ablation
	Plasma	Cleaning and activation	High	Moderate effectiveness, low stability of treated surface

In the current study, a mechanical method was used to strengthen the interface layer between FRP and metals. Generally, mechanical methods increase the surface area and at the same time create undercuts. These undercuts are responsible for mechanical clamping of metals with FRP. Generally, in mechanical methods, the surface of the metal is altered by removing the original passivation layer by introducing surface roughness via sand blasting or with sandpaper to an extent that provides an improved interfacial bonding strength [118].

From literature, it was noted that the flexural strength for a Steel (22MnB5)-GRRP (polyamide-6) hybrid went as high as 586 MPa from 291 MPa when the surface roughness was improved from 0.48 µm (R_a) to 0.89 µm [119]. However, the flexure strength past the R_a value of 0.89 µm started declining and reached to the value of 316 MPa when the R_a was 1.61 µm making it obvious that there is no proper relationship between surface roughness and flexure strength [119]. Nevertheless, in another report, there was a clear increase in shear strength depending on the different mechanical strategies as shown in Figure 2-11a [120]. Four different samples were produced out of which one sample is abrasive blasted and the remaining three samples were surface treated by laser with different structure height. The surface treatment is classified as nanoscopic structures when the modified structure height is less than 100 nm; microscopic structure when the range is between 100 nm – 200 µm; and macroscopic structures if it is greater than 200 µm. It can be observed that shear strength of Al-FRP hybrid was improved by a factor of ~3.4 times when compared to abrasive blasting treatment. Figure 2-11b shows load displacement curve for the steel-CFRP hybrids where the metal surface is treated with 600 grit sandpaper, degreasing, sandblasting and combined with adhesive films which increased the peak force to ~100 N from ~30 N [121].

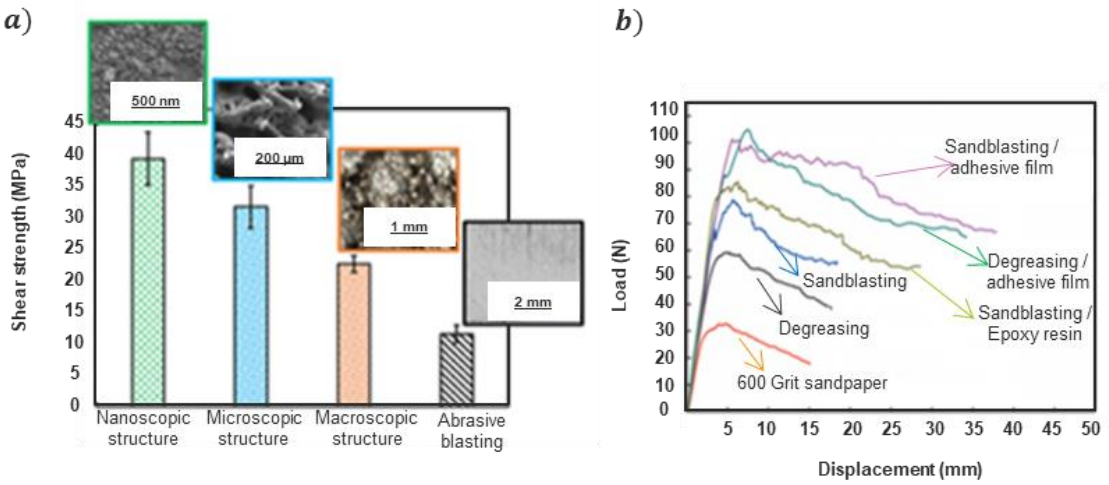

Figure 2-11: a) Tensile shear strengths of AA6082-GF60 joints with various surface pre-treatments [120] and b) load–displacement curves of steel-CFRP hybrid laminates subject to double cantilever beam testing [121].

Sandblasting based mechanical approach was used in the present study to alter the surface of the steel for increasing the surface areas and mechanical locking between steel part and CFRP.

2.4 Metal-FRP Fabrication Processes

In general, the fabrication of metal-FRP hybrid components is classified into two categories based on the sequence of joining and forming process as shown in Figure 2-12. The processes are named after the last step in the manufacturing cycle of metal-FRP processes. In joining, metal and FRP are preformed separately and then joined together using techniques like adhesive bonding, riveting, or welding, etc. The main advantage of forming is that we can use the existing fabrication process of metals and FRPs that are well established. However, joining requires longer cycle time and higher cost due to additional stage of joining metals and FRPs after their individual production. In addition, mechanical joining using bolts adds an additional mass, whereas welding techniques are likely to cause thermal damage to FRPs [18]. However, most of metal-FRP hybrid components for automotive applications are fabricated using joining as they have high geometrical accuracy and consistency [18].

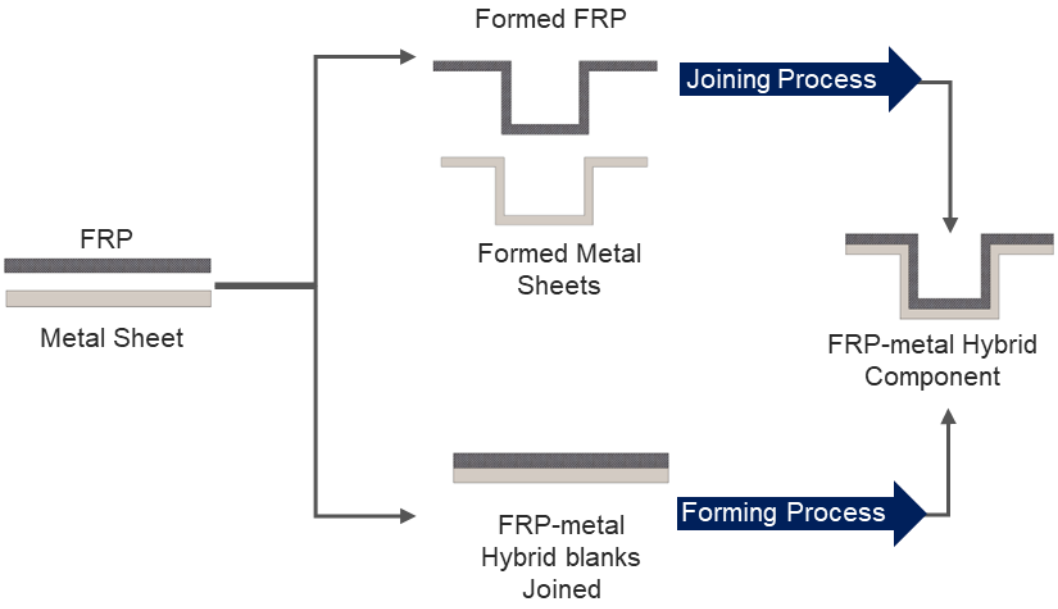

Figure 2-12: Classification of fabrication processes of metal-FRP hybrid components.

In the forming process, both metals and FRPs are joined first and then formed simultaneously so that it can be a simple one stage process. The FRPs in forming can be either a semi-finished product such as prepregs or raw materials like dry fibers depending on the structure and strategy. Both metals and FRPs are placed in the temperature-controlled tools and are formed together to one joined component. Both forming and curing processes are completed in one single step, eliminating the preparing phase of metal-FRP hybrid sheet that shortens cycle time [60]. The performance of hybrid component fabricated by forming process depends on the process parameters such as forming temperature, forming pressure and may also have quality issues such as wrinkles, resin extrusion, and heterogeneous thickness [61]. However, once the parameters are optimized, producing the complex metal-FRP hybrids via forming can be achieved with shorter cycle time in comparison with joining process. A detailed overview on joining and forming techniques of metal-FRP hybrid components along with a comparison is described in the following section.

2.4.1 Joining Approach

Joining processes is a reliable and well-established approach for fabricating metal-FRP hybrid components [18]. This section focuses on joining processes such as adhesive bonding, riveting, welding and intrinsic.

2.4.1.1 Adhesive Bonding

Adhesive bonding is a commonly used technique where an adhesive substrate is either coated or injected between metal and FRP that acts as a stress transfer area when subjected to loading [62]. The mechanical properties of the metal-FRP hybrid components depend on the shear and tensile strength of adhesive with respect to metal and FRP. In addition, interfacial physicochemical reactions play a major role because of the wide difference in physical and chemical properties between metal, FRP, and adhesive substrate. In general, there are 3 major types of adhesive substrates used in automotive industry as listed in Table 11 along with their characteristics.

Table 11: Characteristics of adhesives used to bond metal and FRP [18].

Adhesive Substrate Types	Characteristics	
	Advantage	**Disadvantage**
Polyurethane	Good elasticity, wear resistance, aging resistance, and heat resistance	High curing shrinkage, low bonding strength, and long curing cycle
Epoxy	High bonding strength, low curing shrinkage, good heat resistance, and chemical resistance	High brittleness, low elongation, low peel strength, and poor impact resistance
Acrylic	High bonding strength, short curing time, and wide application range	Pungent odor, toxic, poor corrosion resistance

The functionality of the adhesive in humid nature was reported, where water soak test was carried out where the metal-FRP sample over a time period of 21 days [18]. The shear strength of adhesive substrate decreased with the prolongation of water soak time. Corrosion was spotted on the steel side of bonding interface under microscopic examination stating that the corroded area expanded to the center of bonding area on steel with the extension of water soak time [18]. This effect can be explained because of the water molecules diffusing inward along the bonding interface resulting in corrosion on the steel surface and changing the adhesive from insulator to conductive body accelerating the galvanic corrosion [18] [64]. The acceleration of galvanic corrosion can also be due to the potential difference effect as the electrons on the steel side of the adhesive-bonded joint will run to the SMC side reducing the strength of the bonded joint [18] [64]. The decrease in joint strength caused by interfacial corrosion is the main issue of adhesive-bonding. There are many methods to improve the corrosion resistance of adhesive-bonded steel-FRP joint such as increasing the thickness of the adhesive layer, treatment of steel surface, adding coating on steel surface, etc. [65] [66]. Another biggest challenge using adhesive substrate is long curing time and formation of bubbles that affects the mechanical properties. Novel techniques such as electrical resistance curing method, ultrasonic vibration-assisted hot pressing

etc. are under study for curing the adhesive without any defects for the metal-FRP hybrid components fabrication application [67] [68].

2.4.1.2 Riveting

Riveting is a commonly used mechanical joining method for complex multi material structures, which is widely used in automotive and aerospace industry. Riveting is insensitive to the surface properties leading to a high joining strength usually in comparison with adhesive bonding. There are various types of riveting techniques depending on the structures and materials as listed in Table 12 .

Table 12: Characteristics of riveting used to bond metal and FRP [18].

Riveting Types	Characteristics	
	Advantage	**Disadvantage**
Self-piercing	Stable joint strength, easy to automate, good sealing performance	High equipment cost, requirement of high material ductility
Friction self-piercing	Able to join low ductility materials	Existence of heat affected zone
Electromagnetic	Good fatigue performance, less damage	High energy Consumption, requirement of a pre-drilled hole
Flow drill	Easy to disassemble, easy to automate	Stress concentration, galvanic corrosion, requirement of stack-up sequence, existence of heat affected zone
Friction stir blind	No requirement of stack up sequence, good sealing, and corrosion resistance performance	Existence of heat affected zone

Self-Piercing Riveting (SPR) is a double-sided joining process which is divided into four stages. The semi-tubular rivet penetrates the upper workpiece and its tail flares due to the resistance of the lower workpiece and the constraint from the dye, which can join thermoplastic composite without additional efforts [18]. However, thermosetting composite can only be used as the upper workpiece because of fracture formation when placed as a lower workpiece [18]. Nevertheless, it is inevitable to damage the fibers during the SRP process that can be predicted to a certain level using a two-scale homogenization model of CFRP [69]. SPR was further improved by using a pre-drilled hole on the FRP laminates before riveting resulting in a better interlocking structure than SPR known as pre-holed self-piercing riveting (PH-SPR). It was reported that with this new technique, the joint strength and energy absorption capacity of CFRP and titanium (TA1) sheets were 14% and 110% higher than that of the regular SPR joints [70]. Furthermore, an innovative method was developed where CFRP prepreg sheets and aluminum alloy were joined using SPR and then placed in an autoclave for curing the prepreg at 80 °C for 0.5 h and 160 °C for 1.5 h with a pressure of 0.1 MPa known as post-curing self-piercing riveting (PC-SPR) [71]. As a result, tearing and delamination in regular SPR of CFRP were avoided in PC-SPR along with an improved joint of 45% [18] [71].

Friction Self-Piercing Riveting (F-SPR) is proposed based on SPR process that allows the SPR rivet to generate a large amount of frictional heat through highspeed rotation to soften the local material during the penetration of rivet [72]. F-SPR does not require high ductility of the lower workpiece attributed to the frictional heat, and it is particularly capable of joining difficult-to-form materials [18]. Electromagnetic riveting (EMR) is a novel high efficiency riveting technique that applies electromagnetic force to drive the punch to impact a rivet at high speed. EMR process is similar to SPR Process where the rivet penetrates the workpieces to complete the joint but has an ideal interference-fit due to its uniform shaft expansion, which enhances the sealing performance and fatigue performance of the joints [73]. It was reported that by using EMR process for joining Al alloy and CFRP, the cracks were observed at the Al alloy around the rivet that formed due to the fretting wear between Al sheet and the rivet [74]. Similar behavior was observed in other report where wedge shaped Al alloy and CFRP was joined using EMR process with a significant damage in a rivet tail close to the structure edge [75].

Flow drill screwing (FDS) is a single-sided, one step joining process that combines friction drilling and threading process where the steel screw rotates at a high speed to locally heat the workpiece and forms an extrusion around the screw and then the materials are threaded by the male thread on the screw. Still, FRP sheets can only be placed as the upper workpiece in the joining process of metal and FRP for a better thread profile [18]. FDS also has similar issues like in previous process such as use of thermoset matrix resulting in bending, fracture, and delamination. Also, in FDS process the load bearing capacity is reduced as fibers and matrix particles are drawn into the threaded zone [18]. Alternatively, it was reported that change in screw structure by drilling a hole on the tip reduces the amount of particles entering the threaded area resulting in a higher joint strength [76].

Friction stir blind riveting (FSBR) is a combination of friction drilling and blind riveting where rivet penetrates the workpieces fully at a high rotational speed and then the mandrel is pulled back and breaks at its pre-set notch, forming an expanded shank to lock the workpieces [18]. FSBR process was used to join Al alloy and CFRP and study the parametric influences on the joint performance [77]. In another report, the corrosion performance by salt spray test were studied on Mg/CFRP and CFRP/Al joints that showed no decrease in load bearing of the joint [78]. It was attributed to the mechanical locking between the workpieces formed by the friction stirring process resulting in a reduced clearance between workpieces and formation of protective layer avoiding the contact between rivet and moisture [18]. Following a positive test result in marine conditions, FSBR was modified further by main researcher resulting in multiple subcategories. FSBR-II was introduced based on reduced penetration force so that the damage in FRP was kept to minimum where the rivet tip was cut that resulted in a 42% reduction in penetrating force [79]. FSBR-III was introduced with a conical shaped rivet tip used to join thermoplastic GFRP with Al alloy and Mg alloy [79].

It can be concluded that no matter which riveting method is applied to join FRP and metal, inevitably damage is introduced to low-ductility materials (in particular, thermosetting FRP) and may have an impact on joint strength [18]. Therefore, damages are particularly concerned in the riveting of metal and FRP to fabricate metal-FRP hybrid components. It can be optimized or kept

to minimum by establishing an accurate finite element model to predict the FRP damage behavior during riveting process.

2.4.1.3 Welding

Welding is the most challenging technique in the joining category as the physicochemical properties of FRP are quite different from those of metals. The principal mechanism in metal-FRP welding is similar to adhesive bonding where the solidification of thermoplastic material takes place after being heated, which does not work for thermoset materials. This creates a mechanical interlocking based on molecular and chemical bonds at melting interface. There are mainly 4 types of welding process that can be used for metal-FRP hybrids as listed in Table 13. Figure 2-13 shows the schematic diagram of various welding processes.

Table 13: Characteristics of Welding used to bond metal and FRP [18].

Welding Types	Characteristics	
	Advantage	**Disadvantage**
Resistance spot	High production efficiency, low cost, easy for mass production	Relatively low bonding strength, only applicable to some specific materials, narrow process window
Ultrasonic	High bonding strength, low cost, easy to control the bonding area	Limited application due to double-sided joining
Laser	High efficiency and accuracy, low cost, easy to mass production	Low universality of different materials, generations of heat accumulation and pores
Friction stir (spot)	Relatively high strength, high efficiency	High energy consumption, high equipment requirements, difficult to control the melting zone

In resistance spot welding, the electrode is supplied with a pre-determined current for a fixed time so that the heat generated will melt the matrix of a thermoplastic CFRP and then solidifies after cooling, forming a bond between metal piece and CFRP. The principle was tested using stainless steel alloy with CFRP matrix containing PA6 and PP [80]. It was reported that tensile strength as high as ~13 MPa was recorded between SUS304-CFRP(PA6) by increasing welding current and welding time [80]. However, this process is only applicable for thermoplastic matrix systems.

In ultrasonic welding, the oxide film on the metal surface is removed by applying ultrasonic vibration to the component making impurities on the surface to scatter and forming the attractive force between metal and FRP to create a phase bonding state. Ultrasonic welding was used to weld Aluminum alloy with a thermosetting CFRP as shown in Figure 2-13 [81]. The method was also modified so that the thermoset matrix can be welded by placing a layer of thermoplastic film (PA6) with a thickness of 100 μm along with CFRP in prior to curing the CF/Epoxy prepregs. It was reported that a maximum tensile strength of ~34.8 MPa was recorded for a CF/epoxy-PA6AA5754 ultrasonic welded joint [81]. In addition, by performing optical cross-sectional test on the joint, it was observed that area beneath the sonotrode had carbon fibers embedded into AA5754 and in contact with PA6 forming a mechanical interlock [81].

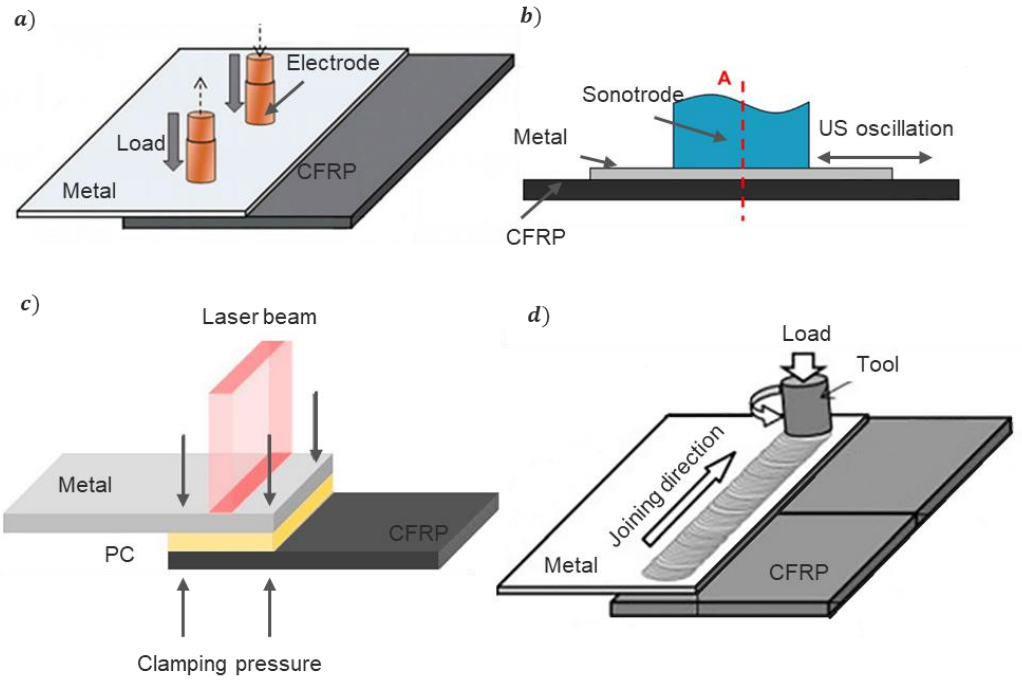

Figure 2-13: Schematic diagram of various welding process for metal-FRP hybrids a) Resistance spot welding; b) Ultrasonic welding; c) Laser Welding and d) Friction stir welding [18].

In laser welding process, the heat from laser is absorbed by the irradiated surface of the metal sheet and then transferred to the contact surface melting the thermoplastic matrix in FRP. Meanwhile, the pressure generated by the expansion of pores in the matrix extrudes and stirs the molten matrix, which closely combines the metal oxide layer with the molten matrix, forming macro- or micro-mechanical locking, chemical molecular bonding and metallurgical bonding at the metal-FRP interface as shown in Figure 2-13c [18]. Laser joining technology has many working strategies depending on the type of matrix system used. For thermoset type matrix it has three different techniques based on the substrate used in between metal and FRP. In the first type, a layer of adhesive is applied to the surface of metal, which is generally known as laser heating-assisted adhesive bonding. In the second type, instead of adhesive layer, a thermoplastic material such as PEEK, PC, PET, etc. or metal film is used between metal and FRP. In the third type, a thermoset prepreg is placed along with the metal that is heated by laser beam and then co-cured [18]. In one of the studies, thermoset based CFRP and aluminum alloy where welded using two different laser techniques [82]. In the first technique, an intermediate layer of thermoplastic was placed between Al alloy and CFRP. Laser was employed as a thermal source heating Al alloy which transferred the heat via conduction phase to melt the thermoplastic layer as shown in Figure 2-13c. In the second technique, a Ni/Al self-reactive coupling layer (SRCL) was utilized as a thermal source to melt PC layers, which also used lower energy and rapid reaction making it ideal fit for joining metal-FRP hybrid components under extreme circumstances, e.g., in space or underwater [82]. However, the formation of excessive bubbles resulting in porosity is of big concern in laser welding that can be avoided by proper control of heat input [83].

High reflectivity of Al alloys makes it difficult for using laser, making Friction stir welding (FSW) more suitable to join aluminum alloys with other materials. Aluminum alloy (AA5052) was welded with FRP (PA6-CFRP) by generating heat through the rotation of the stirring head on the aluminum surface and the frictional heat was transferred from the Al alloy to the CFRP via contact conduction, and a thin molten polymer layer was generated in the welding area as shown in Figure 2-13d [18]. Mechanical interlocking and chemical adhesive are the main bonding mechanisms of FSW formed because of molten layer consolidated under pressure, which resulted in adhesion between metal and polymer. It was reported that shear strength as high as ~43 MPa can be achieved between sandblasted AA2024 and CFRP that are welded via FSW [84].

In summary, the welding processes can be grouped such that resistance spot welding and ultrasonic welding can be classified as spot joining processes, while laser joining, and friction stir welding can be classified as line joining processes. Based on this categorization, spot joining processes are more suitable for complex geometries, while line joining processes are more suitable for flat overlapped structures. In general, it is recommended that welding of metal and FRP are to be used as an auxiliary joining method rather than the primary joining method of load-bearing parts as more research is required [18].

2.4.1.4 Intrinsic Resin Transfer Molding (Intrinsic - RTM)

In intrinsic method, the matrix system itself acts as the adhesive layer joining both FRP and metal. Resin transfer molding (RTM) technique can be used for this intrinsic approach. Intrinsic - RTM is a sub-category of Liquid composite molding (LCM) process where liquid polymer is injected to infiltrate dry fibers. In RTM process, the entire production takes place in a mold so that the finished product achieves A2 surface finish. Firstly, metal parts which are pre-formed to shape of the mold are placed on the lower side of the mold. Dry fibers are cut to the exact shape of the mold and stacked based on the thickness required over the metal. The mold is closed, and a low-viscosity thermoset resin is injected through the injection port into the mold cavity under pressure as shown in Figure 2-14. The resin is injected until the excess resin starts flowing through the vents which are in general placed as close as possible to the structure end so that the entire fibers are impregnated along with removing the trapped air bubbles. The injected resin also helps in bonding the metal part to the FRP structure. After the resin is cured, the mold is opened, and the part is de-molded.

The main advantage of RTM is that it can produce parts close to dimensional tolerance with a volume fraction of about 50%–70%. RTM can manufacture complex-shaped composite parts in a faster cycle with much controlled process parameters. With the help of High-Pressure Resin Transfer Molding (HP-RTM), where pressure as high as 150 bar can be used to produce large structures in short time making it a perfect and suitable process for mass production of large structures [102]. Figure 2-15 shows monolithic CFRP components made for BMW i3 using HP-RTM process [103]. The BMW i3’s body contains CFRP passenger cell (the Life Module, LM) integrated with an aluminum chassis (the Drive Module, DM).

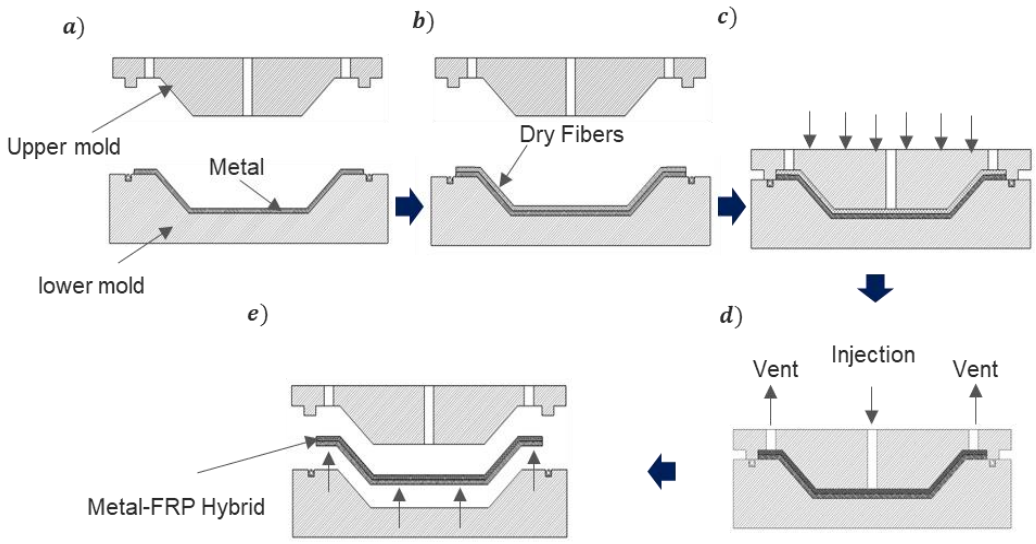

Figure 2-14: Schematic diagram of RTM producing metal-FRP Hybrid a) Placement of metal in the lower mold; b) Dry fiber stacking & placement; c) Mold closure with pressure d) Resin Injection and curing and e) Demolding metal-FRP Hybrid.

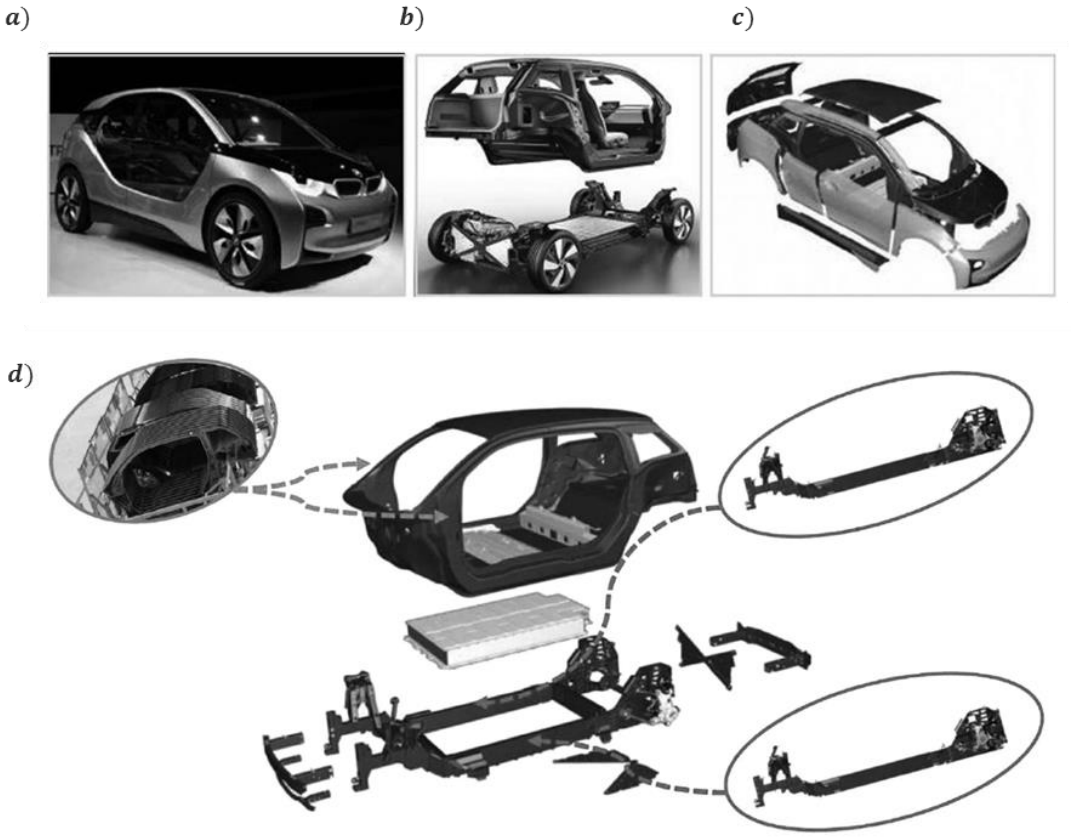

Figure 2-15: a)BMW i3, the first mass manufactured lightweight car with a predominant part of its structure and body manufactured from carbon fiber reinforced composite; b) life capsule and drive module; c) body panels fabricated from hemp-reinforced thermoplastic composites and d) Schematics of BMW i3 structure assembly [103].

Nevertheless, RTM does have few challenges such as race tracking, deformation of fiber structure, macro void formation, resin rich areas, improper impregnation of fibers, etc. Race tracking is one of the biggest concerns as the fibers near the wall or the rib cavities have high permeability that creates an easier path for resin to travel leading to an uneven fluid front path [104]. Resin rich areas are caused because of the ply drop effect which occurs during mold curvature that can be avoided by selecting proper layer thickness of fibers to tool curvature. The main reason for macro void formation is due to race tracking which results in multiple fluid front path trapping air pockets. Due to race tracking, the resin flow from the edge reaches the vents before impregnation of preform resulting in macro void formation. Macro voids can be eliminated by studying the influence of resin viscosity with respect to fiber preform, temperature, injection pressure, gating method, mold geometry. Fiber deformations occur due to injection pressure of resin injection stage. In general, there are four fiber deformation mechanisms: inter-fiber (intra-ply) shear, inter-fiber slip, fiber buckling, and fiber extension [105]. It was reported that a drop of 9% and 22% in stiffness and strength was observed when fibers are misaligned by 5° [106]. In another report a decrease of 4 % in elastic modulus was noted for every 1° of fiber misalignment up to 20° [107].

To extend the application of high fiber volume fraction composites into high-level production runs, the above challenges should be addressed and mapped with the parameter influencing the process. The main stages in RTM process such as mold surface cleaning, applying releasing agent, stacking of fibers and metal, mold filling, resin cure, part demolding should be studied experimentally. In order to counter fiber deviation during injection phase, the fibers are preformed meaning a thermoplastic polymer known as binders are added between each layer and activated via heating and then cooled down resulting in a stronger layup as shown in Figure 2-16. This preform stage is time consuming as it should be accurate so that reproducibility can be achieved. In general, preforms are prepared well in advance using the same mold or using separate equipment. Pre-heating of mold prior to injection can gradually reduce the curing time as the polymers used in RTM are mostly based on exothermic reaction. However, this introduces a new challenge when fast curing polymers are used, as curing is initiated before mold is filled due to reduced gel time caused by temperature. By studying the combination between reduced mold filling times and faster curing resins, cycle time can be optimized. Mathematical models were developed to study polymer flow front during injection process and its influence under temperatures [108]. Level set method was used to predicate the flow of the polymer in fiber using finite element software such as LS-DYNA [109]. The other possibility is to modify RTM process depending on the applications that are discussed further.

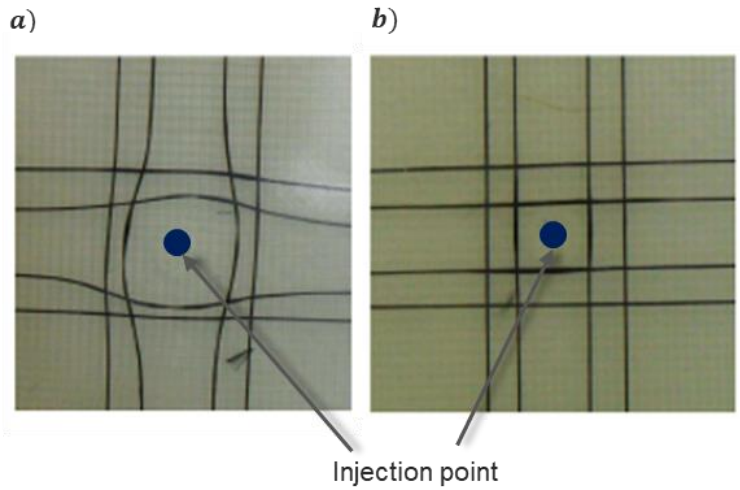

Figure 2-16: Influence of binders on fiber alignment during injection process a) no binder resulting in large deformation of fibers at the injection point and b) with Epikote System 620 binder, no fiber movement [110].

Vacuum Assisted Resin Transfer Molding (VA-RTM)

In the VARTM method, the entire setup is similar to RTM process, but the vents are connected to the vacuum pump which is equipped with a resin trap container as shown in Figure 2-17. The tool is sealed using a sealing material made of polymer at the contour to get vacuum. The purpose of vacuum pump is to drive the resin under atmospheric pressure to aid in impregnate process of reinforcement while evacuating the air bubbles and compacting the fiber preform. Even after the end of injection phase, the vacuum pump is kept running till the curing process is completed. The percentage of porosity formed because of trapped air can be completely eradicated with a well-controlled VA-RTM process. VA-RTM process is commonly used in aerospace, marine, defense industries, etc. [111].

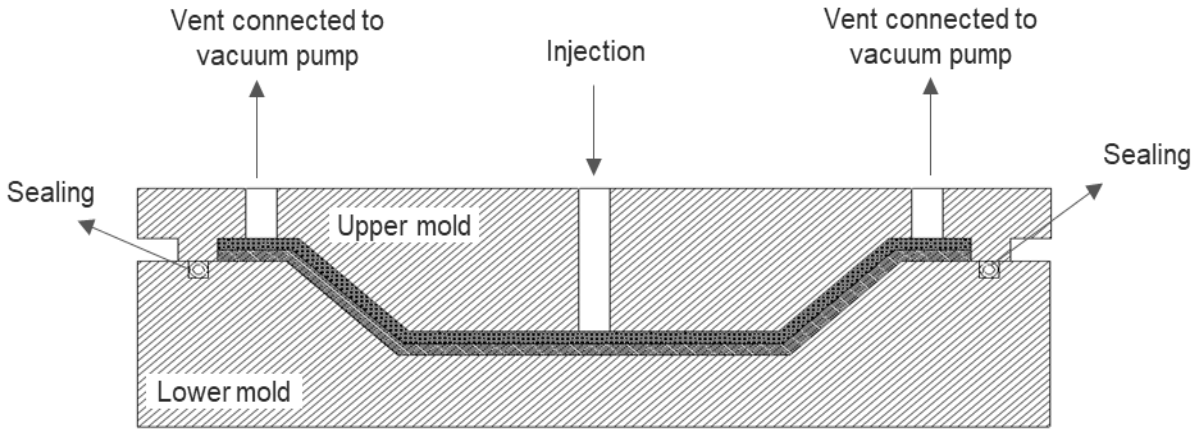

Figure 2-17: Schematic diagram of VARTM producing metal-FRP Hybrid.

Some of the advantages of VARTM are flexibility of mold tooling, low emission of volatile organic compound (VOC) and low porosity. In the alternative version of VARTM, the upper mold is replaced with transparent vacuum bag. Main advantage of using transparent plastic vacuum bag

is to spot visible dry spot occurring during the resin infusion process that can be removed by inserting a vacuum needle at the dry spot and drawing the air out. However, this setup creates additional cost as the vacuum bag setup materials are one-time consumables. Chances of air leakage is high, and this strongly depends on the worker's skill, experience, and the consumables such as sealing tape, vacuum bag, etc. which directly influence the part quality due to dry spots and incomplete resin infusion [112]. A careful and frequent inspection for air leakage is necessary during the entire process, making it a labor-intensive process. The compression pressure on the preform is limited between the environmental pressure and the vacuum that results in lower fiber volume. In order to understand the influence of pressure and other process parameters on mold filling in VARTM, a two-dimensional mathematical model based on dimensionless analysis was introduced [113]. The model divides the resin-saturated porous medium domain into the saturation and flow front regions to make it easy to predicate. It was observed that flow front velocity in the VARTM process decreased significantly as the length of saturated region increased. However, this effect can be overcome by either using fibers with higher permeability or reducing the flow path of the polymer which is discussed below.

Compression Resin Transfer Molding (C-RTM)

The biggest issue with both RTM and VARTM process for a large structure require large fill time which also makes it difficult for the resin flow as resistance increases linearly. C-RTM was introduced to overcome this challenge, where resin travels in thickness direction rather than in length direction as shown in Figure 2-18.

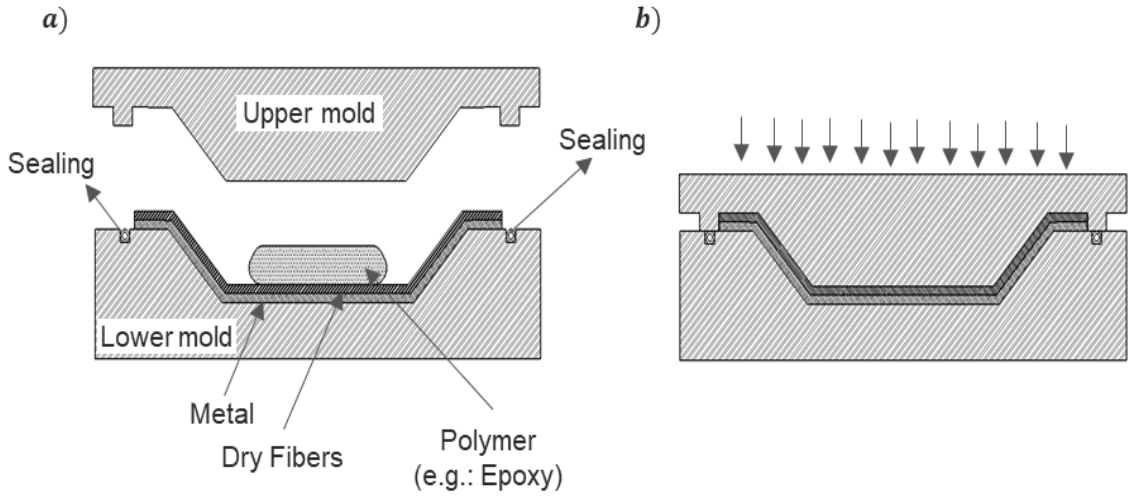

Figure 2-18: Schematic diagram of Compression RTM producing metal-FRP Hybrid a) Placing dry fibers, metal and adding polymer in the mold cavity via external injection system and b) squeezing the polymer into fiber using pressure form mold closing.

In CRTM process, the vertical movement of mold plays a major role as it directly influences resin resistance during preform impregnation and cycle time. The preform impregnation during CRTM process is divided into two subsequent process phases. In the first phase, known as injection phase the mold is moved closer to fiber where the resin is added either by external system or via injection ports of the tool. In the second phase known as compression phase, the tool is closed

to compact the preform to the final part thickness and distribute the resin to fully impregnate the preform. Generally, the gap between tool and the fiber acts as a resin distribution space of low flow resistance for performs with a small geometrical aspect ratio (length/width versus height) of 10–100. This causes a predominant in-plane filling of the injection gap and a subsequent through-thickness preform impregnation [114]. CRTM is well suited for rapid production of high-quality fiber composite parts, where short cycle time and lower pressure are required. However, faster mold filling is typically gained at the expense of complex setup due to use of additional clamp setup. In case of shell structures with a geometrical aspect ratio of 100–1000, it was reported that the gap between fiber and tool mold did not reduce the cycle time but it increased as the time needed for the resin to flow the surface of entire preform was more [115]. It was also reported that there is change in fiber volume contact in thickness direction as top layers have slightly higher resin than bottom layer and higher porosity due to trapped air [115] [116]. To address the above issues, the RTM process was further modified where the race tracking effect was used to reduce the cycle time.

Light Resin Transfer Molding (L-RTM)

In L-RTM process, resin is injected at the corners of the mold. Firstly, the resin runs around the perimeter of the mold as empty channel is provided which has lower permeability in comparison with fibers and then start impregnating the fiber in convergence way towards center where the outlet vent is located which can be connected to vacuum as shown in Figure 2-19. The advantages of L-RTM are high productivity, reduced cycle time, etc.

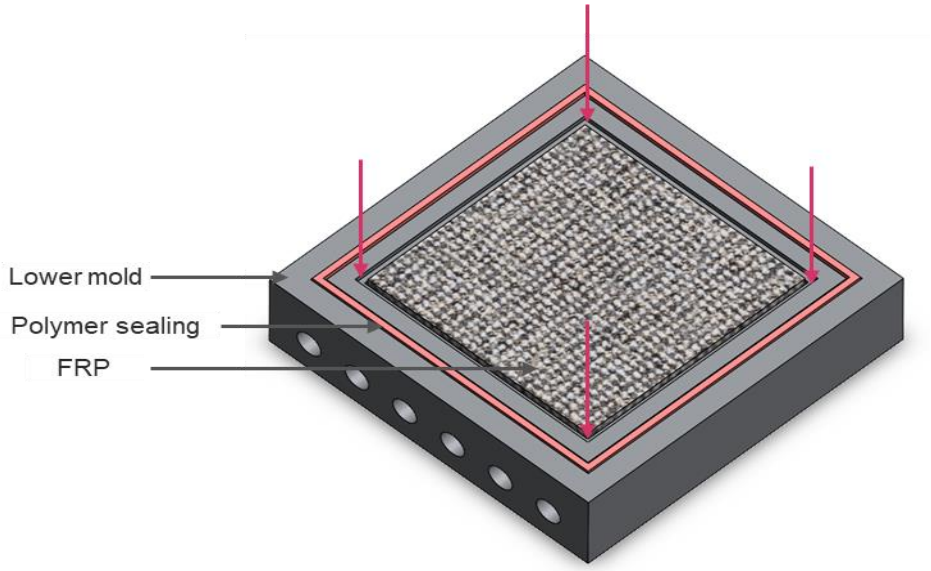

Figure 2-19: Schematic diagram of L-RTM.

In-situ hybridization

A new variant of RTM knows as In-situ hybridization was developed in combination with RTM and deep drawing to produce the metal-FRP hybrid [117]. Figure 2-20 shows the process where metal blanks and fibers are stacked as a semi-finished part initially and then thermoplastic resin is injected that infuses the fibers. Now the forming stage is initiated to obtain the final structure of

the part. The benefit of this process is that resin injection can be utilized at an arbitrary drawing depth to further increase formability. In this process, the control of resin fluidity is difficult which requires further study.

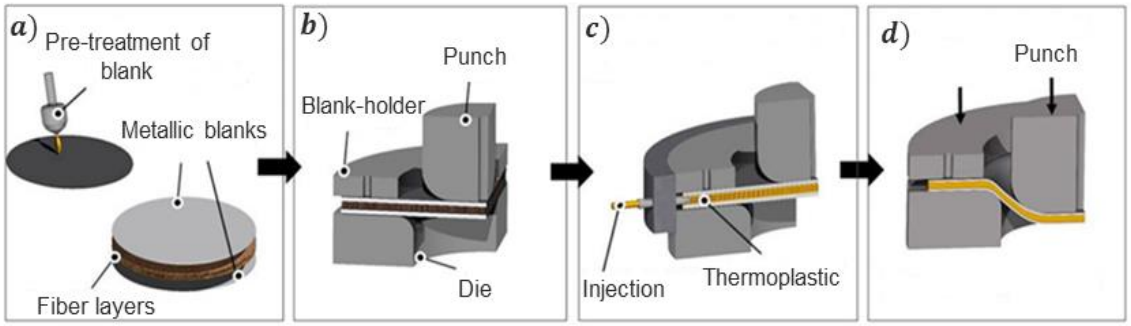

Figure 2-20: Schematic diagram of various steps in In-situ hybridization a) preparation; b) insertion in forming tool; c)T-RTM: injection between sheets and d) curing after forming [18].

It can be concluded that each process has its own advantages and disadvantages for producing metal-FRP Hybrids. The process is selected based on the structure to be produced rather than using the same process for all the structures. For example, to produce a hybrid beam, a simple hand-layup is efficient whereas for producing a bracket a mold is better choice. It also should be noted that all the processes can be combined depending on their feasibility.

2.4.2 Forming Approach

This section focuses on the forming processes such as roll bending, shot peen forming, laser forming, autoclave, compression molding that are reported to be able to produce metal-FRP hybrid structures.

2.4.2.1 Roll Bending

In Roll bending process, first metal and FRP are bonded resulting in hybrid sheets or laminates by hot pressing and then roll bending process is initiated. Figure 2-21 shows the schematic diagram of the process where the top roller moves downwards for predetermined displacement to a desired curvature while the bottom rollers are fixed. The advantages of roll bending process are high efficiency, high flexibility and low cost informing large scale parts with small curvature making it suitable for aviation application. However, in addition to common failure modes, it does have issue of spring-back defects that depends on FRP configuration making it not suitable for complex structures in automotive applications. It was reported that spring back is maximum when the bending direction is along the fiber direction and minimum when its perpendicular based on GLARE laminates [85].

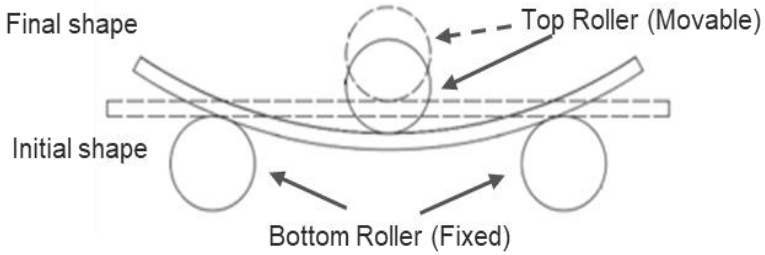

Figure 2-21: Schematic diagram of roll bending [18].

2.4.2.2 Shot Peening Process

The shot peening process follows the same strategy as roll bending where metal and FRP are first bonded and then the shot peening process is initiated which is based on sandblasting technique. Shot peen forming is regarded as a flexible forming technology that is used commonly in aerospace industry to shape large and thin panels, such as wing and fuselage skins [86]. During the shot peening process, plastic deformation of metal sheets is formed due to the kinetic energy released by the stream of small hard shots that are introduced mechanically. This approach also creates compressive stresses in the surface through thickness direction as shown in Figure 2-22a. Generally, to balance the compressive stresses, thin outer layers are stretched along the surface to produce significant bending [87]. With the help of shot-peening process, high productivity and low labor cost can be achieved for metal-FRP hybrids.

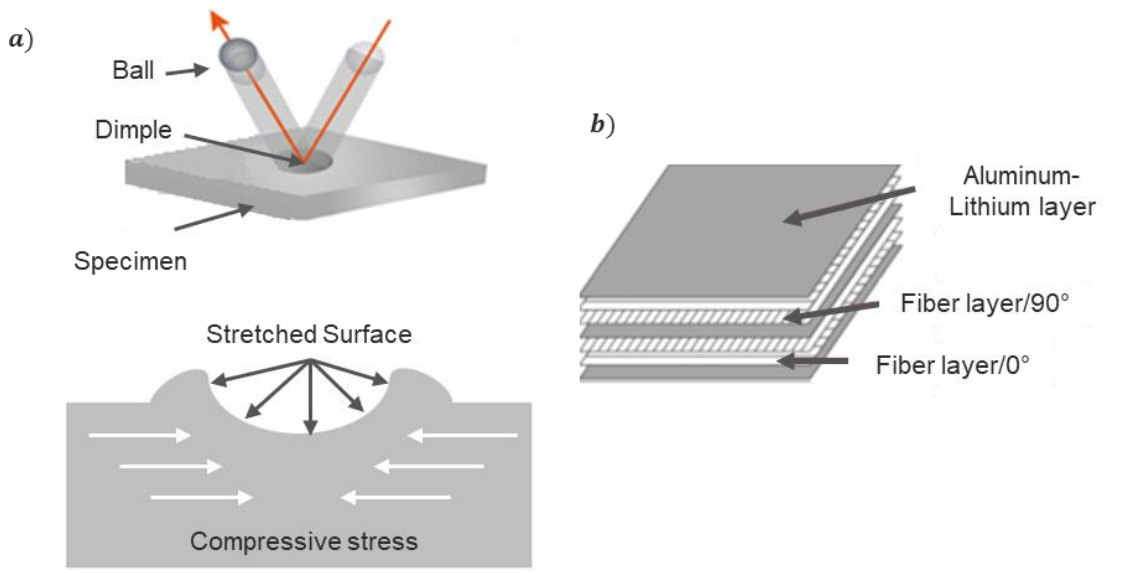

Figure 2-22: a) Schematic diagram of shot peen forming and b) Laminate design of fiber metal laminates based on aluminum-lithium alloys (NFMLs) [87].

NFMLs based on FMLs, and Al-Li were manufactured using shot peening process as shown in Figure 2-22b. Firstly, 0.3 mm layer of aluminum-lithium layers were surface treated using phosphoric acid followed by spraying with J116 structure adhesive. Then three layers of Al-Li sheets were stacked alternatively with glass/epoxy plies between them. The curing process was conducted in an autoclave with optimized temperature and pressure [87]. After the curing process,

the shot peening process was initiated with ceramic balls of diameter 0.212 mm and 0.425 mm; and cast steel balls of diameter 0.584 mm and 1.670 mm. It was reported via microscopic investigation that there are areas where delamination of fiber metal interface, wrappage near edges and cohesive failure of adhesive itself occurred in few cases due to residual stresses [87]. In another report, it was observed that the metal pellets with smaller radii, higher solidity ratio (i.e., the ratio between peened area and overall area of a sample) and lower peening pressure are beneficial to lower the defects in case of GLARE [88]. However, pits and damage are still likely to occur since metal pellets are directly in contact with the outer metal sheets. To address these issues, a tool-free, non-contact process based on laser peen was introduced which provides shockwaves strong enough to bend metal-FRP hybrid sheets through high dynamic loading conditions [89]. The process was validated by forming a GLARE with a reduced curvature radius of 91 mm that exceeds the capability limit of mechanical shot peening process [90].

2.4.2.3 Compression Molding

Compression molding is among the oldest material processing techniques that is also known as matched dye molding. Compression molding is the process by which a charge of fiber reinforced prepreg bulk molding compound (BMC) is molded under heat and high pressure to form complex shaped parts. In general, the BMCs contain chopped fibers with typical fiber length of 6.4 mm to 50.8 mm along with a thermoplastic resin. These loose chips or strands are weighed out to the exact amount required to fill the volume of a given tool. They are heated either in an oven or directly at mold and compressed to a predefined pressure to force the fibers to flow into the mold cavity, filling in every complex feature before cooling. Thermoplastic BMC compression molding requires a degree of mold temperature control not normally required by thermoset compression molding [92].

This process is suitable for a wide range of industrial, commercial, and consumer parts and products ranging from very small to large automobile body panels. Thermoset based sheet molding compounds (SMC) were the first used material in compression molding for ages before thermoplastic found its application. The aerospace industry has been using SMCs for years to fabricate covers and other secondary structures. BMC differs from SMC as the raw material in BMC consists of chopped flakes, chips, or lengths of prepreg fibers rather than a sheet of material made from continuous or discontinuous fibers. Carbon fiber is well suited for the aerospace industry due to its high strength and stiffness. Carbon fiber thermoset BMCs are currently being used on aircraft structures, for example, a V-22 Osprey access door was produced by compression molding. In general, thermoplastic BMCs are being recognized as a replacement to thermoset SMCs/BMCs when increased durability, inherently low flame-smoke-toxicity (FST), and faster part production times are desired. In a study, a glass mat reinforced thermoplastic (GMT) hybrid beam was manufactured via compression molding as shown in the Figure 2-23. It was reported that there was a significant increase in strength, stiffness, and energy absorption between a GMT beam in comparison with metal-GMT Hybrid beam which is integrated with metal belts [93]. Due to addition of two metal belts, the hybrid variant had 52 % more mass than the GMT. But at the same time, the energy absorption and mass-specific energy absorption increased by 1105 % and 693 % respectively [93].

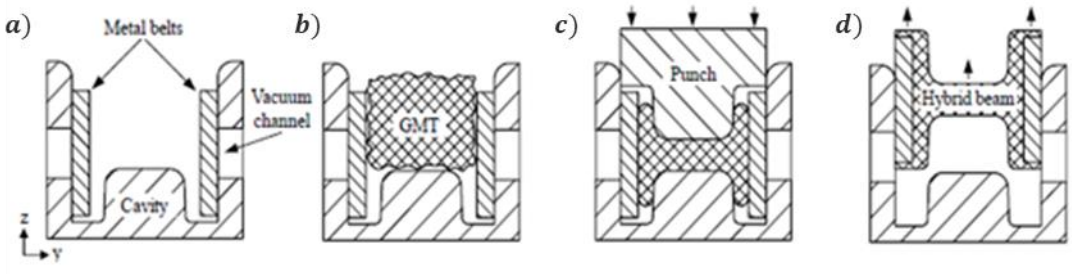

Figure 2-23: Schematic diagram of compression molding forming metal-FRP Hybrid Beam a) Insert placement; b) GMT insertion c)compression molding and d) Hybrid beam eject [93].

However, the biggest drawback is that the thermoplastic BMCs require higher temperatures to process in comparison with thermosets. In addition, they also require a controlled cool down process to manage the crystallinity of the polymers. Nevertheless, there are few variants in compression molding to accommodate different materials such as cold forming and sintering for thermoplastic but there may be necessity of postprocess such as additional pressurization, annealing, and/or machining to finalize the shape and properties. Items for the electrical industry are often made by these methods. In case of polycarbonate or ABS, cold forming compacts them by a factor of 3-6 a granular charge at 21-35 MPa without prior heating [94]. Phenolic thermosetting material can also be cold molded and then cured in an oven. The other drawback in compression molding is when the structures are too long, it results in longer flow path for materials where some portion of cavity maybe not be filled properly and chemical decompositions along its flow path [95]. Nevertheless, this issue can be addressed by using analytical mathematical models to predict the mold filling process prior to production. It should be noted that the material mold should capture the flow as viscous fluid described in one, two, and in three dimensions even though the thickness is smaller when compared with structure length [95].

2.4.2.4 Hand Layup Technique

In hand layup technique, both FRP prepregs or dry fiber can be used. In case of dry fibers, the fibers are laid manually onto a pre-formed metal part which is already pre-treated based on requirements. Now, polymers such as epoxy or polyurethan are poured on to the dry fiber and pressed using roller with balanced pressure so that there won't be a significant change in dry fiber thickness. The rolling stage can be performed for each layer of dry fiber or all together depending on the number of layers. As the number of layers increases, it is recommended to apply polymer for each layer separately for a better bonding of layers. Now the entire setup can be cured at atmospheric condition, or it can be placed in oven so that the curing can be accelerated as shown in Figure 2-24. The process can also be combined with vacuum setup to extract the air. Pressure plays a major role in ensuring a tight bonding between FRP and metal during curing. In comparison, metal structure serves as the tool in the curing process of metal-FRP hybrid component. FRP layers can be adhered to arbitrary locations of the metal part, and the number of prepreg layers can be varied freely [18].

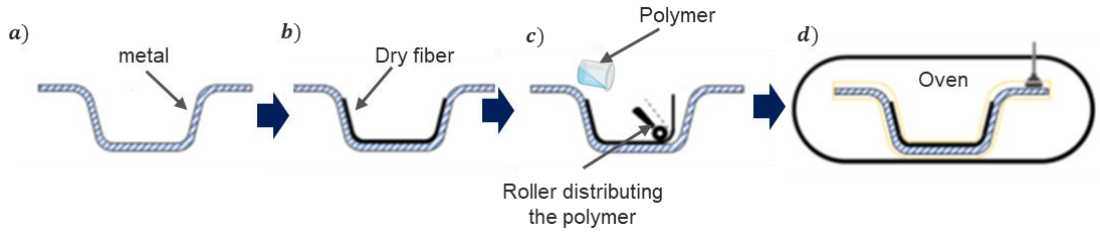

Figure 2-24: Schematic diagram of hand lay-up technique of forming prepreg to metal parts followed by co-curing; a) surface treatment; b) hand layup process of dry fibers; c) disturbing polymer using roller across its length and d) heating and curing.

Hand layup techniques are common in concrete Beam manufacturing industry where FRP are bonded with steel rails [96]. In a study, a total of six rectangular beams were tested to find the effectiveness of GFRP in beams with a dimension of 200 mm x 250 mm x 2000 mm. The load capacity of the beam increased to 120 % that is from 37 kN to 78 kN when using GRFR [96]. However, as the lay-up processes are mostly carried out manually at present, this forming process is labor-intensive and needs a long cycle time.

2.4.2.5 Vacuum Bagging

Vacuum bagging process uses a flexible transparent film that acts as a vacuum bag to enclose and compact metal-FRP (prepreg) using atmospheric pressure as shown in Figure 2-25. The entire setup is connected to a vacuum pump to extract the air inside the vacuum bag and then compresses the part under atmospheric pressure. There are various materials used between FRP and vacuum bag as listed in Table 14. The parts fabricated with this process yield better mechanical properties than a hand layup process even though the materials used are cheap. Since the applied pressure is evenly distributed over the entire surface regardless of the quantity, vacuum bagging can produce thinner laminate parts with lesser voids [97]. The excess resin is either observed by the bleeder or extracted via vacuum pump as they are equipped with resin trap pot which collects the excess resin resulting a better fiber volume fraction. The vacuum bag technique was used to fabricate yacht's primary structures such as decks, hulls, superstructures, bulkheads, and secondary structures such as partition panels and interior joint work [97]. In general, there are two types of vacuum bagging processes namely single vacuum bagging (SVB) that discussed above and double vacuum bagging (DVB). DVB uses a double vacuum bag setup to efficiently evacuate volatiles produced during curing process. The entire setup of DVB is similar to SVB but it uses an additional outer vacuum bag over the assembly with a perforated steel tool in between the two bags as shown Figure 2-26 [98]. The perforated steel functionality is to prevent the collapse of outer bag into the inner bag during the vacuum stage. A full and partial vacuum is pulled on the outer and inner bags, respectively, resulting in a pressure differential creating "ballooning effect" that aids the evacuation of entrapped air and volatiles. The outer bag is purged to atmospheric pressure and the inner bag is vacuumed to maximum for consolidating during the final curing stage. It was reported that the escape of volatiles and entrapped air was more efficient in the DVB technique than in the SVB technique [97]. In another report with carbon prepreg with a fiber content of 58%, DVB laminates and SVB laminates had surface porosity of 0.04 % and of 0.1 %, respectively [98].

Table 14: Function of Vacuum Bagging Components [99].

Component	Function
Release Agent	Permits the release of the cured prepreg from the tool.
Peel Ply	A porous material that allows the passage of excess resin to flow through it during curing. It aids the removal of the bagging system from the parts after curing. An example of this material is a perforated Teflon sheet.
Release Film (separator)	A lightly porous material that permits the flow of air and volatiles only onto the breather; however, it restricts the further flow of resin.
Bleeder Fabric	Typically, a fiberglass mat that absorbs excess resin as it flows out during the molding process
Breather Fabric	A highly porous material that allows the removal of air and volatiles from the composite assembly. Examples of breather materials are fiber glass, polyester felt, and cotton.
Vacuum Bag /Sealant Tape	A sticky polymeric tape placed around the entire assembly to provide an airtight seal vacuum bag.

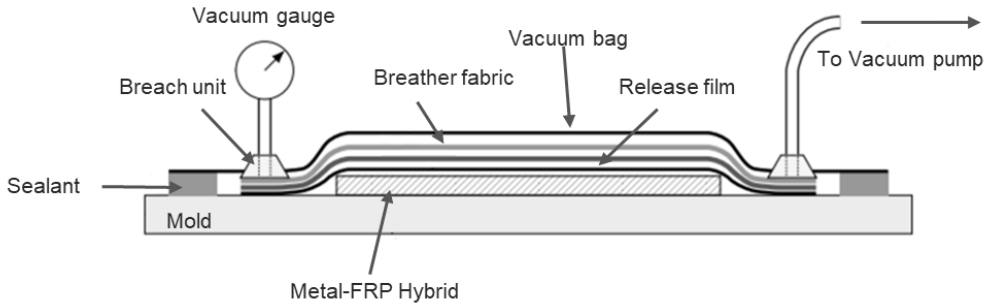

Figure 2-25: Schematic diagram of Vacuum bagging setup [97].

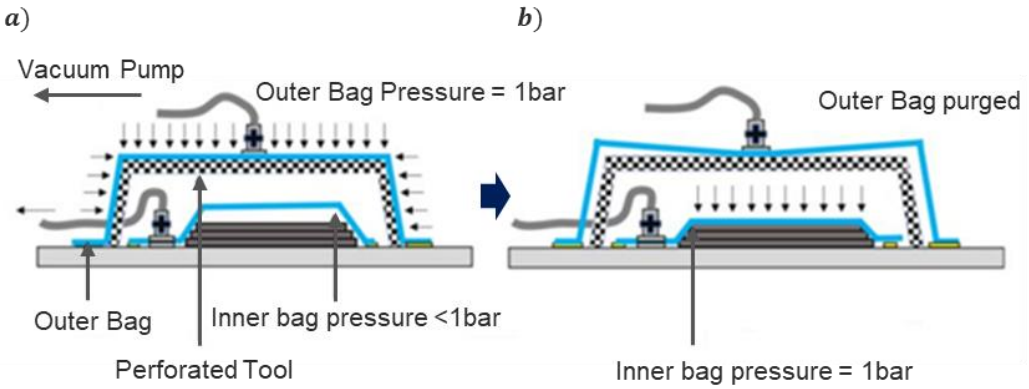

Figure 2-26: Schematics of a flexible double-vacuum-bagging setup with a perforated tool during (a) degassing phase and (b) compaction phase [98].

However, one of the disadvantages of vacuum bagging process is its labor intense for processing bigger and complex structures as the process needs to be completed once started without any breaks in between. Another major disadvantage is failure to calculate the fiber volume fraction when over-bleeding is used.

2.4.2.6 Autoclave

Autoclave is similar to vacuum bagging process which is an open molding process where it has a mold on the lower side and vacuum bagging on the top side of the structure. This process involves stacking of FRP-prepregs in a mold which is already coated with a release agent to avoid polymer sticking to it. The mold along with the stacked FRP is placed in a vacuum bag. The application of vacuum is to serve in assisting the ply consolidation and continuous removing of volatiles that may form during the molding operation to reduce the incidence of porosity. Special breathers are used as a layer between vacuum bag and FRP-prepreg for better surface quality. Now, the whole assembly is moved to the autoclave machine, where both heat and pressure are applied for curing of the FRP-prepreg as shown in Figure 2-27. Autoclave enables excellent control of pressure and temperature with appropriate ramps and dwells using a control unit. Once the curing is achieved the structure is removed from the mold. In case of manufacturing metal-FRP hybrids, the metal part can replace the lower mold or stacked on top of the lower mold followed by FRP [32].

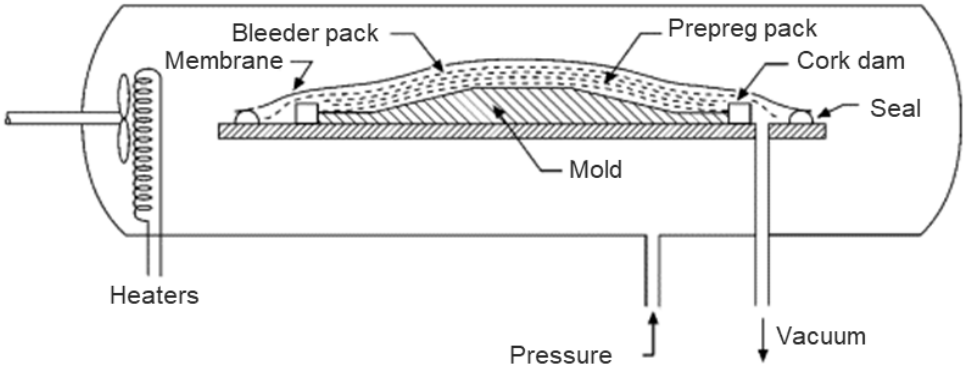

Figure 2-27: Schematic diagram of Autoclave setup [100].

In the autoclave process, both thermoset and thermoplastic polymers can be used as the process supports high fiber volume fraction. The fiber content in autoclave process typical ranges in 60-70% with high degree of dimension control [101]. Autoclave process also supports use of insert along with the FRP as the interfacial bond between metal and FRP are well suitable for load bearing [100]. The void formation is minimum or can be completely avoided in autoclave process via vacuum bagging mechanism so that the bubble effect between metal and FRP can be avoided making their interface better. This process has been widely used to manufacture numerous engineering parts mainly by aerospace, marine and military industries. Despite all the benefits, the autoclave process does come with few challenges such as low production rate, involvement of skilled labor, expensive technique because of autoclave machine, etc. As an alternative to autoclave, many out of autoclave processes were introduced.

2.5 Sealing Techniques

Sealing plays a very important role in process control of VA-RTM process. Typically, the contours of the mold used are sealed during the injection process until the resin has reached a certain degree of curing. The sealing of the mold influences the part quality as they are used to prevent leakage as the matrix system has relatively low viscosity and is injected with high pressure [32]. The sealings also help in evacuating the mold in a controlled environment. Many techniques were suggested and used for RTM process in sealing the molds. Initially, in a mold a pinch zone and resin overspill zone are provided to control the resin flow and prevent it from contaminating the working area. The pinch zones are designed in such a way that fiber volume percentage are high in pinch zone so that it prevents the resin to flow further but it's not always successful resulting in additional resin overspill zone and the process can't be equipped with vacuum technique [32]. Alternative to pinch zone, use of metal inserts at the mold contour was suggested but it fails to obtain vacuum and reduce pressure drop.

To overcome the above challenges, polymer sealing was introduced, which has variable hardness that can be used based on the process and requirement. In some cases when the injection pressure is more than 100 bars, the polymer sealing contains more than one component, such as an O-ring and a backup ring, or possibly an O-ring and two backup rings. Sealings that are used internally on a sliding or moving assembly are called Packings and classified as dynamic sealings. The dynamic conditions can be reciprocating, rotary, oscillating, at many places. When they are used on non-moving fittings and bosses are classified as gaskets. The most widely used polymer sealing type is O-ring that has a round-cross section which is economical to produce and provides a bi-directional sealing that is easy to install as shown in Figure 2-28a. Round cross section of O-ring makes it possible to apply in dynamic conditions as it provides a point load with a minimal surface contact area. However, it tends to roll or spiral in long stroke reciprocating applications making it a drawback for fatigue process.

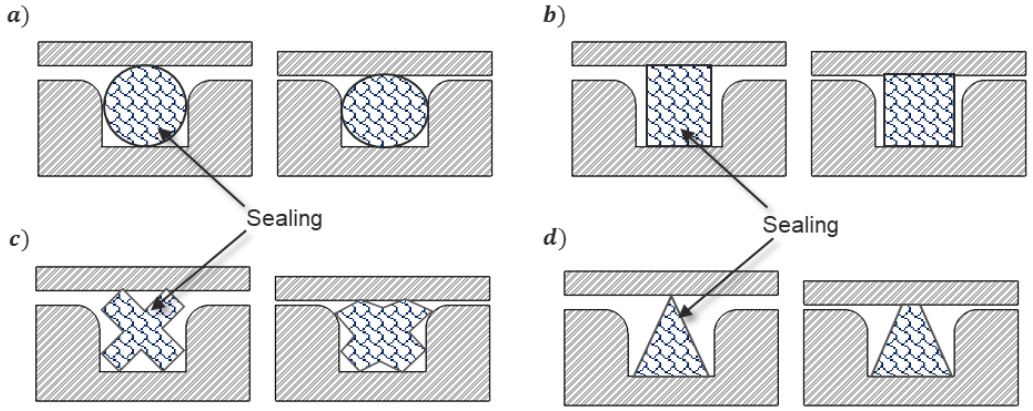

Figure 2-28: Cross profile of typical seals in Injection Molds a) O -ring; b) Square-ring; c) X-Ring and d) Delta-ring.

A square ring as shown in Figure 2-28b can be used in reciprocating applications but not for dynamic conditions as they tend to tear under dynamic conditions. Figure 2-28c shows a square ring which is also called as quad ring that is perfectly suitable for both static and dynamic conditions. They are generally used in rotary motion applications. Delta ring, also known as V-

ring, which is used in high pressure applications. All these four types are also available in hollow profiles and are used based on their applications. There are many other cross sections of sealings as shown in Figure 2-29. Generally, these sealing profiles are found in hydraulic applications where the pressure is as high as 350 bars that fits the H-RTM application where similar pressures are used but the compatibility should be checked. In these sealings, lips refer to the initial contact area to the mold [142]. Sealings are mostly made from polyurethane or silicon and are classified based on their hardness values which is equivalent to compression ratio.

Figure 2-29: Cross-sectional profiles of few seals a) U-ring; b) Double lip wiper; c) Single lip wiper; d) Asymmetric rod seal – positive squeeze and e) Double acting piston seal with integral bearing and f) Vee pack [142].

Figure 2-30 shows a typical silicone-based polymer used as a sealing material for intrinsic manufacturing of metal-CFRP hybrid omega profiles by VARTM process [143]. These seals undergo tremendous mechanical wear due to high clamping forces and thermal wear due to mold temperature and matrix reaction. This results in replacing of sealing after certain production cycles depending on the material of sealings that cause unproductive downtime of mold.

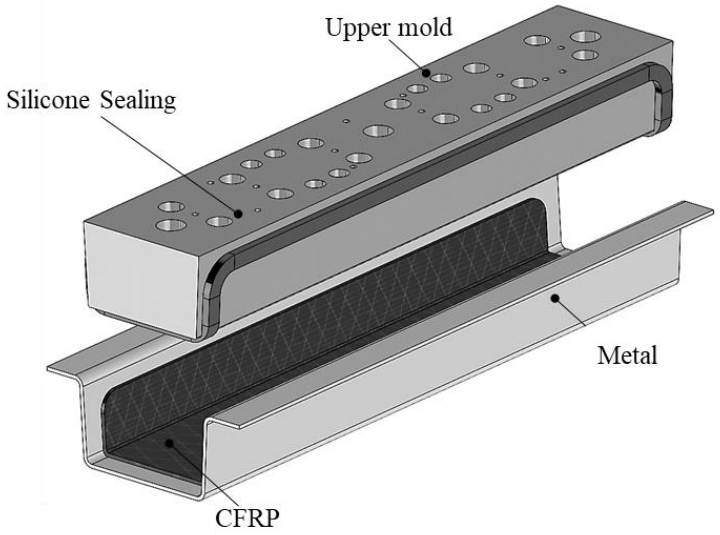

Figure 2-30: Tool with silicon sealing technique for intrinsic VARTM processes [143].

2.6 Maintenance of Molds

Mold maintenance is another important factor that affects the part quality and production cycle. Molds in RTM process are bound to get contaminated that should be removed before next production as it affects the part quality and has the potential to damage the mold itself. One of the biggest advantages of RTM process is to ensure A2 surface of the produced component, which can be unfulfilled if the surface of mold is contaminated. Mostly the mold is cleaned manually or in a semi-automated process. Table 15 shows most widely used cleaning process for molds.

Table 15: Advantages and disadvantage of various cleaning process for mold.

Method	Advantages	Disadvantages
Blasting process (dry ice)	▪ Simple system technology ▪ Short cleaning times without disassembly ▪ Low abrasive and corrosive substrate influence	▪ Dry ice has a limited shelf life ▪ High operating costs ▪ Extraction technology required ▪ Noise intensive ▪ Manual cleaning ▪ Ventilation required
Laser beams	▪ Thorough cleaning ▪ Fast process	▪ High investment costs ▪ High security regulations ▪ Removal of the tool ▪ Removal of only thin (<100 µm) homogeneous impurities ▪ Complex handling
Chemical cleaning	▪ Reliable plant technology ▪ Removal of heavy contaminants ▪ High throughput	▪ Removal of the tool ▪ Damage to the tool possible ▪ Polluting ▪ High operating costs ▪ Time consuming
Ultrasonic	▪ No damage to the surface as it is contact-free ▪ Short cleaning times ▪ Suitable for complex geometries ▪ Fully automated cleaning ▪ Environmentally friendly with reduced use of solvents or with bio-cleaners ▪ Low operating costs	▪ Shape expansion ▪ Drying necessary ▪ High investment costs
Thermal cleaning	▪ Removal of unmixed impurities ▪ No drying	▪ Shape expansion ▪ High energy requirements ▪ Structural influence ▪ Post processing required ▪ High investment costs due to cleaning the exhaust gases

Most widely used cleaning process is ultrasonic because of its efficiency and suitability for complex geometries that is discussed further. In Ultrasonic cleaning process, contaminated mold is immersed into solution bath that uses high-frequency vibrations to generate imploding air bubbles. On contact with the mold surface, these air bubbles tend to explode removing the contamination on the mold. The concept behind this working method is cavitation where bubbles are formed, expand and collapse by releasing energy. These phenomena are achieved by connecting Ultrasonic transducers to the bath system. There can be multiple transducers in one ultrasonic cleaning unit depending on the size of the bath and necessity. Once the mold is cleaned, they are characterized to check the surface quality of the mold. Most widely used testing technique is surface roughness values R_a and R_z. R_a is the arithmetic average of the absolute values of the profile heights over the evaluation length and R_Z is the average value of the absolute values of the heights of five highest-profile peaks and the depths of five deepest profiles within the evaluation length as shown in Figure 2-31. However, it can be argued that even if surface has a different profile, R_a and R_z value can be same because of its measuring method. Another measuring technique is the gloss meter testing method. Here a light is bounced on the surface at fixed intensity and angle and the amount of reflected light is measured. The measuring unit in this method is gloss unit (GU) rated up to 100. They are classified into three types namely high gloss (> 70 GU), medium gloss (10-70 GU) and low gloss (< 10 GU). However, this technique is not recommended for highly reflective surfaces as the GU value must be scaled to 2000 GU rather than 100 GU making it difficult to attain better accuracy. Then GU values can be related to surface quality via ISO grade numbers such as ASTM C346, ASTM D523 etc.

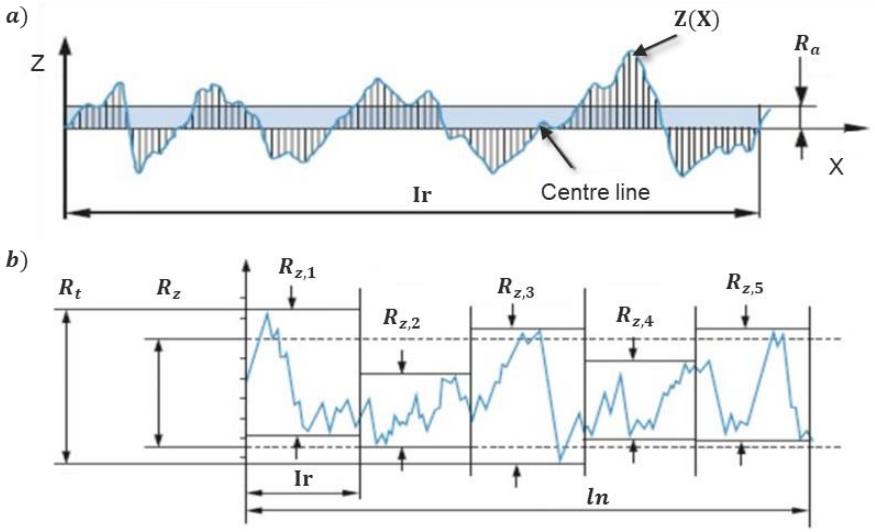

Figure 2-31: Surface roughness measurement showing the profile of a surface tested a) R_a and b) R_z.

Ultrasonic process has many stages that are labor intense such as transporting the dye to the cleaning station, removing all electrical connections and corrosive parts, drying the dye, reinstalling the electrical and corrosive parts in the dye, and then transporting the dye to the press to resume production. In the current study, this challenge is addressed by optimizing ultrasonic cleaning further with a potential for automotive process setup.

3 Experimental setup

Mechanical testing is an important stage to study the material or structure behavior under different conditions. In the current study, three different mechanical characterizing were used to study hybrid structure behavior and determine their respective values. Interlaminar Shear Strength (ILSS) tests were used to determine the shear stresses in hybrid structures as it determines the load transfer conditions. In addition, Torsion and Crushing tests were performed to determine the stiffness and energy absorption of the hybrid structures produced. Both torsion and crushing tests are selected based on the demonstrator that is explained in chapter 5.

3.1 Interlaminar Shear Strength (ILSS)

One of the major failure modes in FRP is delaminating which occurs due to the presence of inter-laminar shear stresses that are unique in composite structure. This delamination results in a reduced strength of the entire structural component. ILSS are classified as out of plane stresses that vary between each layer as fiber orientations is one of the influence factors.

Classical Laminate Theory (CLT) is a commonly used theoretical approach to predict the stress-strain in FRP structures that can also be used to study ILSS with an appropriate method. An appropriate evaluation of ILSS leads to an accurate prediction of failure mechanism in the FRP structure. Short Beam shear test (SBS) is used to determine ILSS of FRP components. SBS can be performed based on the different ASTM standards such as D2344, EN 2563 or EN ISO 14130. Table 16 and Figure 3-1 shows specimen dimensions and the test step of ILSS, respectively, based on ASTM ISO 14130. The radius of the loading member r_1 should be 5 mm ± 0.2 mm and that of the supports r_2 should be 2 mm ± 0.2 mm. The loading member applies the load mid-way between the supports. The span (distance between the supports) are adjustable. It should be noted that this particular test is for FRP laminates but in the present study they are used for testing the metal-FRP hybrids.

Table 16: Specimen dimension relation.

Thickness, h / mm	Overall length, l / mm	Width, b / mm
2± 0.2	20 ±1	10±0.2

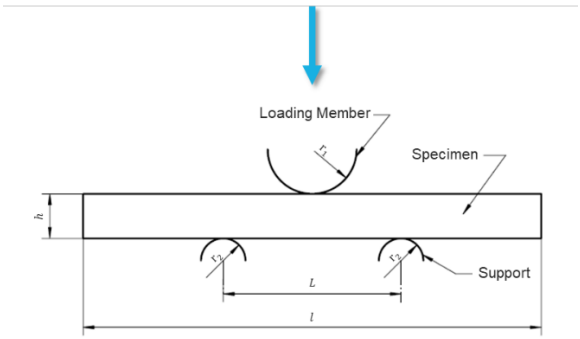

Figure 3-1: Loading configuration for ILSS for FRP.

3.2 Static Crushing Test

Static crushing test is based on compression mode of force application where the energy absorption capacity of the structure or material is studied. Energy-absorbing components are commonly used in engineering structures such as in the front anti-collision devices of a bridge, in high-speed rail, aircraft bottom landing devices, or buffer structures under cabin floors, crash management of automotive, etc. [47]. Generally, the static crushing test can be performed using Universal testing machine where the force vs displacement is recorded for a fixed compression length of the sample as shown in Figure 3-2.

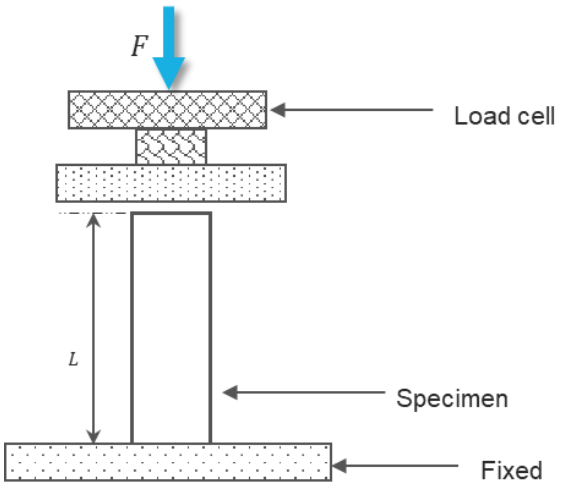

Figure 3-2: Typical loading configuration for crushing test.

The data from Force vs displacement is used to calculate the energy absorption indicators such as total energy absorption (EA), Mean crushing force (P_{mean}), Specific energy absorption (SEA) and crushing force efficiency (CFE) [47].

EA is the total energy absorbed during the crushing test that is used to determine the energy-absorption capacity using Equation 1

$$EA = \int_0^d F(x)\, dx \qquad \textbf{Equation 1}$$

Where d is the total displacement during the crushing test and F(x) is the instantaneous crushing force at the crushing displacement 'x'. P_{mean} is the mean value of the load in the stable crushing stage and can be calculated using Equation 2

$$P_{mean} = \frac{EA}{d} \qquad \textbf{Equation 2}$$

SEA is the energy absorbed per unit mass that represent the energy-absorption efficiency and can be calculated using Equation 3

$$SEA = \frac{EA}{\mu d} = \frac{P_{mean}}{\mu} \qquad \textbf{Equation 3}$$

Where μ is the mass per unit length of the specimen. CFE is the ratio of P_{mean} to Peak crushing force (PCF) that represent the consistency of load during crushing that can be calculated using Equation 4

$$CFE = \frac{P_{mean}}{PCF} \times 100\% \qquad \textbf{Equation 4}$$

3.3 Torsion Test

In Torsion testing, the structure is deformed under stress via angular displacement. Torsion testing can be split into two categories based on testing requirements. It can be used to test raw materials like metal wires or plastic tubing or finished structures such as screws, pharmaceutical bottles, and sheathed cables, etc. The most measured mechanical properties by torsion testing are modulus of elasticity in shear, yield shear strength, ultimate shear strength, modulus of rupture in shear, stiffness, and ductility [137].

The best example for the necessity of torsion test in an automotive is the drive shaft that experiences a complex combined loading when in use, with torsion being the main component. The other forces observed in drive shaft are compression and tension. In a typical torsion test, torque with respect to degree of rotation is recorded and the test setup is shown in Figure 3-3. The most widely used geometry for torsion tests are cylindrical shapes that are clamped on both ends with special fixtures. When the clamps are not perfect, there is a possibility of sample slipping during testing phase that affects the results. One of the ends is fixed while the other end is rotated with a fixed angle with respect to time using hydraulics. In the Figure 3-3, side 'A' is fixed while side 'B' is rotated and the torque is recorded using the load cell. There are various analytical methods to determine the torsional torques of a structure. The simplest analytical method involves two parameters to calculate the torsion as shown in Equation 5, where 'r' is distance at which force 'F' is acting. In the current study both static and fatigue-based torsion tests were performed for the metal-FRP hybrid shafts.

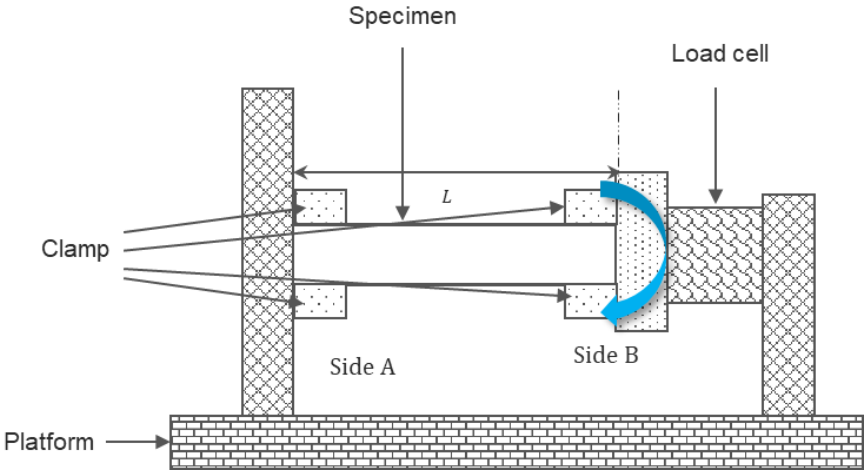

Figure 3-3: Typical Loading configuration for Torsion test.

$$\tau = r \times F \qquad \textbf{Equation 5}$$

4 Concept Development Approach

In current study, two different techniques that are Self-sealing and In-Mold cleaning were proposed for RTM process that has potential for automation. These techniques are also suitable for injection molding processes.

4.1 Self-Sealing Process

In traditional RTM process, a polymer sealing is used at the contour of the molds to prevent matrix leakage. Generally, matrix systems used in RTM process are highly reactive, making the polymer sealing undergo chemical stresses in addition to thermal stresses due to production temperatures and mechanical stresses occurred due to mold closure force. These stresses tremendously reduce the sealing functionality over time making it mandatory to replace after certain cycles with an increasing production cycle time and material wastage. As a potential replacement for traditional polymer sealing, a technique based on accelerated curing of matrix along with reduced cross-section of mold and possibly with catalysts that provide increased flow resistance resulting in a Self-sealing mechanism is suggested. As a result, the matrix cures close to contour and therefore seals the cavity. Due to this Self-sealing effect, there is no need for further sealing materials. In the case of vacuum assist, the conventional polymer sealing can be placed in areas with lower thermal and mechanical stress. The downtime for replacing the sealing material is thus eliminated. Figure 4-1 shows the block diagram of Self-sealing's working principle for an intrinsic manufacturing technique in place of traditional polymer sealing (zone 2 and 3). This concept is universally applicable to processes involving matrix injection with low viscosity (10-500 mPas).

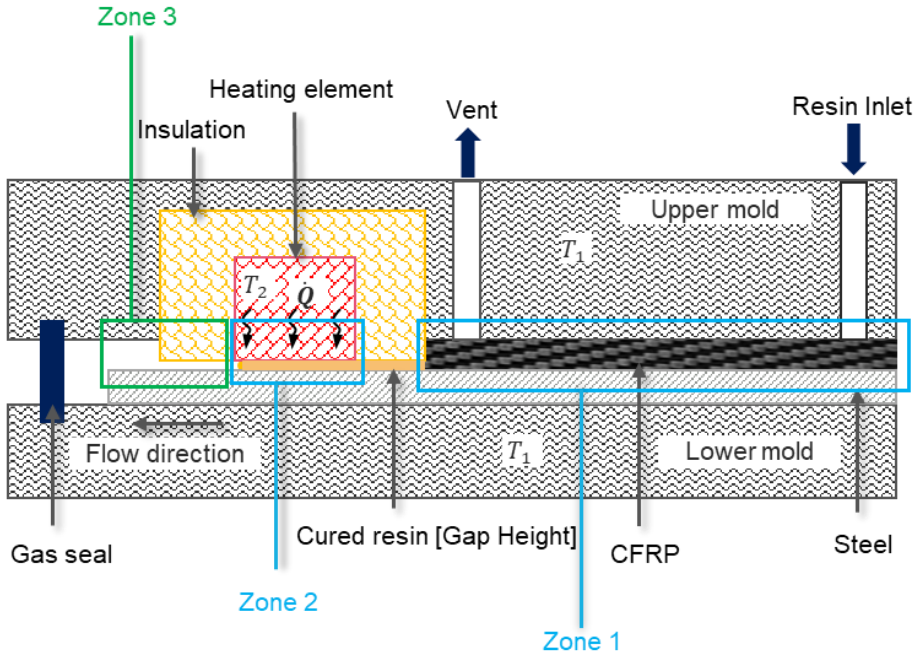

Figure 4-1: Block diagram showing the cross-section setup of self-sealing process in a VA-RTM Mold.

To validate the sealing concept a mold was designed based on thermal and theoretical calculations. The mold was divided into 2 zones based on temperature requirement. Zone 1

provides the temperature (T_1) required for manufacturing the sample and zone 2 provides high temperature (T_2) for sealing at contour replacing the traditional sealing material in VA-LRTM method. To prevent the flow of heat from Self-sealing (zone1) to the production area (zone 2), a special insulation material was installed between them. The Self-sealing area consists of a rigid heating element and thermal insulation, where the functionality of heating element is to deliver a significantly higher temperature at contour than the rest of the mold and the insulation prevents the main mold from heating up excessively.

DMADV technique based on Lean six sigma method was used to track the objective and fulfill the functionality of the self-sealing process. DMADV is a five-stage process that has Define, Measure, Analyze, Design, and Verify stage. DMADV is a commonly used technique in manufacturing industries for designing a new process/product or to redesign an existing product/process. In the below, DMADV techniques stages are listed in corresponding with self-sealing process.

In the Define stage, the project objective should be clearly listed so that the project sticks to its original objective without any deviation. The objective of the self-sealing process is drafted and listed below:

1. Sealing the contour of the mold with the proposed concept.
2. Design and production of Mold that works based on Self-sealing process, traditional sealing process and compatible with the In-mold cleaning process.
3. Process study with respect to mold and demonstrator geometry.
4. Validating the influence of Self-sealing process with respect to traditional sealing process.

The Measure stage deals with developing a Critical To Quality (CTQ) to address the above-mentioned requirements. CTQs are mainly used to identify the needs of the process and translate it into a measurable method. CTQs are developed for each milestone separately to track progress in a transparent way and address the issues separately. The CTQs for the self-sealing are listed below with respect to the milestones mentioned in Define stage.

1. The resin flow distance in zone 2 and zone 3 (Figure 4-1) will be used to measure the functionality of the Self-sealing process. Here the criteria will be lesser the better meaning the smallest distance of resin flow in zone 2 and zone 3 is desirable for the process with respect to T_2 Temperature and Gap Height (H_1). The thickness of insulation material (t_{in}) should also be kept to a minimum.
2. The mold design concentrates on reducing the number of components that are exchanged for different processes, which will be the measuring quantity.
3. Process study was evaluated based on mechanical properties. Here the Criteria is defined as higher the better, meaning better mechanical properties are preferred.
4. The Self-sealing process was also evaluated based on mechanical properties of the sample produced and compared with sample produced using conventional sealing. Here the criteria were set to equal to or greater i.e., the mechanical properties of the sample produced using Self-sealing should be greater or equal to in comparison with the sample produced using conventional sealing process.

In the Analysis phase, the best possible solutions are identified to fulfill the objective of the project with respect to CTQs. Self-sealing analyses are listed below with respect to the Define and Measure stages.

1. Two different configurations are designed for validating the sealing concept that is discussed further in Chapter 5
2. Two different possible designs for mold are suggested based on requirements that is further discussed in Chapter 5
3. Process study is classified into two categories namely parameter study and interface study between metal and FRP. The samples produced were tested experimentally and the best possible parameter and interface is determined.
4. ILSS test were selected to evaluate and compare self-sealing process with conventional process.

Design is the fourth stage in DMADV technique where the best possible solution from Analysis is converted into prototype. Chapter 5 and Chapter 6 cover the Design stage in detail for the self-sealing process.

In Verify stage, the prototype produced in the Design stage is validated for its functionality by testing. This is done to make sure that the drafted solution in Analysis stage meets the milestone of the project based on CTQs. In some cases, DMADV is repeated or if any possibility for improvement is spotted then DMAIC process is used, which will be discussed further. Verify stage for the Self-sealing process is addressed in Chapter 6 in detail.

4.2 In-Mold Cleaning Process

Ultrasonic is the most widely used process for cleaning molds that are used in injection manufacturing process. In a typical ultrasonic process, the entire mold is demolded from the press and prepared for the cleaning stage. Preparation involves removing all electrical and corrosive components as the ultrasonic process involves using of solution that are acid in nature. The mold is then moved to cleaning station and immersed in tank that are filled with cleaning solution and are equipped with piezoelectric device. The piezoelectric device is then powered on to initiate the cleaning process. This process is time-consuming as the mold should be prepared before and after the cleaning and at the same time require huge space for the cleaning station. As an alternative to this, an In-mold cleaning process is proposed that overcomes the above-mentioned issues. The In-mold cleaning process is based on ultrasonic technique that is modified so that the cleaning takes place in mold itself. A special piezoelectric device is inserted into the cavity of mold and if necessary, spacers are used to adjust the cavity volume followed by injecting the cleaning solution. After the cavity is filled with cleaning solution and heated to a desired temperature, the piezoelectric device is initiated with a predefined parameter for cleaning phase. As a result of this technique, the production and cleaning process can be automatic and takes place at the press itself. This method eliminates the necessity of mold preparation for cleaning stage, where all the electrical connections and corrosion elements are removed. Figure 4-2 shows the block diagram of In-mold cleaning technique based on modified ultrasonic method for an RTM mold. This concept is universally applicable to processes involving plastic injection, where contamination is typical.

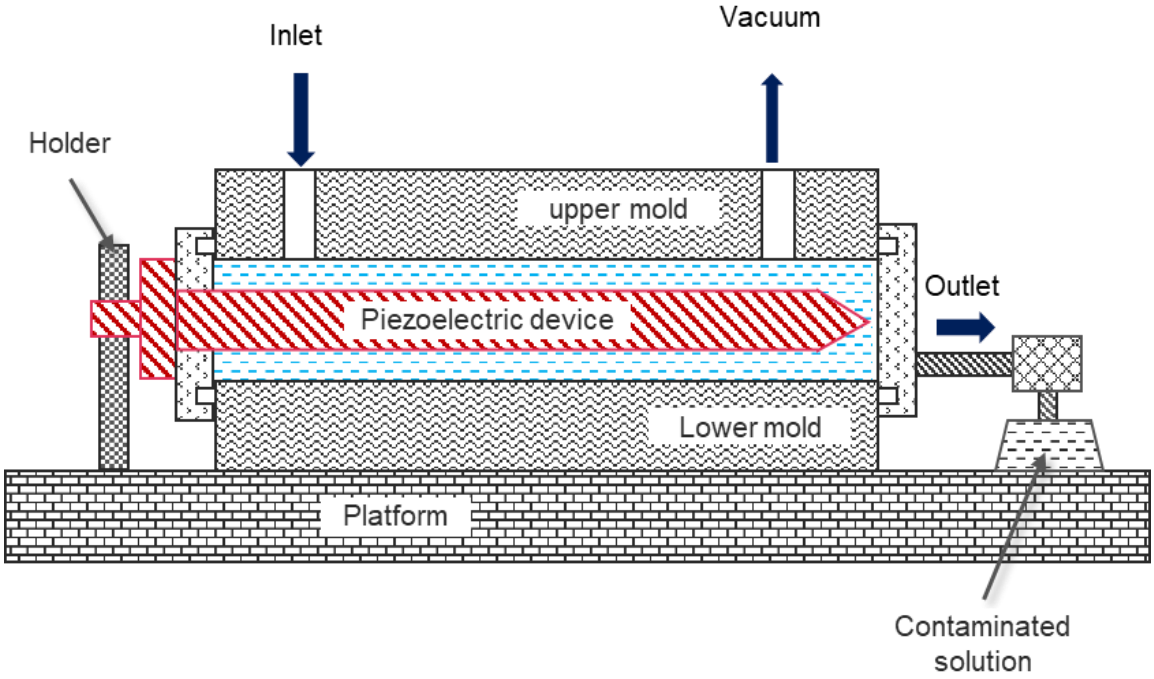

Figure 4-2: Block diagram showing the cross-section setup of In-mold cleaning process based on ultrasonic technique in a VA-RTM Mold.

To validate the concept of In-mold cleaning process, the mold design was modified so that piezoelectric device can be incorporated in the cavity to perform cleaning of mold. Lean six sigma

based on DMAIC technique was used to track the objective and fulfill the functionality of the Optimized cleaning process. DMAIC is also a five-stage process similar to DMADV that has Define, Measure, Analyze, Improve and Control stage. DMADV is a commonly used technique in manufacturing industries for improving an existing process or measuring the performance of a process. In the current study, DMAIC is used to improve the ultrasonic based cleaning process in an efficient way.

Define phase is all about defining the problem that needs to be addressed. The problems in the current ultrasonic cleaning process are listed below that are set as the project objectives.

1. Larger space for the cleaning station.
2. Movement of the mold from press to the cleaning station
3. Longer pre-processing time for cleaning stage involves removal of corrosive parts and electrical connections in the mold.
4. A large amount of cleaning solutions is used.
5. Surface of mold after cleaning.

Measure is the second stage that aims in defining a method that can measure the problems mentioned above in a metric scale. The Measure criteria for the cleaning process is listed below based on the objectives listed in Define stage.

1. Space required can be quantified using the area (m^2) formula which should be lesser the better. Since the area is pretty much fixed and a scalar quantity, the reliability can be rated as Good.
2. Movement of mold can be measured using the distance (m) it moved from point A (press) to point B (Cleaning station). Here the criteria should be lesser the better. Same as before, the distance is already a scalar quantity making its reliability as Good.
3. Pre-processing time (sec) can be recorded as the time needed to remove all the components from the mold that doesn't require cleaning and moved to the cleaning stage and then moved back to the press and all components are assembled back so that production starts. Here the criteria are the same as before, the shorter the better. Reliability here depends on the individual who is assigned on that particular date and can be rated as neutral.
4. The amount of cleaning solution can be measured in scalar quantity of liters which can be rated as good in terms of reliability. Criteria should be lesser the better.
5. The surface of mold can be quantified based on surface roughness which is also scalar quantity and can be rated as good in terms of reliability. Criteria should be lesser the better.

Analyze stage is all about finding the best possible solutions for addressing the above-mentioned problems all together or individually. Here we can evaluate our current knowledge of the process and find the areas that can be optimized. Care should be taken so that the changes won't have a negative influence on the other stages of the process. In the current study, for optimizing the cleaning process, a literature study has been carried out in Chapter 2.

In Improve stage, a solution to address the mentioned problems in Define stage is implemented. For ultrasonic process, a universal solution addressing all the four problems is suggested below.

- An In-mold cleaning process based on ultrasonic method was proposed, where the cleaning of mold takes place in the press itself in a well-controlled environment as shown in Figure 4-2

More details and a schematic design used to set up the mold for the mentioned cleaning process is addressed in Chapter 5 and Chapter 6. Control stages addresses if the proposed concept has improved the process and its stability aligning with the project goal. Chapter 6 addresses the control phase in detail.

Based on both DMADV and DMAIC process, the mold was designed so that 95 % of the structure stays the same for validating both Self-sealing and In-mold cleaning process. The remaining 5 % of the mold was designed as inserts that can be integrated into the mold as per the procedure. One insert was designed based on Self-sealing and the second insert was designed for validating the In-mold cleaning process. The mold also has a third insert that represents the traditional way of RTM production, which is used for process study. A fourth insert was designed with an AM printed cooling channel for optimizing the Self-sealing further. The mold can also be designed where both Self-sealing and In-mold cleaning are integrated without any inserts, but in the present study they are studied separately for better control and understanding their influence.

5 Mold Design and Production

To validate the proposed concepts, a mold was designed that can validate the functionality of both Self-sealing and In-mold cleaning process, which is addressed in this section. The mold is designed based on demonstrator geometry, theoretical and analytical calculation.

5.1 Selection of Demonstrator Geometry

In the current study, various structures of an automobile were studied to find the potential application of hybrid structures that results in weight saving and at the same time improved properties. Based on literature, some of potential areas that can use hybrid structures in an automotive are A-pillar, B-pillar, C-pillar, Crash-box, and Drive shaft. One of the common challenges in hybrid structures is residual stresses generated due to different thermal expansion coefficients of metals and FRPs. However, this can be reduced with tailoring the fiber directions or can be used to increase the adhesive force between metal and FRP if the structure is cylindrical. Out of five structures mentioned above, drive shaft cross-section is cylindrical in shape that can use residual stresses for a better adhesiveness between metal and FRP. Based on this approach, a cylindrical shaft geometry that resembles the cross section of vehicle's drive shaft as shown in Figure 5-1 was selected.

In addition to residual stresses approach, a drive shaft should fulfill a few important characteristics such as stiffness, vibration damping, crash optimization, etc., where hybrid structure can be advantageous. The drive shaft is an important component in a power transmission system, which is used to transmit the engine torque/power to the drive wheels so that vehicle can move/accelerate. For continuous motion of vehicle, the torque transmission must be smooth and uninterrupted under various loading conditions. In addition, it must compensate for variations in angle or length resulting from maneuvering or deflection from the road lanes. Improved stiffness of the structure can reduce the energy losses due to these loading condition without increasing its weight or cost significantly, which can be fulfilled by using hybrid structures. At the same time, the drive shaft should have better energy abortion during crush events, which can also be fulfilled by hybrid structures. In addition, the efficiency of the drive shaft depends on its weight, speed, and natural frequency. The drive shaft has many parts connected to it besides cylindrical shaft such as spline, universal joint, torsion dampers, anti-lock system rings etc. If entire drive shaft is made from FRP's, then it becomes difficult to connect to other parts of the power train, which can be challenging making metal-hybrid approach more suitable as additional parts of the power train can be connected to the metal section of the hybrid drive shaft.

The next step is to select the dimensions of the hybrid drive shaft, which should be determined before designing the mold. Diameter, thickness, and length are three different dimensions that should be determined. The thickness of the drive shaft should be as minimum as possible so that the inertia is kept to minimum. The typical thickness of shafts ranges from 3 mm to 15 mm depending on the type of vehicle. Diameters range from 42 mm to 60 mm depending on the material used and type of vehicle. Length of the dive shaft depends on the type of drive shaft configuration and material used that ranges from 850 mm to 2000 mm. The configuration of the drive shaft is classified based on the number of segments it's made from. For example, a three-

part drive shaft is dived into three segments and are connected using universal joint to reduce the bending loads when the length of power train to long as shown in Figure 5-1
In the current work, the thickness of the drive shaft was kept to minimum that is 3 mm and a mid-value of 54 mm was selected for the outer diameter. Since the length of drive shaft has lesser influence as they can be made from number of segments was kept to a minimum value, which is 320 mm. The percentage of weight reduction by using CFRP with respect to other materials for the selected dimension is shown in the Table 17. In current study, a hybrid shaft was considered, which is heavier in mass than CFRP but lower than Steel mass and cost effective in comparison with CFRP.

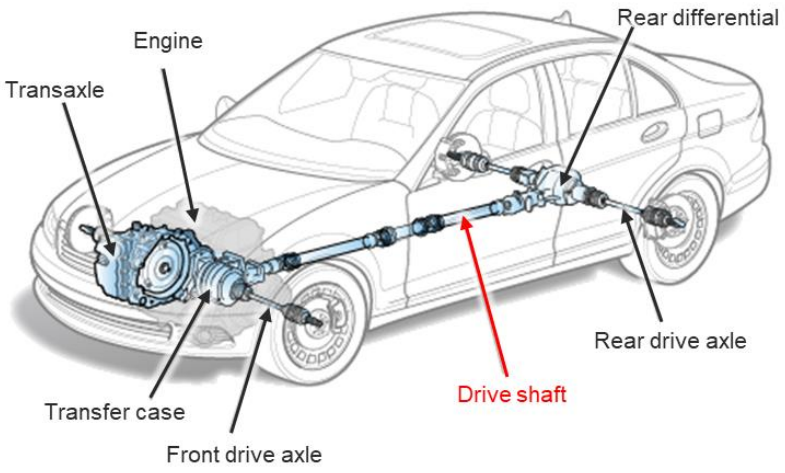

Figure 5-1: Drive shaft location in a power transmission of a car [150].

Table 17: Mass of shaft with respect to different materials.

Type	Data				Calculated	
	Length / m	Outer Diameter / m	Inner Diameter / m	Density / kgm^{-3}	Volume / m^3	Mass / kg
Hollow Steel	0.32	0.054	0.048	7850	0.000153	1.2
CFRP	0.32	0.054	0.048	1665	0.000153	0.3
Steel - CFRP Hybrid	0.32	0.054	0.05	1665	0.000104	0.5
	0.32	0.05	0.048	7850	0.00004	

5.2 Theoretical Approach

In current work, theoretical approach is divided into two sections. Initially, existing material models were studied to understand the importance of parameters with respect to fluid front and draft parameters that can be controlled with the Injection machine for a parameter study. In the second section, theoretical approach is used to select the power of the Heating element of the self-sealing with respect to temperature and gap height.

5.2.1 Selection of Parameters based on Mathematical models

One of the important factors in VA-LRTM process is the nature of resin flow through porous medium and its affecting parameters. The porous medium refers to fiber structure. The flow can be studied mathematically using the Equation 6 based on Darcy's Law [32]

$$V = {}^{K}/_{\eta} \left({}^{dx}/_{dy}\right) \qquad \textbf{Equation 6}$$

where 'V' is flow front velocity, 'η' is the resin viscosity, 'K' is the permeability tensor of the preform, and '$({}^{dx}/_{dy})$' is the pressure gradient that can also be represented as '∇P'. For arbitrary reinforcements, three orthogonal directions can be calculated if respective permeabilities are known. However, this formula can't be used when temperatures based on time are considered. As the temperature changes, so does the viscosity making this equation inaccurate to predict the flow front with respect to time. To capture the relation between temperature, viscosity, and time, Equation 7 were formulated based on dual Arrhenius model [150]

$$In\,\eta(T,t) = In\,\eta_{\infty} + {}^{\Delta E_n}/_{RT} + \int_0^t k_{\infty} \exp\left({}^{\Delta E_k}/_{RT}\right) dt \qquad \textbf{Equation 7}$$

where 'T' is Temperature, 't' is time, 'η_{∞}' is calculated viscosity of the material at $T = \infty$, 'ΔE_n' is the Arrhenius activation energy, 'R' is the gas constant and 'k' is an apparent kinetic factor. It can be noted that Temperature, Viscosity and Pressure gradients at the fluid front are important parameters, determining the flow process. Thus, these parameters are further studied in Chapter 6. The fiber volume fraction can be calculated using Equation 8, which is based on ASTM D2584 [38]

$$V_f = \frac{\rho_m\, w_f}{\rho_m\, w_f + \rho_f\, w_m} \qquad \textbf{Equation 8}$$

where 'V_f' is volume fraction of fibers, 'w_f' is weight of fibers, 'w_m' is weight of matrix, 'ρ_f' is density of fibers, 'ρ_m' is density of matrix. The fiber content was calculated to be ~ 55 % for 6-layer CFRP sample. It should be noted that the moisture content in the fibers is not considered for this calculation.

5.2.2 Selection of Heating Cartridge

In case of Self-sealing process, it can be noted from Equation 7 that the activation energy plays a major role because the main functionality of the heating element is to cure the resin before it reaches the other end, so that the leakage is prevented. In terms of experiments, this depends

on the two parameters, heating element width that is parallel to resin flow and the height of the resin flow (Gap in the sealing zone) itself. After selecting these two values, the amount of energy required to cure the resin can be determined. Once the energy is calculated, a suitable heating cartridge can be selected based on its time efficiency. For initial calculations, the gap height of resin flows was kept to 0.1 mm to keep the amount of resin cured as low as possible, since it has no relevance for the functionality of the finished part. The width of the heating element was set to 25 mm and its length to 157 mm. The mold temperature was set to 120 °C and the heating temperature was set at 260 °C. The temperature selected were based on the matrix system. Based on these values, the energy required in the sealing zone was calculated using Equation 9 for a worst-case scenario, i.e., the entire heating zone is filled with epoxy.

$$Q = m * c * \Delta T \qquad \textbf{Equation 9}$$

Where 'm' is mass of epoxy, 'c' is specific heat capacity and 'ΔT' is temperature difference. The energy required for this setup is 63 J which can be supplied in 0.32 sec if a heating cartridge of 200 W is used according to Equation 10.

$$t = \frac{Q}{P} \qquad \textbf{Equation 10}$$

Where 't' is time, 'Q' is energy and 'P' is power of the cartridge. The calculated time can be used in combination with experimental fill time of the mold to know the distance of fluid flow in the seal zone before the curing is initiated. These values should be scaled to a factor of safety. Based on these calculations a heating cartridge of 300 W was selected, which can supply more energy or increase the sealing temperature up to 300 °C if needed.

5.3 Injection Strategy

Figure 5-2 shows few of typical strategies used in RTM process. Most widely used injection method is converging flow, where the matrix system in injected at the end and flows towards its center as shown in Figure 5-2a. The outlet vents are connected to the vacuum pump for easy flow and removing the air particles trapped between fibers. Converging flow has less fill time, making it impossible for tarped air to escape creating a porous laminate. Another challenge for using multiple injection requires a complex injection system equipped with multiple sensors to make sure the injection pressure is constant at all injection ports.

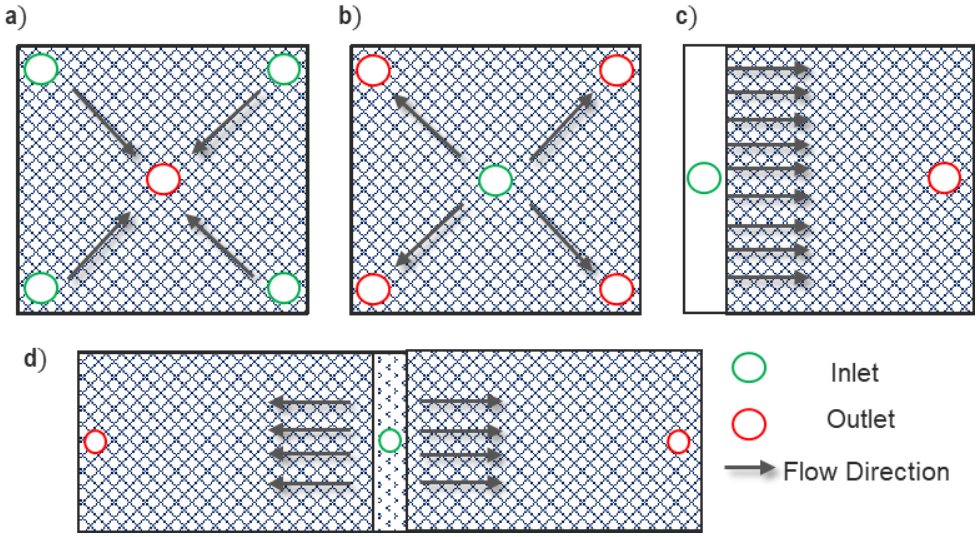

Figure 5-2: Typical injection strategies used in RTM process a) Converging flow; b) Diverging flow; c) Linear flow and d) Linear flow integrated with diverging flow.

Diverging flow is opposite of convergency flow, where injection takes place at center and matrix flows towards the corners that are provided with multiple outlet vents as shown in Figure 5-2b. Diverging flow has larger fill time and there is possibility that the matrix system reaches its gel time before exiting the vents for large structures. Figure 5-2c shows linear flow also known as light technique makes use of race tracking effect of matrix system, where the matrix flow around the circumference of the mold and then infiltrates the fiber. Linear flow can be used in combination with divergency or convergency depending on the geometry. In the current work, light technique based on divergency flow was used as shown in Figure 5-2d. The word “Light” in Vacuum Assisted Light Resin Transfer Mold (VA-LRTM) refers to this technique. To obtain divergency flow, the outlet vents are placed at the ends of the mold.

A self-sealing flowstop developed and patented by TARTLER GmbH was used in the current work, which prevents the material return after injection phase as shown in Figure 5-3. The flowstop can be integrated into the mold and placed at the entrance of the injection channel in the mold. The material flow generated by the mixer opens the flowstop and the material flows into the mold. If the material flow stops, the flowstop seals itself automatically and prevents the backflowing of material.

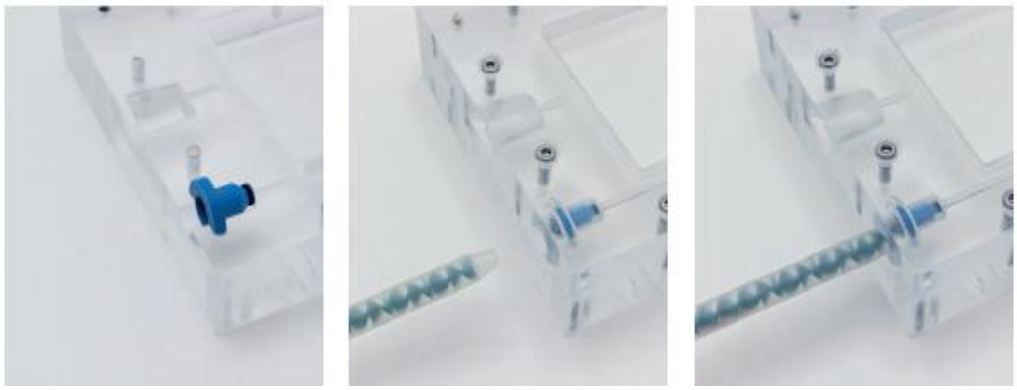

Figure 5-3: Schematic diagram showing the functionality of flowstop with respect to mold [151].

5.4 Mold Design

Mold design plays a very important role in both cost management and process cycle. In RTM process, mold is solely responsible for the geometry and tolerances of the part. The mold dictates how the resin enters and leaves the mold guiding the filling process. At the same time, mold must also withstand the loads from mold closure and resin pressure. Another important specification of mold is to provide the necessary heat for curing the resin or accelerating the cure of resin. The selection of optimized location for sealing in the mold for VARTM contributes to factors like production cycle, resin overfill, ease of handling, etc. It should be noted that Mold design is directly linked to structure of the component to be produced. For example, changes in initially calculated fiber volume can have a dramatic effect on mold closure forces affecting the clamping arrangements. Because of this sensitivity, the mold design and component design processes must proceed in parallel. Mold material is one of the factors that should be considered in the early stage. Properties of mold such as chemical, mechanical, and thermal play a vital role. Chemical properties of the mold include compatibility with matrix system (resins, curing agents and additives), release agents, catalyst, and corrosion resistance in the production environment, etc. The mechanical properties include strength, stiffness, resistance to handling induced damage, etc. Thermal properties include coefficient of thermal expansion, thermal conductivity, and specific heat. In general, there are three types of molds made for RTM process namely direct method via CAD/CAM, indirect method where mold face is casted or laminated and hybrid methods [32]. CAD/CAM method is widely used as it supports complex shapes. In CAD/CAM, the mold cavity is directly machined on block of material. The materials of mold can be polymers, foams, metals, ceramics, etc. Most widely used material is made of tool steel that is classified under metal and has better properties such as good formability, corrosion resistance and better thermal conductivity. In brief, the requirements of mold design for RTM can be summarized below [32].

- The mold must form a cavity of accurate and reliable dimensions.
- It must be possible to introduce resin into this cavity in such a way that the reinforcement filling the cavity can be uniformly wetted out with resin. Excess resin must be able to exit the cavity and the mold cavity may have to be evacuated.
- Contact between resin and sealing should be kept to a minimum.
- Fiber packing and injection pressures must be maintained without any deflections or any damage to the mold structure.
- The heat required to cure the molding must be provided and for very rapid curing systems it may be necessary to provide cooling to limit peak exotherm temperatures.
- For molds that are to be thermally cycled, both heating and cooling may be required to gain the necessary control over the cycle time.
- The lay-up of reinforcement or preforms into the mold must be facilitated and the ejection of cured parts must be possible without damage to the mold or component.

Another requirement in the current study is selection of a suitable method to prevent the heat flow from self-sealing zone towards the production zone of the mold. This can be achieved in two different methods, i.e., either using special material made of composites such as fiberglass, rocks and slag wool, cellulose, natural fibers, rigid foam etc. or cooling channels made out of metals. In

current study, both approaches were designed, tested, and compared. In addition to thermal functionality, the insulation material/component should also withstand the forces occurred during the mold closure, withstand pressures during matrix injection phase and should be compatible with the In-Mold Cleaning process. Table 18 shows the thermal conductivity of few typical insulation materials that can be compared with steel which has a thermal conductivity of 50 $Wm^{-1}K^{-1}$ at 20 °C.

Table 18: Thermal conductivity of special insulation materials [144].

Material	Density / $kgdm^{-3}$	Tensile Strength / Nmm^{-2}	Adhesive Material	Temperature Limit / °C	Thermal conductivity / $Wm^{-1}K^{-1}$
DB110	1.4	120	Phenol	120	0.2
210LW	1.5	-	Polyester	210	0.18
DB260	1.9	280	Epoxide	260	0.21
K - Therm AS 600M	2.2	170	Silicon	600	0.26
K - Therm AS 550M	1.8	50	Silicon	650	0.37

DB110, 210LW and DB260 belong to DuroBest® insulation material category manufactured by AGK Hochleistungswerkstoffe. DuroBest® basic framework is made from high-quality substrates such as cellulose paper, cotton, aramid, and filament glass fabrics that are combined using resin system based on phenol, epoxy, melamine, polyester, silicone, and polyimide. Even at high temperature, DuroBest® retains 60% of its strength. In addition to insulation properties, they are low weight, high voltage resistance and dimensionally stable. DuroBest® can also be used in electrical applications for both low and high voltage range under oil or with increased humidity. DuroBest® are available in a wide variety of shapes such as solid blocks, cylindrical, hallow shafts etc. and can be machined to specific shapes. K-Therm® AS M series of materials offers electrical insulation for temperatures up to 800°C. K-Therm® are made from different crystal structures of mica such as muscovite's and phlogopite's and pressed with high pressure and temperature using silicone resin as adhesive. In current work, K-Therm® AS was used to validate Self-sealing process as temperatures up to 300 °C were considered and because of its low water absorption making it a better choice in comparison with DuroBest® category.

The biggest disadvantage of composite based insulation materials are machinability and their strengths as they are not applicable for all applications. Most of these insulations are weak for shear force making it difficult to turn or grind in parallel plane to their alignment. This challenge can be avoided by using cooling channels made of metals. Typical traditional cooling channels are made via drilling methods that are limited to length, diameter, and structures. Due to these limitations, the cooling channels are generally in a particular plane and usually made of simple

paralleled straight channels that results in a lack of performance to cool complex shapes. For a complex shape, they are made as a separate component and wrapped around the mold using forming techniques. Figure 5-4 shows few of the cooling channel designs that are used as a separate component in the system. The biggest issue here is the cooling process takes place in combination of conduction, radiation, and convection mode rather than just convection, which is more complicated for theoretical prediction and can only be validated experimentally. In case of Figure 5-4 setup, the excess heat/energy produced by the component must reach the cooling channel surface via radiation and then transferred to the cooling medium via conduction. Finally, the convention process takes place as the cooling medium carries away the excess energy. This process can be more efficient if the cooling channels are in direct contact with the surface of the components that are difficult to manufactured via traditional process.

These can be addressed by using additive manufacturing (AM), which is gaining more application and potential in both tooling industry and direct manufacturing for components. Figure 5-5 shows a conformal cooling system produced for an injection molding application using AM that works based on convection mode of thermal management. In the current study, AM is used to produce a cooling channel for the RTM mold application.

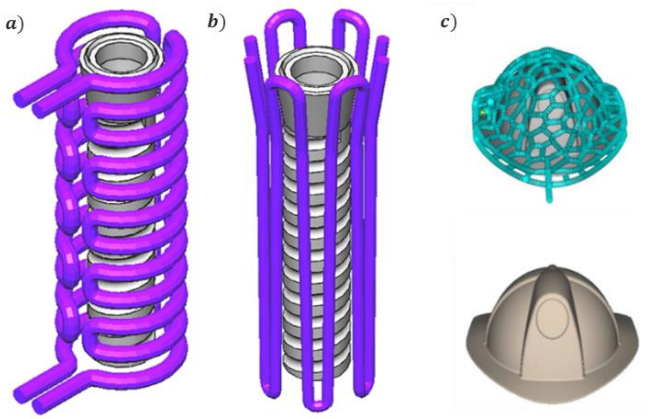

Figure 5-4: Cooling channels manufactured as a separate component for various geometry with variants [145] [146] [147].

Figure 5-5: Conformal cooling system manufactured for Injection molding application by B&J Specialty [149].

Based on the above factors, the mold for the current study was designed as a two-part mold. A centering mechanism was used at the corners of the mold to align the two halves of the mold during opening and closing stages. The design of lower mold is explained as the upper mold is symmetric in nature except for few sealing cavities. Figure 5-6a shows the lower mold with injection ring based on light-RTM process and alignment slots for installing centering mechanism components at the corners. Since the production process involves high temperature, heating cartridges were selected and placed on the mold in a homogeneous way. There are two possible ways to arrange the heating cartridges as shown in the Figure 5-6b and Figure 5-6c. Both ways of heating cartridges are suitable if the mold is used just for producing the components in the traditional way. However, in current work, the same mold should be used to validate both Self-sealing process and In-mold cleaning process along with a parameter study so that production cost and time can be minimized. To use the same mold for all the above-mentioned processes, the possibility to use inserts either in zone A or zone B was investigated. When Zone B was considered for incorporating an insert technique for the various processes, two challenges were spotted that are matrix inlet and center mechanism. These two challenges can be ignored if Zone A is considered for incorporating insert technique. Another important factor is to install a vacuum element that also acts as a resin overspill collector during the Self-sealing process, which will be easy to install in zone A rather than zone B. This concern makes Figure 5-6c more suitable so that heating cartridge won't be contaminated due to resin overspill and won't be a hindrance to design vacuum element.

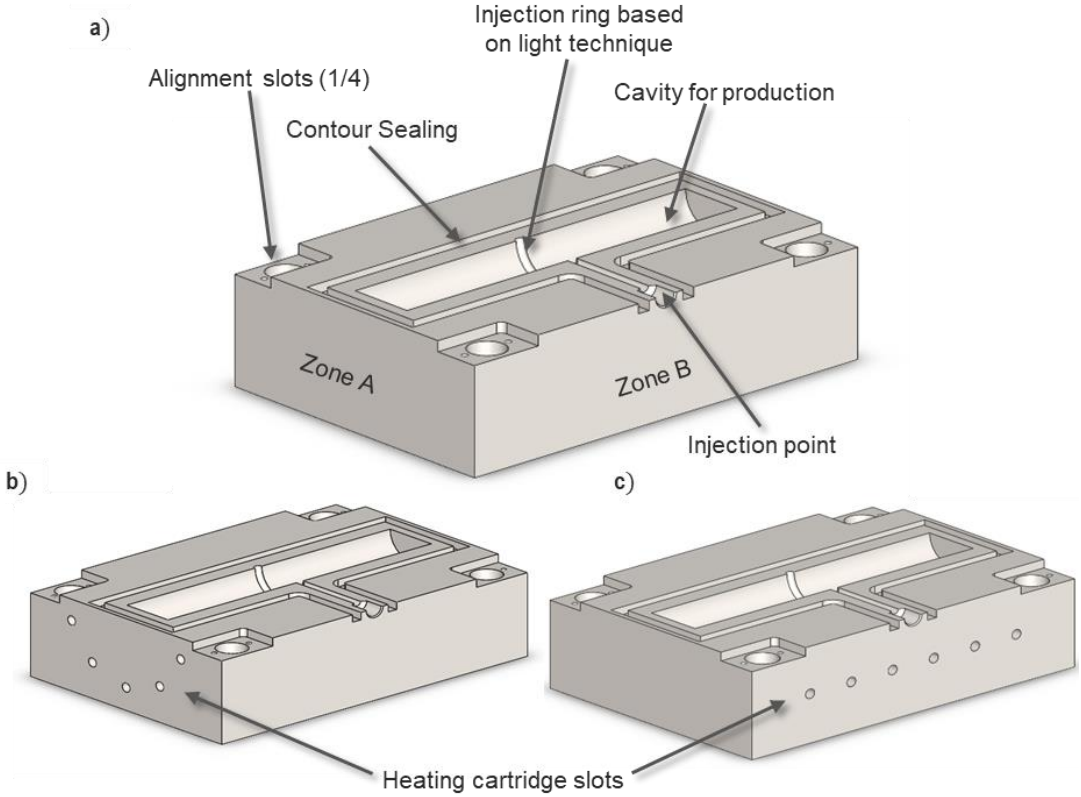

Figure 5-6: a) CAD model of lower mold design for producing hybrid shaft with an outer diameter of 54 mm; b) Heating cartridges across parallel to the sample length and c) Heating cartridges across perpendicular to the sample length.

Figure 5-7 shows the modified mold, which has two slots for adopting various inserts for validating the Self-sealing and In-mold cleaning concepts. Both ends of the mold have the same design with two slots. H7 surface with diameter of 10 mm was designed to add the heating cartridge perpendicular to the sample length for providing temperature to accelerate the resin curing depending on the requirement. As mentioned before, the injection area was modified so that a flow stop adapter can be used which prevents the back flow of resin after injection phase. Injection holder is designed to hold the flow stopper and injector head in position. A total of four inserts were designed that can be integrated into mold during various stages such as production and cleaning.

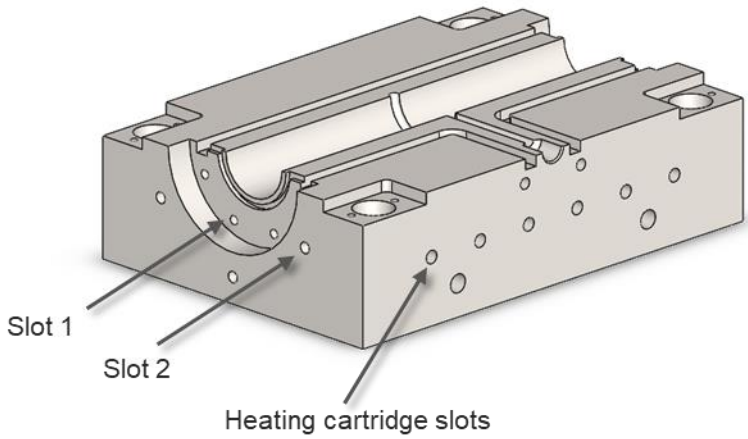

Figure 5-7: CAD showing the final version of lower mold with 2 slots where inserts can be integrated to study various concepts.

Insert 1 was designed based on conventional sealing for studying parameters and interface influence on mechanical properties of hybrid samples that are produced via VA-RTM process. Insert 1 was split into two components matching the lower and upper mold geometry. Figure 5-8 shows the CAD model of insert 1, which will be installed on both ends of the mold. The conventional sealing was installed into mold via slot 1, which prevents resin leakage and also to obtain vacuum in the mold.

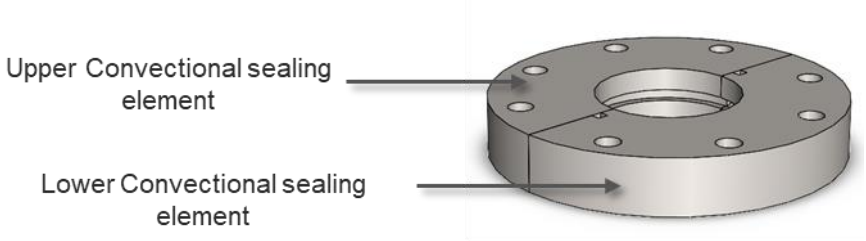

Figure 5-8: Inserts – 1 design for current mold based on conventional sealing process.

Self-sealing based on insulation material was designed as a second insert. In total there are six components that make up insert 2 as shown in Figure 5-9. The components were split equally

between lower and upper mold for ease of production. Insert 2 consists of an insulation element, heating element and vacuum element. Insulation element is made of K-Therm® AS, which prevents thermal flow from Self-sealing to mold production zone. Heating element is the component where the heating cartridge is installed to supply high temperature. The heating cartridge used is made of highly deformable material that can be shaped as per requirement. Vacuum element was used to obtain vacuum in the mold and collect the resin spill in case Self-sealing fails reducing the contamination. Both insulation element and heating element were installed via slot 1, whereas vacuum element was installed via slot 2 to the mold.

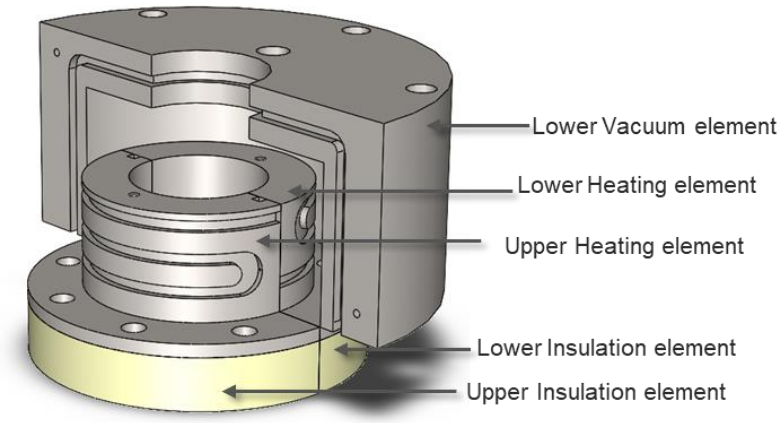

Figure 5-9: Inserts – 2 design for self-sealing process based on insulation materials.

Insert 3 was designed to replace insert 2 and overcome the challenges faced by insert 2. Insert 3 is made of two components that were installed to mold via slot 1. Insert 3 makes use of cooling channel to prevent the flow of heat from heating zone to mold zone. A lattice structure is designed on the opposite side of the cooling channel to prevent the heat dissipation, making it energy efficient as shown in Figure 5-10.

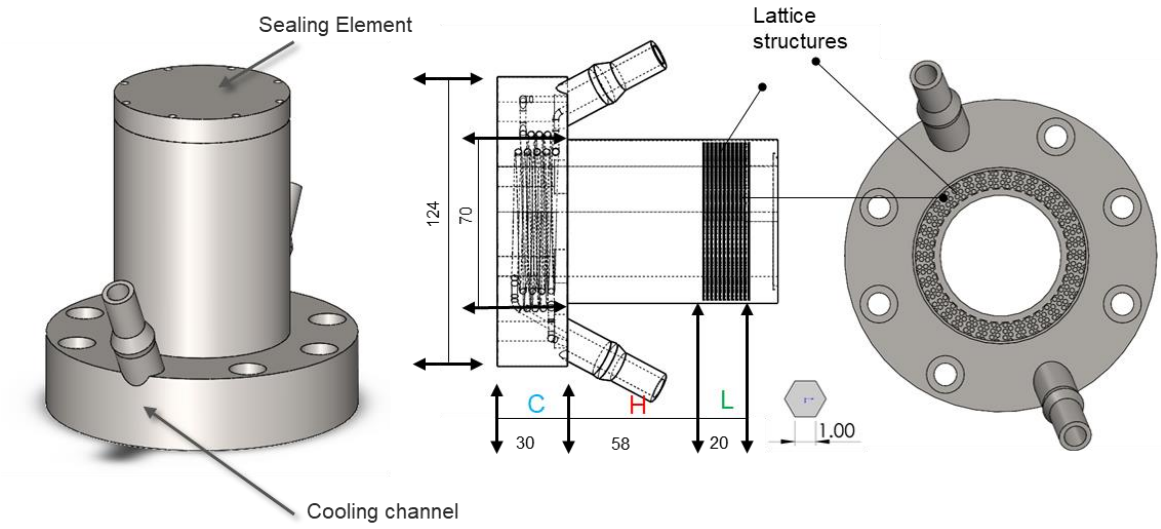

Figure 5-10: Inserts – 3 design for Self-sealing process based on cooling channel**,** C is where cooling channels are located, H is where heating element is installed and L is where lattice structure is located.

Insert 4 is designed to hold the ultrasonic device and at the same time prevent the leakage of both water and cleaning medium using sealing systems as shown Figure 5-11. Insert 4 consists of two components installed to lower and upper mold each. Both insert 1 and insert 2 have same dimensions except the inner diameter. Insert 2 is installed to mold via slot 1. There are two more components used in insert 4, which were not integrated into mold but to the press itself.

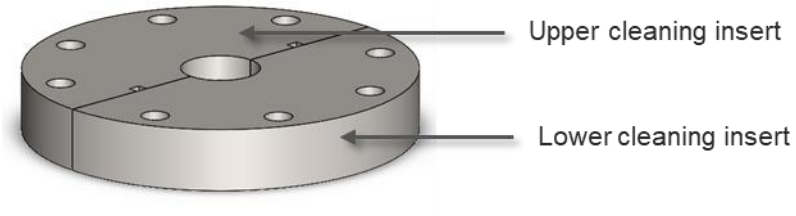

Figure 5-11: Inserts – 4 design that function as a holder for Ultrasonic device with a different inner diameter than insert 1.

5.5 Steady State Thermal Analysis of self-sealing zone of mold

Insulation material thickness was selected based on steady state thermal analysis using Finite Element Method (FEM). Hyper-works/ Opti-struct was used in the current study to perform steady state analysis. Material properties for the simulation were taken from the data sheets obtained by the respective companies as listed in Table 19. Both convection and conduction type of the heat flow is used to represent the system as close as possible to the real time scenario. Convection heat flow was used to represent the surrounding of the mold with a room temperature of 25 °C. Conduction heat flow was used to represent heat flow between various components in the mold from the heating cartridge. Figure 5-12 shows the CAD model used for the simulation along with boundary conditions.

Table 19: Material Parameters used for steady state analysis.

Materials	Young's Modulus [E]	Poisson's ratio [υ]	Density [ρ]	Thermal conductivity [k]	Specific Heat Capacity [H]
	GPa	-	kg/(m^3)	W/(m*K)	J/(kg*K)
Tool Steel - 1.2085	210	0.3	7.85 * 10^3	20	508
AS 600	6	0.4	2.2 * 10^3	0.25	1200
AS 550	4	0.4	1.8 * 10^3	0.37	1280
CFRP (CF + Epoxy)	129	0.32	1.55* 10^3	3.9	900
Resin	2.35	0.4	1.2 * 10^3	0.18	1180
Silicon Sealing	0.05	0.49	1.44 * 10^3	0.3	1100

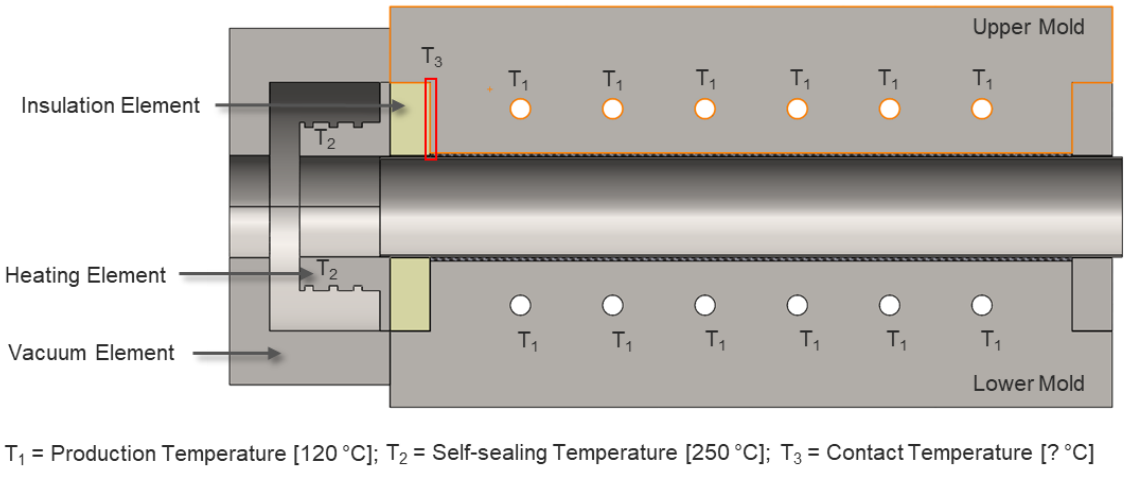

Figure 5-12: CAD model showing the boundary conditions used for FEM analysis.

Production Temperature (T_1) and Self-sealing Temperature (T_2) are input values given, whereas Contact Temperature (T_3) is determined via FEM. Five FEM simulations with same element size of 1 mm were performed with different insulation material thickness and type. Table 20 shows the temperature measured on the contact surface of the mold where insulation was installed. The goal here is to have the temperature close to production temperature which is set to 120 °C for all five FEM simulations. It can be noted from Table 20 that 20 mm thickness of AS 600 can maintain temperature ~ 126 °C. Figure 5-13 shows the heat flow from heating element of Self-sealing zone towards a 20 mm AS 600 insulation material. Based on these results, the thickness of the insulation was increased to 25 mm for the Self-sealing process that is made from AS 600.

Table 20: Temperatures measured using FEM on the contact surface of the mold for various insulation material and thickness.

Insulation Material	Thickness [mm]	Temperature, T_3 [°C]
AS 600	12	142
	15	131
	20	126
AS 550	15	153
	20	146

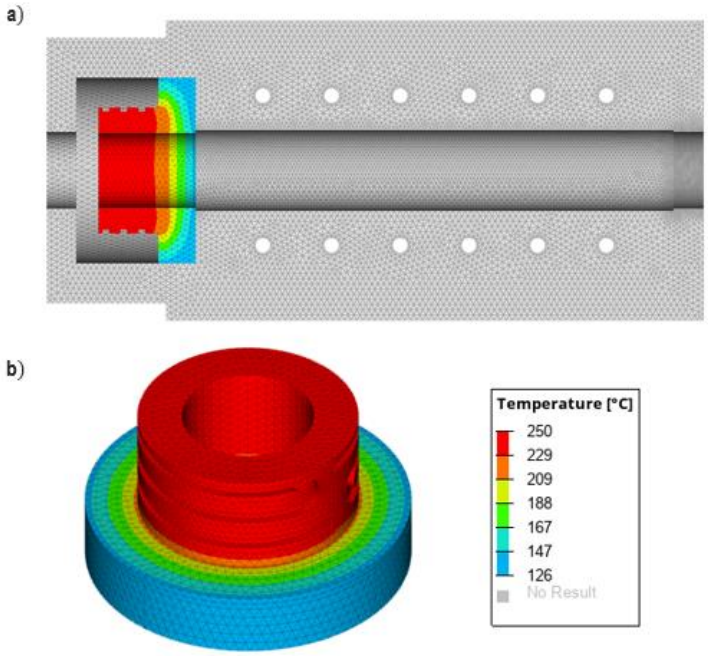

Figure 5-13: a) Steady state analysis results of mold with a 20mm thickness of insulation material made out of AS 600 and b) Self-sealing based on insulation.

6 Process Development

In the current study, three different approaches based on VA-LRTM process were used for manufacturing hybrid samples. First, general process parameters regarding the manufacturing process and the interface conditioning were studied. In the Second approach, the process is modified by adding the self-sealing system. In the third approach, the cleaning approach was investigated. Figure 6-1 shows the block diagram of current work's process development steps.

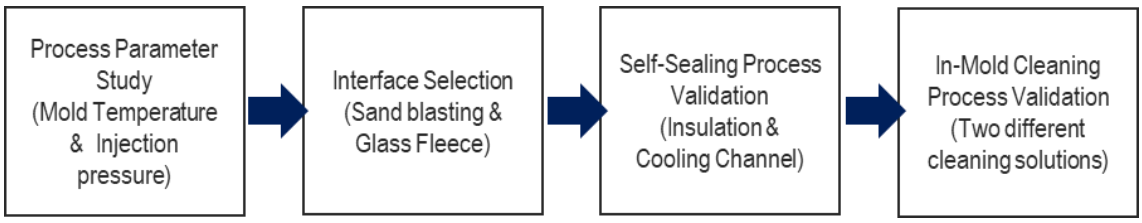

Figure 6-1: Block diagram showing process development steps.

6.1 Process Parameter study

The first manufacturing process is based on conventional sealing process where typical polymer-based sealing is used for sealing the mold contour. In this process both process parameters and the interface between metal and FRP were investigated separately to reduce the number of samples produced and study their influence in detail.

Process parameters have greater influence in mechanical properties, production cycle time, production cost, etc. For example, in RTM process if the injection pressure is set as 2 bar, then the upper mold can be simple vacuum bag which reduces the production cost but at the same time the production cycle is increased as it needs more time to fill the cavity. It can also be formulated in other ways such as parameters are selected based on the production methods and materials used. In the present chapter, parameter influence in RTM process was studied. In RTM process, there are many process parameters such as resin injection pressure, mold temperature, location of inlet and vents, fiber volume, fiber layup, application of vacuum, injection mass flow rate, etc. that influence the mechanical properties of the final composite fabricated as shown in Figure 6-2. It should be noted that process parameters are also influenced by material characteristics.

Injection pressure of the resin plays a very important role in the final property of the structure. It was reported that if the injection pressure is too high, it causes fiber wash resulting in displacement of fiber alignment [138]. At the same time if the injection pressure is too low, then the cavity is not fully filled before curing initiates. In another study, three sheet samples were produced using injection pressures of 2.9 bar, 3.8 bar and 4.8 bar respectively [139]. It was observed that the sample manufactured at 3.8 bar exhibited better mechanical properties than the other two samples. The main reason for the decrease in mechanical properties at the other pressures is due to high void content. In the case of 4.8 bar pressure, the pressure was too high for this particular sample, which lead to a preferential channeling of the resin between fiber tows resulting in a non-uniform flow front and caused the entrapment of air bubbles. At 2.9 bar, the

resin tends to flow around the fiber bundles (through macropores) rather than to flow through the fiber reinforcement (through micropores) during the mold filling process because of its shear rate-dependent viscosity resulting in a difference in impregnation rate.

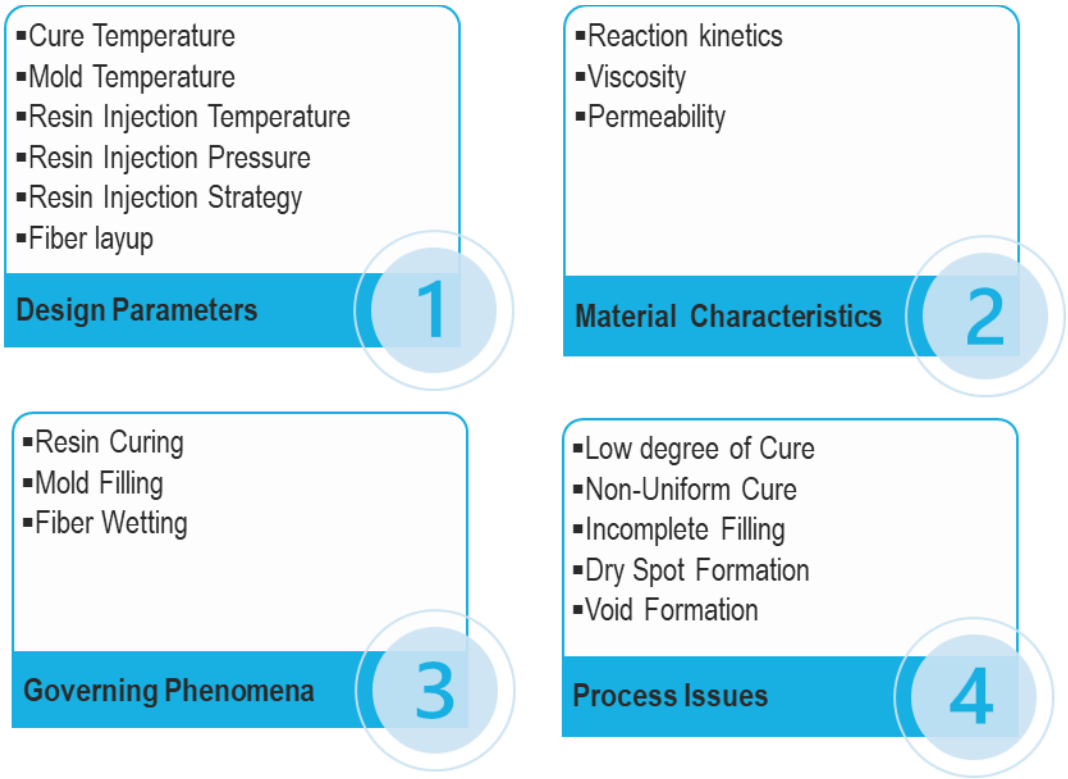

Figure 6-2: Process design parameters in RTM process.

Both resin injection temperature and the mold temperature are important factors that should be studied together. Viscosity of the matrix system is related to temperature that influences both filling time and wetting the fibers as shown in Figure 6-3. The mold temperature should be adjusted based on resin injection temperature and the cavity volume. For example, if the matrix is injected at 100 °C and the mold is also maintained at 100 °C then the fill time should be less than 2 min, if not, the matrix starts curing (gel time exceeding) resulting in dry areas reducing the mechanical properties. In general, this can be compensated for by increasing the injection pressure or the mass flow rate so that the fill time is within its gel time with respect to the selected temperature.

Mass flow rate is another important factor as it has direct influence on the fiber wetting and fluid front. Typically, higher mass flow rate creates multiple fluid front resulting in an uneven flow front trapping the air particles creating porous structure. However, controlling both injection pressure and mass flow rate is not possible as both are interlinked. Based on the above literature, hybrid samples were produced based on different mold temperature and injection pressure and tested. Three different values for mold temperature and injection pressure were used to produce hybrid samples. Mold temperature was selected based on the matrix system used as it directly influences its viscosity. Injection pressure was selected based on the machine limitations and factor of safety.

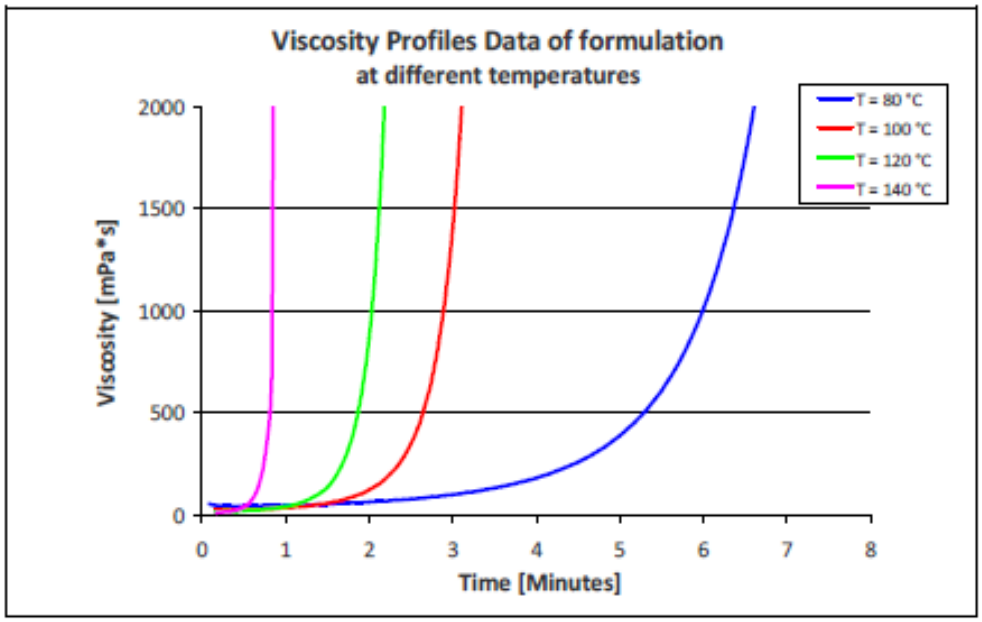

Figure 6-3: Viscosity with respect to time at various temperatures of epoxy based Epikote Resin 05475 and Curing Agent 05443 [141].

In order to reduce the number of samples and get more reliable relations, the design of experiments (D.O.E) was used. There are two techniques in D.O.E that can be used for two variables with three parameters each, which are the Two Factorial method and Taguchi method. In current study, the Taguchi method was selected as it has the option to control the number of experiments and at the same time evaluate the parameter influence. A two-level Taguchi method was used with L9(2^3) array with 3 values for each parameter with a total of 9 different samples as shown in Table 21.

Table 21: Sample details based on Taguchi L9 array for parameter study.

Sample	Mold Temperature / °C	Injection Pressure / bar
Sample 01PA_01IN	80	5
Sample 02PA_01IN	80	7
Sample 03PA_01IN	80	9
Sample 04PA_01IN	100	5
Sample 05PA_01IN	100	7
Sample 06PA_01IN	100	9
Sample 07PA_01IN	120	5
Sample 08PA_01IN	120	7
Sample 09PA_01IN	120	9

In order to minimize errors and improve the reliability, each sample is produced three times resulting in a total of 27 samples for parameter study. In parameter study, the steel was not sandblasted, nor glass fleece was used, which can be referred to as interface 1. The ILSS test was used to evaluate hybrid samples. After producing the samples and testing the ILSS of the hybrid samples, the best mold temperature and injection pressure was selected and used for producing further hybrid samples.

After the selection of appropriate mold temperature and injection process, the interface between metal and FRP was investigated further. Four different types of samples were planned for interface study as shown in Table 22. Similar to the parameter study, each sample was produced thrice for ILSS tests making a total of 12 samples. Additionally, 24 more samples based on interface study were produced to check if change in interface layer has any influence in its energy absorption and stiffness values. Based on these results, a hybrid sample was produced with interface that has high ILSS value along with selected process parameters from process study. This sample will be used as a reference sample to compare with the next two manufacturing processes.

Table 22: Sample details for interface study.

Sample	Steel Type	Interface/Glass Fleece	Parameters
Sample 10PA_01IN	Normal	No	▪ Mold Temperature - ? ▪ Injection Pressure - ? ▪ Mass flow rate - 0.15 kg/min
Sample 10PA_02IN	Normal	Yes	
Sample 10PA_03IN	Sandblasted	No	
Sample 10PA_04IN	Sandblasted	Yes	

6.1.1 Parameter Study

Figure 6-4 shows the mold setup used in parameter and interface study, which is integrated with insert 1 that is based on conventional sealing type. Resin is injected into the mold using a Nodopur 3 K VSAR system supplied by TARTLER GmbH as shown in Figure 6-5. The machine supports up to three-part resin system, whereas in the current work a two-part resin system was used. Table 23 shows few details about the injection system. The mixing ratio can be controlled via inputting the density and mixing ratio into system using control panel. There is a possibility to add a third component such as additive or catalyst that can be used in configuration 2 to validate the Self-sealing concept. In order to program the mixing ratio to the injection system, selection of material is carried out that are briefed next.

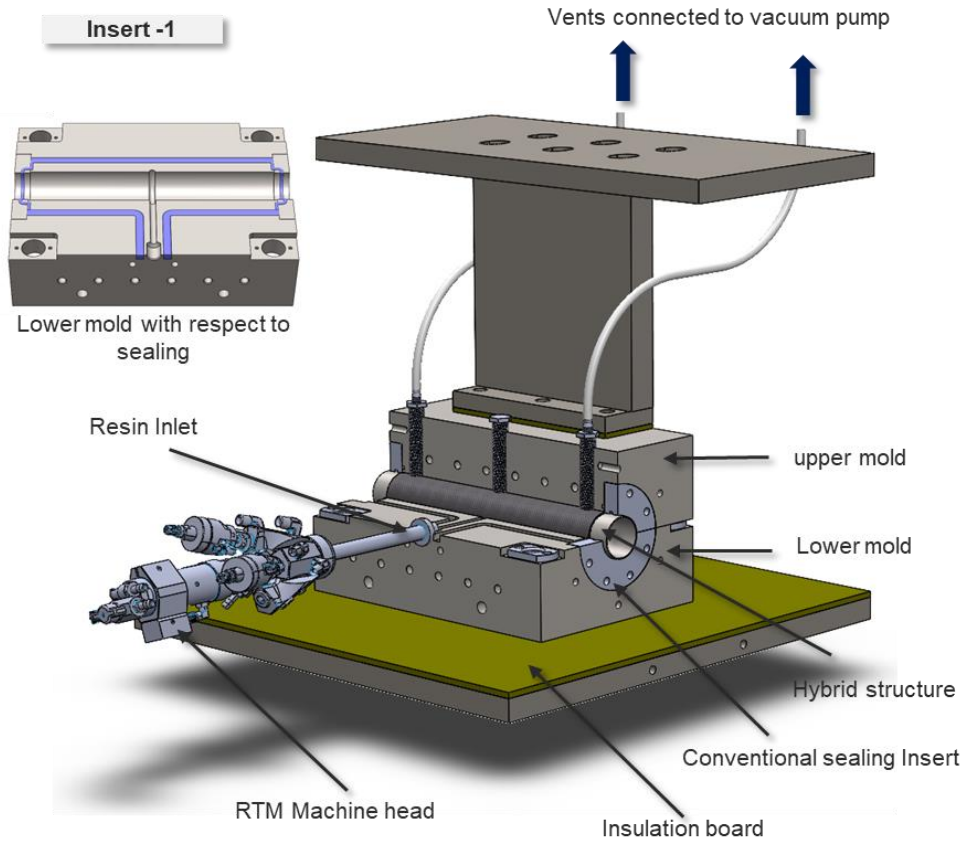

Figure 6-4: CAD model of the Mold configuration for parameter study (Cross section view).

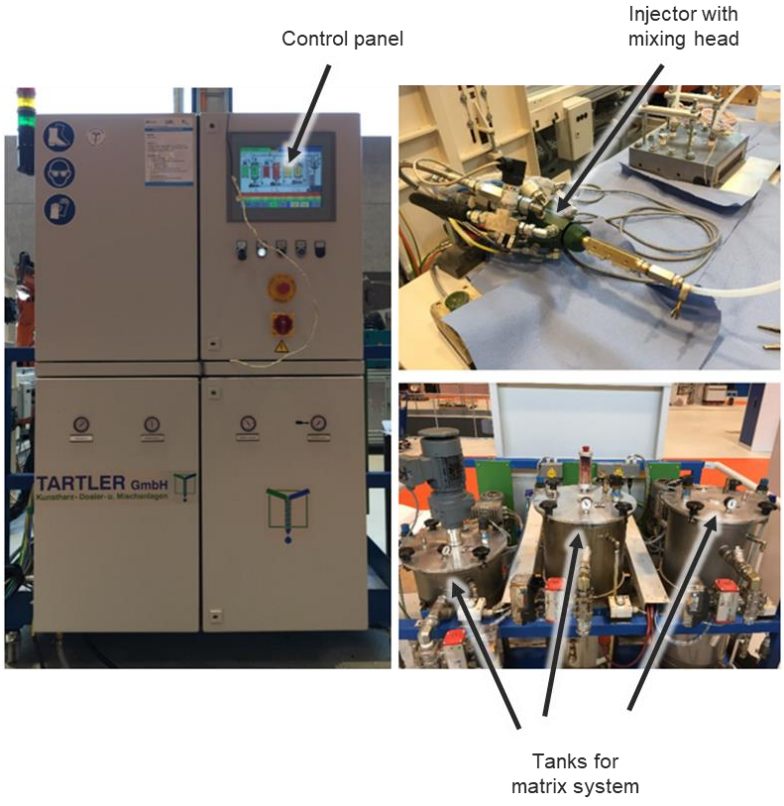

Figure 6-5: Injection system used for the current study.

Table 23: Injection system details.

Nodopur 3 K VSAR	
Manufacturer	Tartler GmbH
Type	Dosing and mixing system for liquid polymer resins
Maximum Injection Pressure	60 bars
Injection Capacity	1 Kg/min
Number of components used at a time	3
Mixing ratios of A:B:C	1:1:1
Measuring system/sensors	Injection pressure, Temperature, Mixing ratio

Precision steel tube made of E235+C with an outer diameter of 50 mm and a thickness of 1 mm was used as the metal part for the demonstrator. The length of shafts has two different dimensions, 340 mm for process study and 410 mm for self-sealing configuration. The main reason for an increase in length of the steel tube is to study the resin flow front in the Self-sealing. For phase 2 of parameter study, the shafts were sand blasted using SMG 25 Duo with sand particle size in range of 210 µm to 297 µm with a pressure of 4 - 4.5 bars.

Dry fiber tubes made of Torayca® T300J 400 tex (6k) carbon fiber was used for the hybrid drive shaft. The fiber tube has a fiber angle of 45 ° with a diameter of 60 mm and thickness of 0.27 mm. The diameter of the fiber hose can be adjusted by stretching or compressing, which likewise changes the fiber angle. Figure 6-6 shows the relationship between fiber angle and the diameter. The diameter in the current study varies from 50 to 54 mm that results in the fiber angle of 35 ° to 37 °.

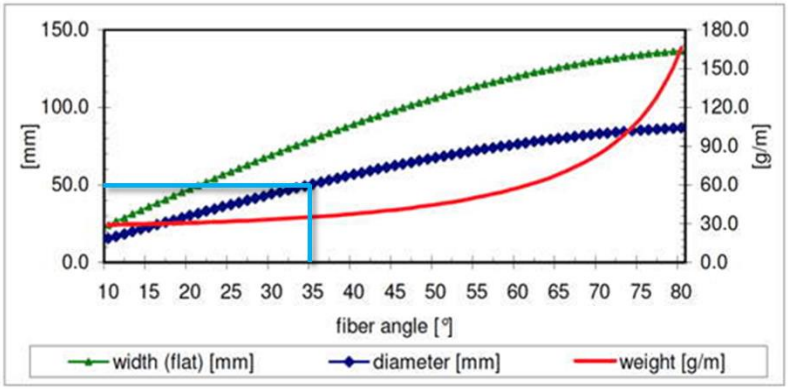

angle [°]	width (flat) [mm]	diameter (mm)	weight [g/m]	weight m² [g/m²]
30	69.3	44.1	33.3	240.0
45	98.0	62,4	40,7	207.8
60	120.0	76.4	57.6	240.0

Figure 6-6: Angle of fibers with respect to different diameters [149].

The matrix system used in this work is an epoxy resin of type EPIKOTE Resin 05475 and the amine hardener of type EPIKURE Curing Agent 05443, both manufactured by Momentive Performance Materials Quartz GmbH. The matrix system shows a relatively low viscosity and a short curing time. The viscosity of the matrix system is highly dependent on temperature. The viscosity of the resin-hardener mixture with respect to temperature can be seen in Table 24. In addition, the temperature has a great influence on the curing speed. The higher the initial matrix temperature, the faster the matrix system cures. A powder version of EPIKOTE Resin 05475 was used as a binder to bind the dry fibers in preform stage. The amount of binder used in each sample is calculated based on 1%-2% tolerance between EPIKOTE Resin 05475 and the amine hardener of type EPIKURE Curing Agent 05443.

Table 24: Material properties od epoxy and steel shaft.

EP 05475 + EK 05443 (100:24)		
Viscosity/mPa.s	at 25 °C	1200 ± 100
	at 80 °C	30 ± 5
	at 100 °C	13 ± 3
Pot Life/min	at 25 °C	120 ± 10
Gel Time/sec	at 80 °C	330 ± 30
	at 100 °C	210 ± 30
	at 120 °C	150 ± 30
	at 140 °C	90 ± 30
E235+C		
Yield strength/MPa		235 – 355
Tensile strength/MPa		480 – 640
Elongation at break/%		≥ 4 - 6

Johns Manville's glass nonwoven ForTex Type SH35/1 with a thickness of 0.37 mm is used as an intermediate layer to prevent contact corrosion between steel and carbon fiber. Despite all advantages of using hybrids, the biggest issue is when CFRP and metals are joined, the metal structures are prone to become galvanically active resulting in corrosion because of the presence of Carbon element in CFRP that acts as an open-circuit potential (OCP). In humid conditions, a perfect galvanic cell is formed resulting in galvanic corrosion attack on the metal structure. These can be avoided by using an interface layer that is not made out of Carbon elements in it [150]. In current study, the interface layer is a glass nonwoven consisting of glass fibers with an average fiber diameter of 13 µm. Nonwoven is characterized by dimensional stability and good wet strength.

Catalysts are selected to initiate the curing of the resin near the self-sealing under low temperature or accelerate the curing process. In order to determine the influence factor of the selected catalyst, DSC study was carried out for the following catalysts.

- DABCO (1, 4 - diazabicyclo [2. 2. 2] octane)
- DBTL (Dibutyltindilaurate)
- UL-28 (Dimethyltin carboxylate)

Figure 6-7 shows the results of 5 % of all the three-catalyst behavior in comparison with normal specimen without catalyst in dynamic DSC processes. It was recognized that curing is an exothermic process. A baseline was used to determine the onset temperature, exothermic peak, and exothermic enthalpy. The onset temperature is the temperature at which the curing behavior begins. Lower onset temperature requires less energy for curing, which is the most preferred characteristic in curing process. The peak or the top of the exothermic curve means that the fastest curing takes place at this temperature. By calculating the area below the baseline, the total heat of reaction of the specimen was determined during the process. By comparing, the peak temperature for DABCO was recorded to be ~86 °C, which is ~24 °C before the sample without any catalyst that has peak temperature of ~110 °C. Both DBTL and UL-28 had peak temperature of ~116 °C which is ~6 °C more than the sample without any catalyst as shown in Figure 6-7. Based on this result, DABCO was selected for further DSC test as it has lower peak temperature than all other samples and is used to determine the right percentage for current Self-sealing process.

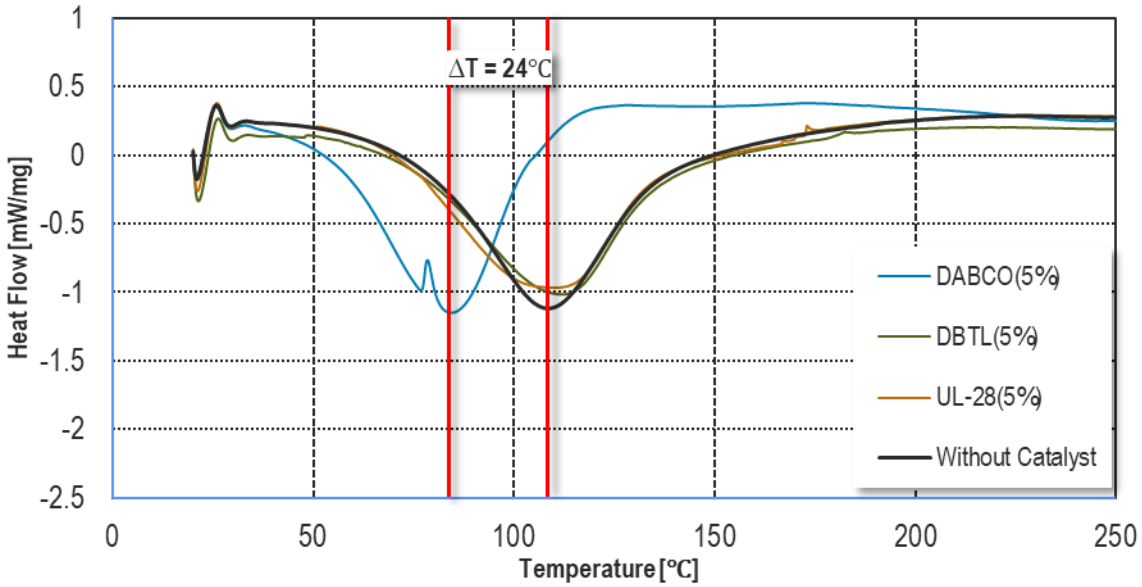

Figure 6-7: Dynamic DSC results of Epoxy specimen with various catalysts and without catalyst

Two additional and higher percentages of DABCO i.e., 10% and 15% were used to evaluate if the peak temperature can be reduced even further. Both higher percentages had a negative influence on the peak temperature i.e., they increased the peak temperature in comparison with 5% DABCO. The peak temperature for 10% and 15% DABCO are ~95 °C and ~104 °C respectively. Nevertheless, the peak temperature of both 10% and 15% DABCO is less than the sample without

any catalyst. In addition, it was observed that the amount of heat released for samples ranged from 325 J/g to 356 J/g. By comparing these results, it can be determined that DABCO at 5 % has an excellent effect on the curing reaction of the epoxy resin system. Therefore, DABCO with 5% was used for optimizing the Self-sealing process. However, it was noted from the DABCO material data sheet that the boiling temperature is ~174 °C. Temperature above these limit temperatures can lead to uncontrollable reactions. Considering the safety factor and the temperature at the innovating sealing, the catalyst was planned to manually add between the thermal insulation and the preform where the temperature was recorded to be ~146 °C if needed.

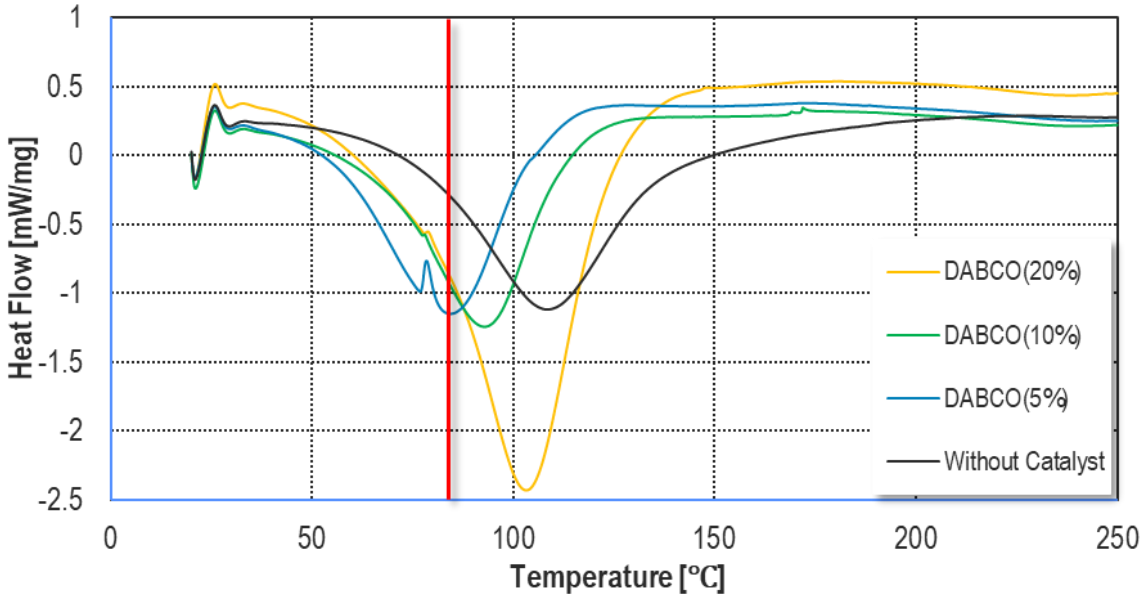

Figure 6-8: Dynamic DSC results of Epoxy specimen with various percentage of DABCO catalyst.

The production of samples starts with cutting the dry fibers based on the dimensions required. A total of 6 layers of dry fibers are cut to form a 2 mm thick composite layer with 55 % fiber volume. The CFRP are stacked on the steel one by one with binders added for each layer manually. Once the fibers are stacked with binder, they are tapped with a special shrinkage tape of 0.05 mm thick, which shrink when temperature is applied on it providing a strong compression force as shown in Figure 6-9. The sample is moved to the mold for preforming, where a temperature of 140 °C is applied for 10 min. Due to this step, the binder melts and then solidifies when kept at room temperature creating a bond between fibers of different layers. The preform is now ready for production. After discarding the release foil, the preform is placed in the mold. The mold is now closed as shown in Figure 6-12 and the injection pressure is adjusted according to the sample number based on Table 21. Another parameter that can be controlled is the initial mass flow rate of the matrix system before the process reaches the injection pressure. Once the injection pressure is reached, the mass flow rate is automatically reduced to maintain the given injection pressure. The machine mass flow rate can be as low as ~0.12 kg/min and past that value, machine cannot record data points. An offset of 0.5 bar was given in the machine so that the pressure can range from 6.5 bar to 7.5 bar for 7 bar injection pressure. Figure 6-10 and Figure 6-11 show the injection pressure and mass flow rate recorded over the time during the injection

phase. The initial mass flow rate was kept at 0.15 kg/min for all hybrid samples. The machine can record the data points every second only. Additionally, for all the hybrid samples, the machine was programmed to inject 0.21 kg of resin into the mold and stop automatically. Based on theoretical calculation, 0.14 kg of matrix system should be injected in order to maintain 55% fiber volume for the hybrid samples produced. However, an extra 0.07 kg was added in order to offset the matrix wasted because of inlets head volume and to maintain a minimum of 90 sec on injection time. The excess resin is collected at the outlet vents that are equipped with resin trap pot. During the entire production cycle, the mold was connected to a vacuum pump via outlet vents at both ends of mold and maintained at ~0.015 bar (absolute pressure).

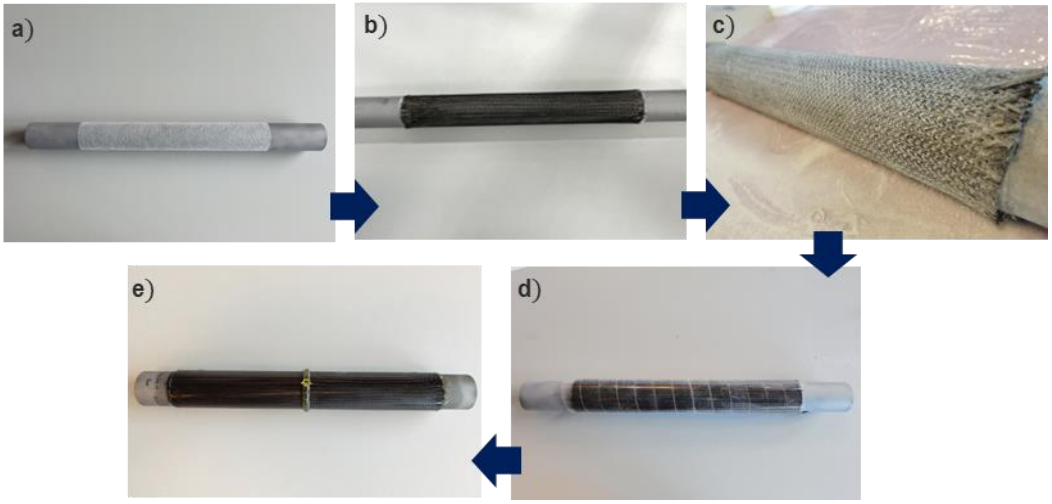

Figure 6-9: Schematic diagram showing the production cycle of Hybrid sample; a) adding glass fleece; b) adding CFRP; c) adding binders; d) tapping the sample with shrinkage tape for preforming and e) Hybrid shaft.

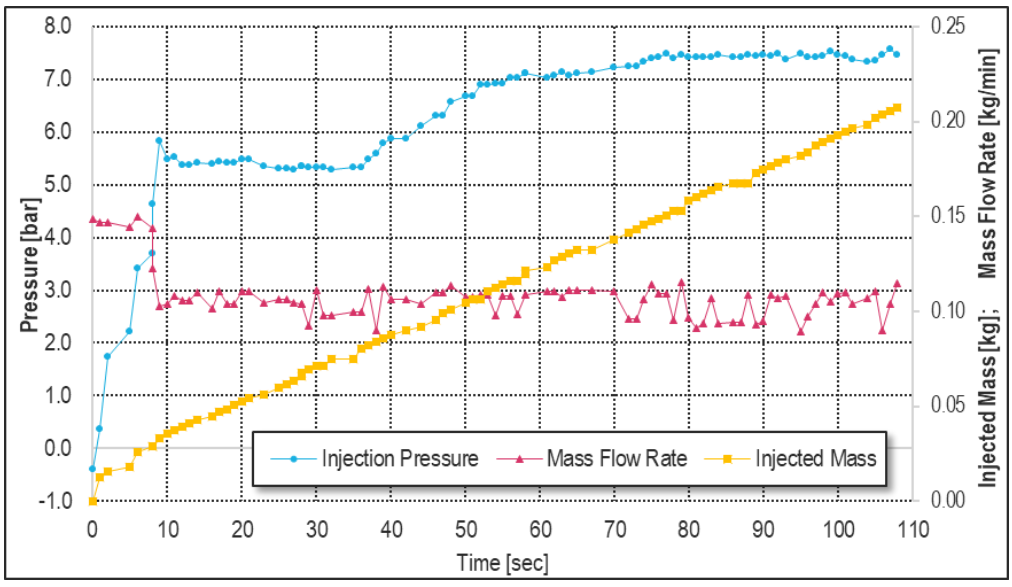

Figure 6-10: Production data points when injection pressure was set to 7 bar and initial mass flow rate of 0.15 kg/min.

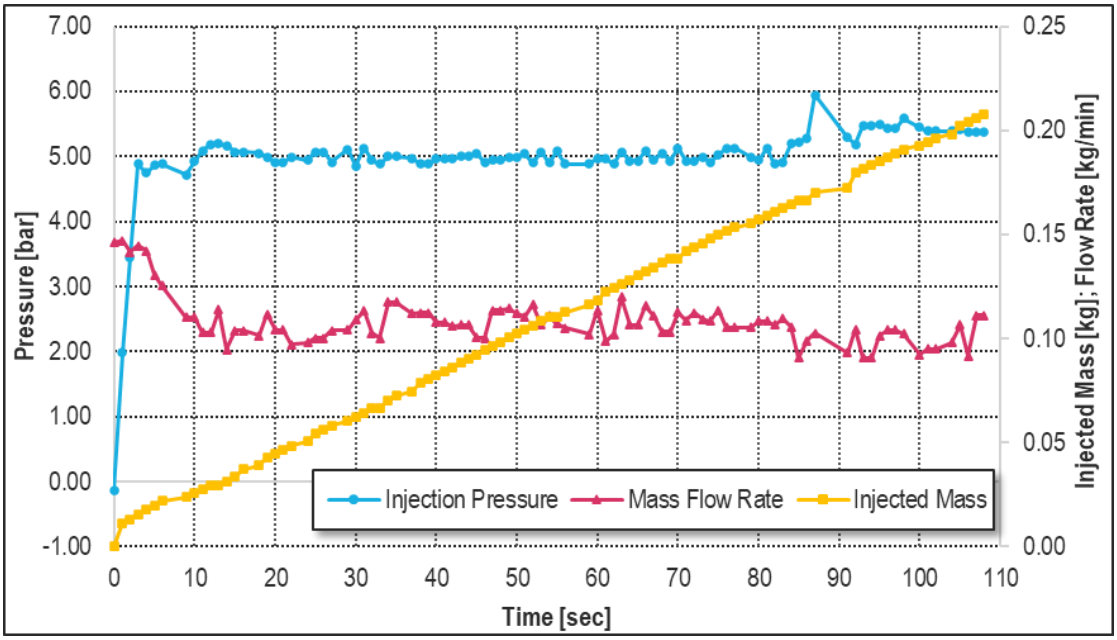

Figure 6-11: Production data points when injection pressure was set to 5 bar and initial mass flow rate of 0.15 kg/min.

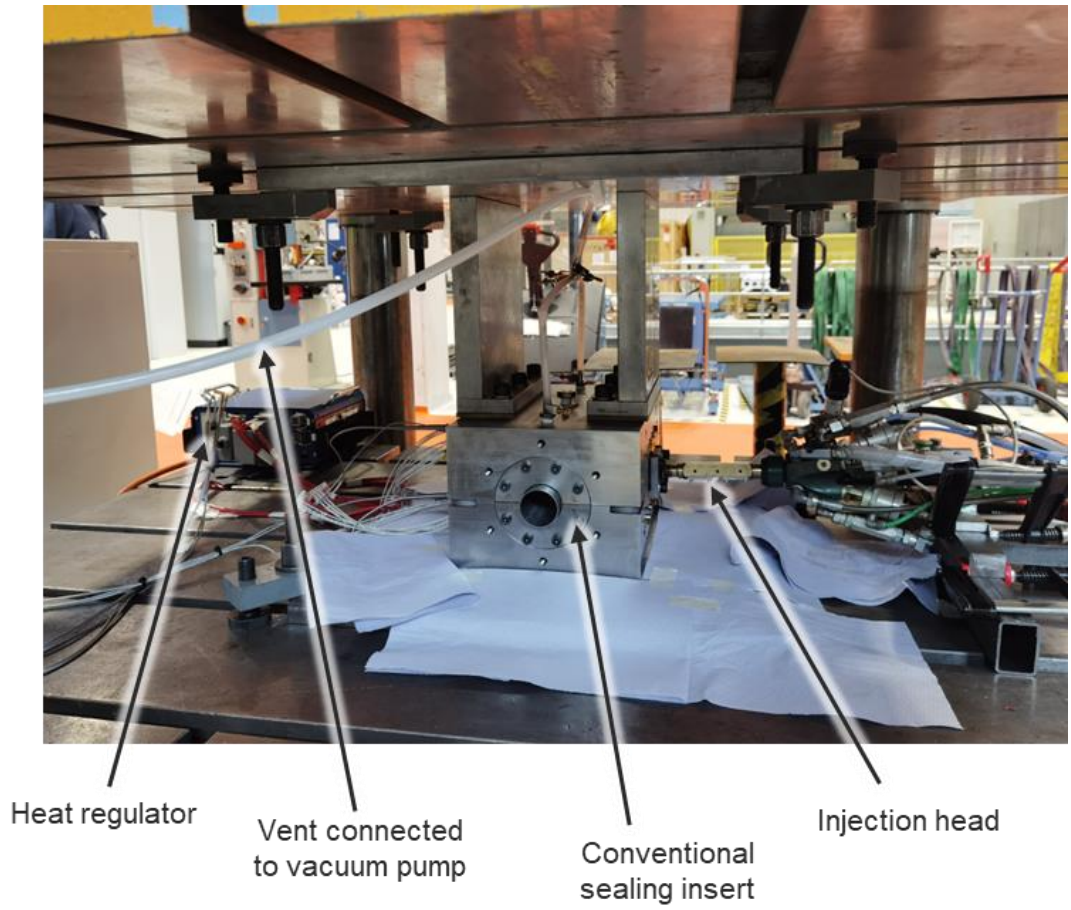

Figure 6-12: Schematic diagram showing the production setup for VA-LRTM.

All 27 samples according to Table 21 were produced with respective injection pressure and mold temperature. To evaluate these 27 samples, ILSS for cylindrical shaft was developed that is based on the shear strength testing of flat composite specimens. For this purpose, the hybrid shaft is cut into 20 pieces across its length into rings of 5 mm thickness. These rings are then inserted into a shear-edge device that presses the steel ring out of the CFRP structure. In this process, the recorded force is normalized to the shear surface (steel/CFRP interface), allowing shear strength to be determined. By designing the die and the punch accordingly, the force flow can be directed very precisely through the interface and thus a defined stress state can be set. Figure 6-13 shows the ILSS test setup and specimen before and after the test.

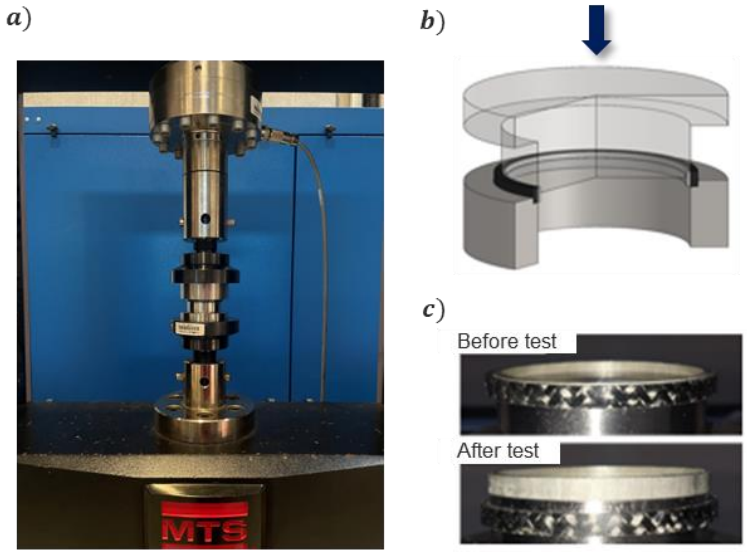

Figure 6-13: a) ILSS test setup for testing Hybrid shafts; b) CAD model of test rig and c) ILSS Specimen before and after test**.**

The samples are tested and grouped based on injection pressure and mold temperature as shown in Figure 6-14 and Figure 6-15. The samples in Figure 6-14 and Figure 6-15 are same and are only grouped in a different way to reveal the influence of parameter clearly. The results are based on an average value of 20 specimens on each sample and their standard deviation is recorded as an error bar. A difference of 26% in ILSS can be noted between best sample (injection pressure – 5 bar & mold temperature 120 °C) and worst samples (injection pressure – 9 bar & mold temperature 80 °C). Figure 6-14 is grouped based on temperature and a liner trend can be spotted based on 9 samples. Even with different injection pressures, higher mold temperature has better ILSS values. This phenomenon can be derived from the temperature vs viscosity of the matrix system. Higher temperature results in lower viscosity which makes the matrix flow better between fiber tows and better at wetting the fibers. Figure 6-16 shows the surface of the samples with different mold temperatures. It can be noted that the number of dry areas is reduced for a sample that was produced with mold temperature of 120 °C, which confirms the importance of mold temperature. Further increase in mold temperature from 120 °C can't be considered for the selected resin as the Gel time is reduced to 150 sec at 140 °C affecting the Injection time. Injection time is the total time the machine needs to pump the 0.21kg of resin into the mold.

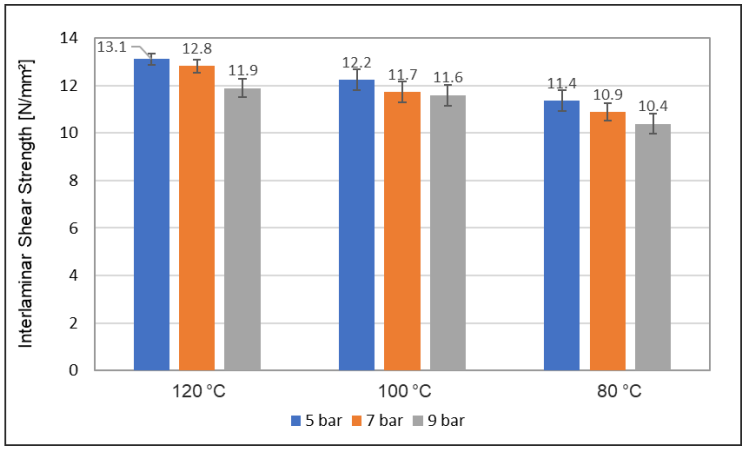

Figure 6-14: ILSS results of samples with respect to mold temperature and injection pressure.

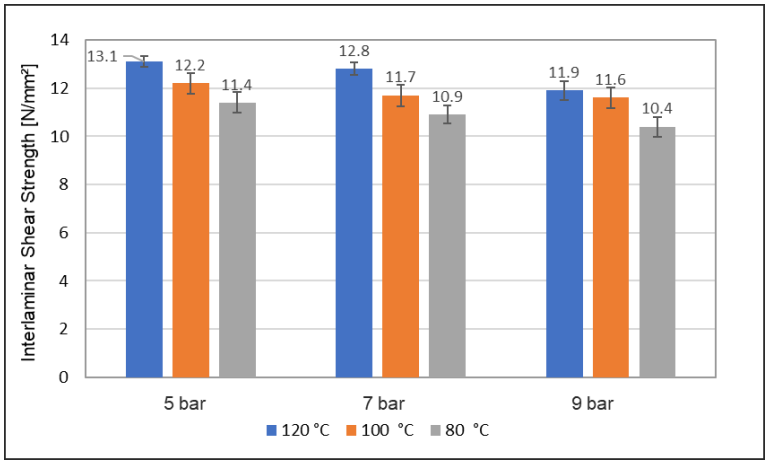

Figure 6-15: ILSS results of samples with respect to mold temperature and injection pressure.

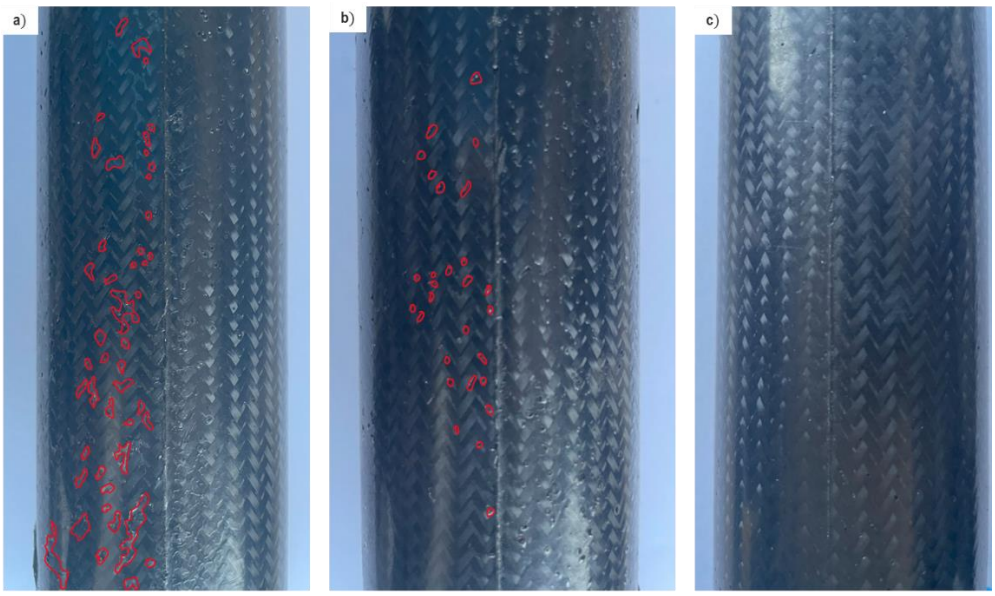

Figure 6-16: Dry areas spotted on sample surface with respect to mold temperature a) 80 °C b) 100 °C and c) 120 °C **Note**: Only partial dry surface areas are marked, while remaining is left for better visualization to spot the dry areas for readers.

Figure 6-15 shows the samples rearranged based on injection pressure. Similar to mold temperature, a linear trend can be observed based on all 9 samples. Change in ILSS value with respect to injection pressure can be related to two factors, i.e., fill time and fiber deformation near injection area. Fill time is the time recorded when resin enters the mold and spotted at the outlet vents for first time. Based on fill time, a proper relation could not be concluded. Figure 6-17 shows the fill time recorded for the samples with respect to injection pressure and mold temperature. The data is averaged based on 3 samples for each case. The sample with longest fill time of 58 sec has a ILSS value of 11.4 MPa, which is 15% less than the maximum ILSS value recorded for a sample that has a fill time of 52 sec. However, sample with shortest fill time of 43 sec has a ILSS value of 11.4 that is same ILSS value of the sample with longest fill time. Inspection of the sample surface doesn't provide any further information to conclude a relationship based on fill time. Figure 6-18 shows the sample surface based on fill time.

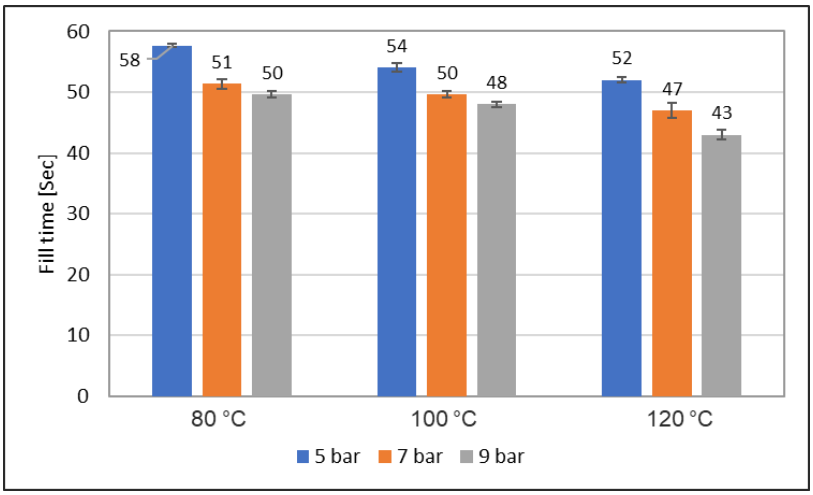

Figure 6-17: Fill time of samples with respect to injection pressure**.**

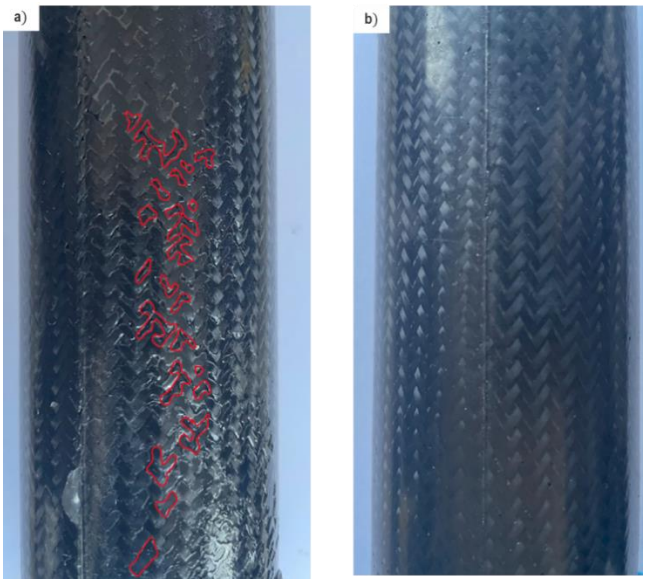

Figure 6-18: Dry areas spotted on sample surface with respect to mold temperature a) 43 sec and d) 58 sec Note: Only partial dry surface areas are marked, while remaining is left for better visualization to spot the dry areas for readers.

Fiber deformation is another typical challenge in RTM process that occurs near injection area. In order to check this influence factor, the ILSS value across a sample is investigated with respect to injection pressure of 5 bar and 9 bar as shown in Figure 6-19, Figure 6-20, Figure 6-21 and Figure 6-22. The values are based on three samples for each case and standard deviation is recorded as the error. Three different trends can be observed based on these results if a few data sets (maximum ignored data set is 4) in every sample are ignored. The first noticeable factor is that for all samples expect one sample (mold temperature - 80 °C with injection pressure of 9 bar), the ILSS value near the injection area is lowest which lies between specimen 10 and specimen 11.

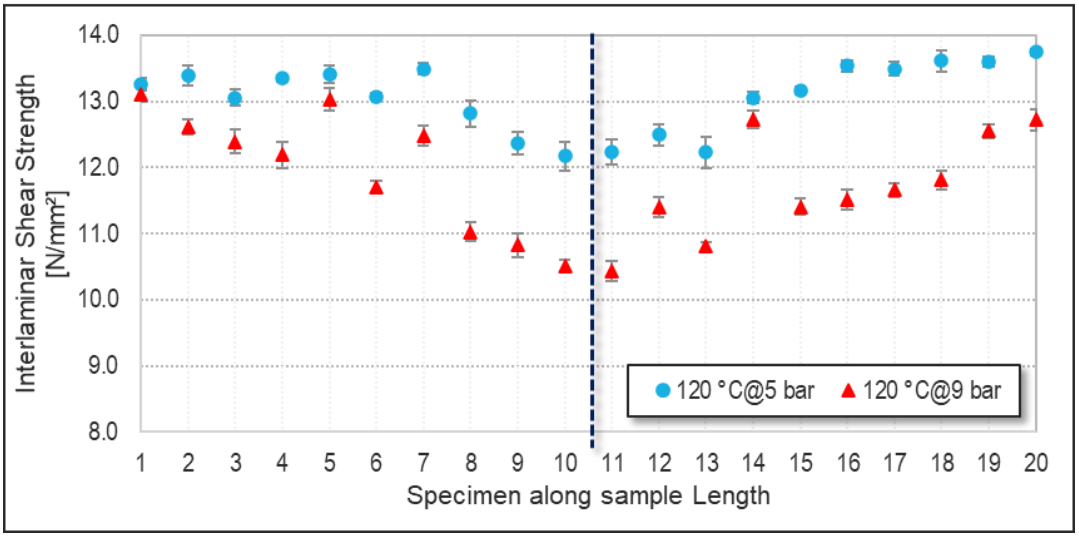

Figure 6-19: ILSS values across sample length based on 3 samples averaged for each parameter at 120 °C of mold temperature. **Note:** Specimen refers to rings that are cut on sample along its length. So, each sample has 20 specimens on them.

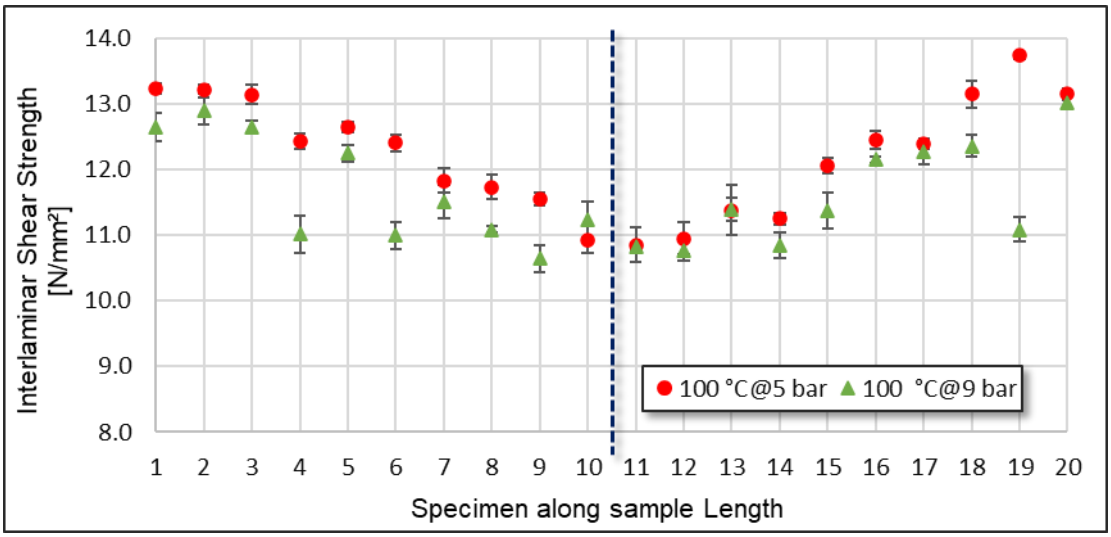

Figure 6-20: ILSS values across sample length based on 3 sample averaged for each parameter at 100 °C of mold temperature.

The second notable factor is the standard deviation between specimens near the injection zone and at the end of sample (maximum distance from injection area which is 130 mm). The standard deviation near the injection zone is high in comparison with the end specimens of the sample which implies that the values near the injection zone are inconsistent. The third notable factor is that the ILSS value across the sample tends to decrease, and the standard deviation tends to increase with decrease in mold temperature. Figure 6-22 shows the ILSS value recorded across the two samples that had maximum ILSS value and minimum ILSS value when all 20 data points are averaged. It can be noted that if mold temperature was 80 °C (lowest value used in our study) with injection pressure of 9 bar (highest value used in our study) are used to produce a sample, the ILSS values are scattered across its length without any proper factor. In case, if the mold temperature was kept to maximum possible, which is 120 °C and minimum pressure of 5 bar was used, the ILSS are not scattered but they tend to have lower value in the injection area.

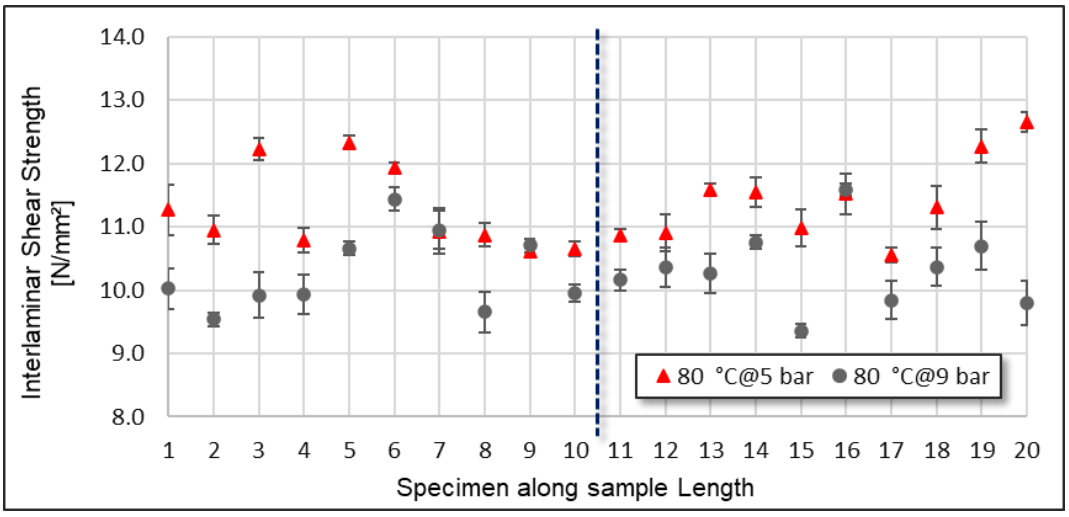

Figure 6-21: ILSS values across sample length based on 3 sample averaged for each parameter at 80 °C of mold temperature.

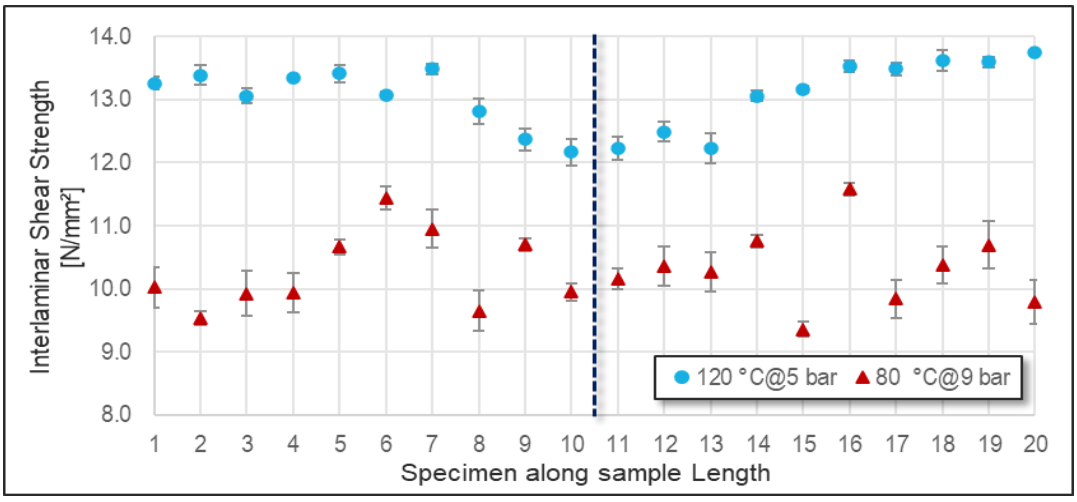

Figure 6-22: ILSS values across sample length based on 3 samples averaged for maximum and minimum ILSS value recorded.

It can be concluded that the values for pressure should be low (5 bar) and mold temperature should be maximum (120 °C) for better ILSS properties with respect to current geometry and mold design. The parameters for interface samples were selected based on these results, which are listed in Table 25

Table 25: Parameter selected for Interface study**.**

Parameter	Value
Initial Mass Flow Rate	0.15 kg/min
Mold Temperature	120 °C
Injection Pressure	5 bar

6.1.2 Interface study

The second stage of process optimization is to select a suitable interface between steel and CFRP as it plays a main role for load transfer between them. In the present study, four different combinations were used to produce the samples based on two modifications as shown in Table 26. In the first modification, the steel tube was sandblasted to check the effect if a rough surface can increase the adhesive between CFRP and steel. The surface roughness of the steel was changed from 1.41 µm to 2.83 µm for R_a and 2.13 µm to 4.27 µm for R_z respectively. For the second modification, the last layer of CFRP is replaced with a glass fleece layer, which has a higher layer thickness and lower density of fibers than CFRP. This layup creates more space for resin at the interface in comparison with the rest of the layers. The layer thickness of CFRP is 0.27 mm, whereas glass fleece is 0.35 mm. The parameters for all four interface samples were same as shown in Table 26. The produced samples were tested to see if there is any influence based on interface type.

Table 26: Sample details based on interface with updated production parameter.

Sample	Steel Type	Interface/Glass Fleece	Parameters
Sample 10PA_01IN	Normal	No	▪ Mold Temperature - 120 °C ▪ Injection Pressure - 5 bar ▪ Mass flow rate - 0.12 kg/min
Sample 10PA_02IN	Normal	Yes	
Sample 10PA_03IN	Sandblasted	No	
Sample 10PA_04IN	Sandblasted	Yes	

Figure 6-23 shows the results of ILSS test that were conducted in a similar way as before for four interface samples. It can be noted that there is an increase of ~ 40 % in ILSS value when sample interface is modified with sand blasting and additional of glass fleece in comparison to the sample without sandblasting or glass fleece as intermediate layer. When compared between glass

fleeces and sandblasting separately, the glass fleece sample's ILSS value increased by 33%, whereas sandblasting approach resulted is 14% increase of ILSS value when compared to the sample which is not sandblasted, or glass fleece is used. Increase in ILSS for a sandblasted sample can be related to increased mechanical locking that was also reported in literature studies [121]. In case of glass fleece, the increase in ILSS value can be related to increased resin content in the sample. The fiber content for sample with glass fleece is 51% (46% of CF + 5% of GF), which is less than the normal sample or the sand blasted that has fiber content of 55% (all CF). The change in fiber content is created because of the replacement of the interface layer between steel and CFRP to reduce the galvanic corrosion. For better understanding of these behaviors, microscopic analysis should be carried out near the interface zone. However, in the current work, the focus is more on mechanical properties and microscopic analysis is not planned. Based on these results, it can be suggested that modifying the interface layers does influence the ILSS values of the samples.

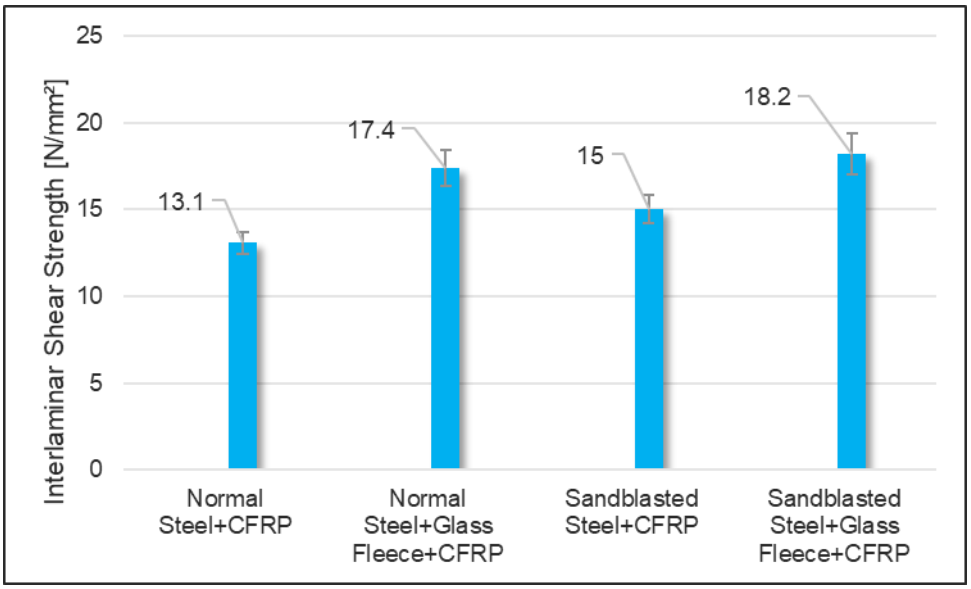

Figure 6-23: ILSS results of interface samples with same production parameter.

6.1.2.1 Compression Test

One of the important characteristics of a drive shaft is to withstand crash events and absorb as much energy as possible. This value can be determined using a compression test. The compression tests were carried out using a Servo motor spindle press that can provide up to 300 KN force. The samples were cut to a length of 150 mm out of 320 mm using a saw machine. To maintain consistency, always same part of the samples (with respect to mold marking) were tested and the center of the sample was always facing the moving part of the press. A special load cell was installed to the press that measures both the displacement and corresponding forces as shown. The test speed was set to 5 mm/min and compressed up to 90 - 100 mm of its length. Two different samples were selected based on interface study for compression test. First sample a normal sample, which interface is not modified i.e., normal steel with 6 layers of CFRP (going further this will be referend as normal hybrid sample). The second sample is the one which has glass fleece in its interface and sand blasted steel with 5 layers of CFRP (will be referred as

modified hybrid sample). For comparison, a steel tube without any CFRP was tested as a reference as shown in Figure 6-26 and Figure 6-27. The steel tube had both buckling and diamond buckling mode of deformation as shown in Figure 6-25a. In hybrid shafts, diamond buckling along with shear cracking and wrinkles can be spotted as shown in Figure 6-25a. The common phenomenon in all interface samples is complete debonding of steel and CFRP. The peak force has increased by 60 % for a hybrid tube in comparison with normal tube, whereas mean peak force has an increase of 88 %. It can be noted that the maximum peak force recorded was 120 KN for a normal sample, which is not modified at the interface. The modified sample has a maximum peak force of 113 KN, which is 6 % less than the normal sample. However, the mean force for normal sample is 59 KN which is 8 % less than modified sample, which had a mean force of 64 KN as shown in Figure 6-28.

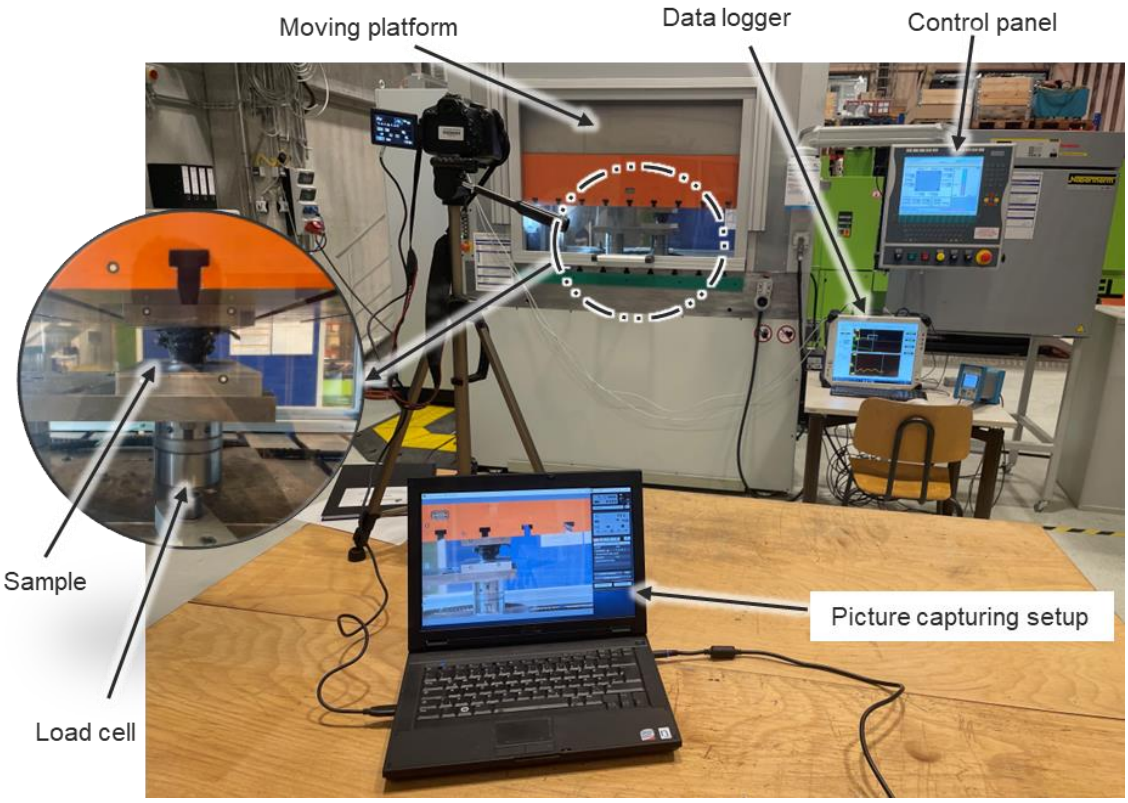

Figure 6-24: Compression test Setup for Hybrid shafts.

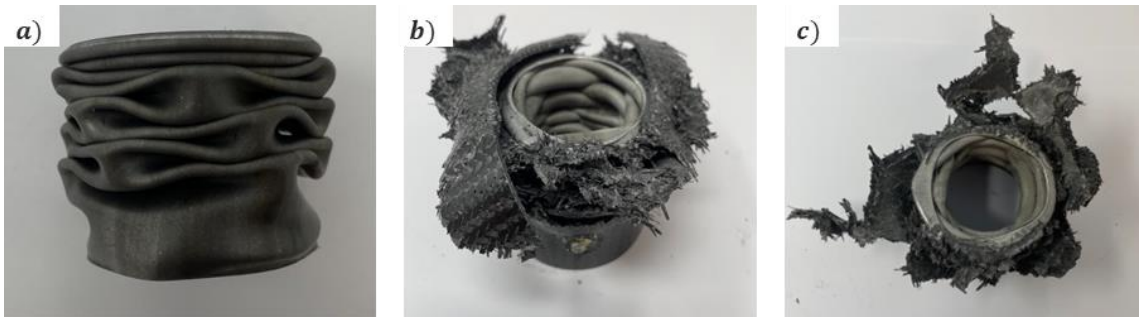

Figure 6-25: Interface samples after compression test a) Steel; b) Normal Steel + CFRP and c) Sandblasted Steel + Glass Fleece + CFRP.

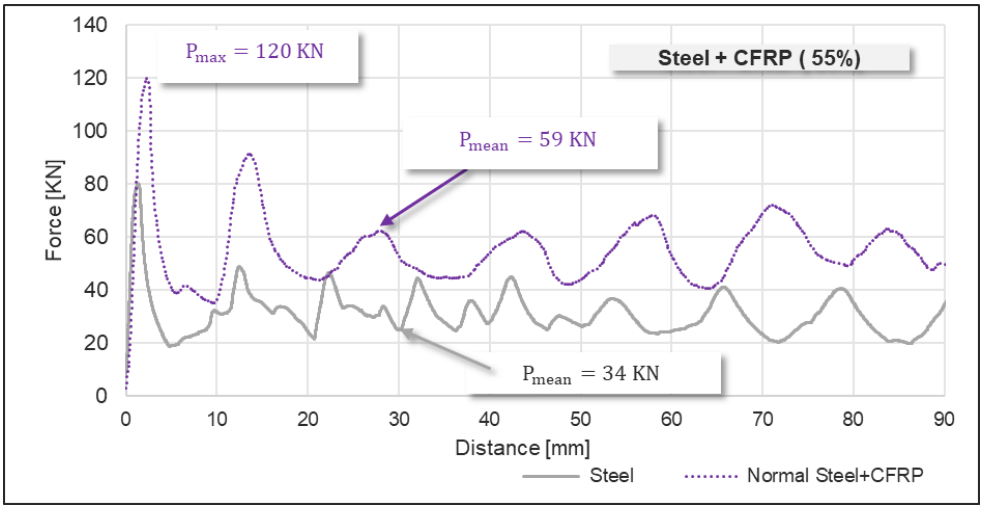

Figure 6-26: Compression results of interface sample (Normal steel + CFRP) with respect to steel tube.

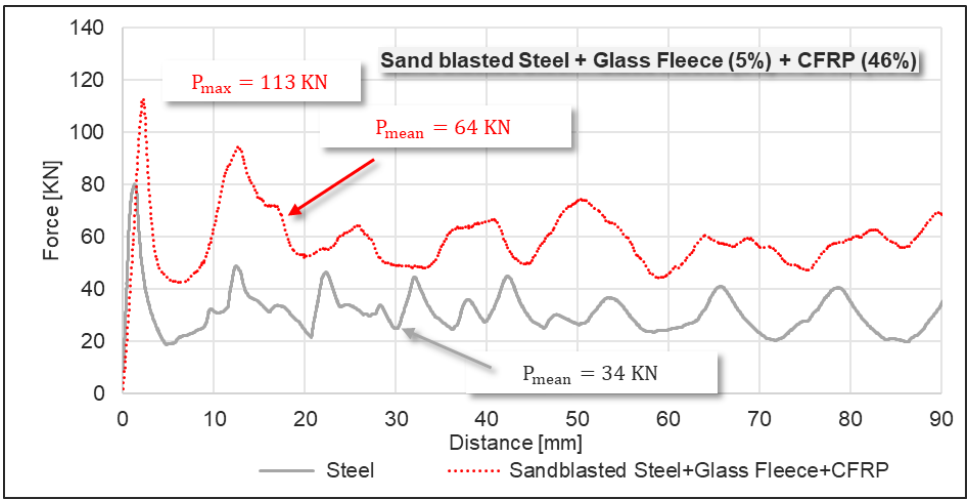

Figure 6-27: Compression results of interface sample (Sandblasted steel + Glass Fleece + CFRP) with respect to steel tube.

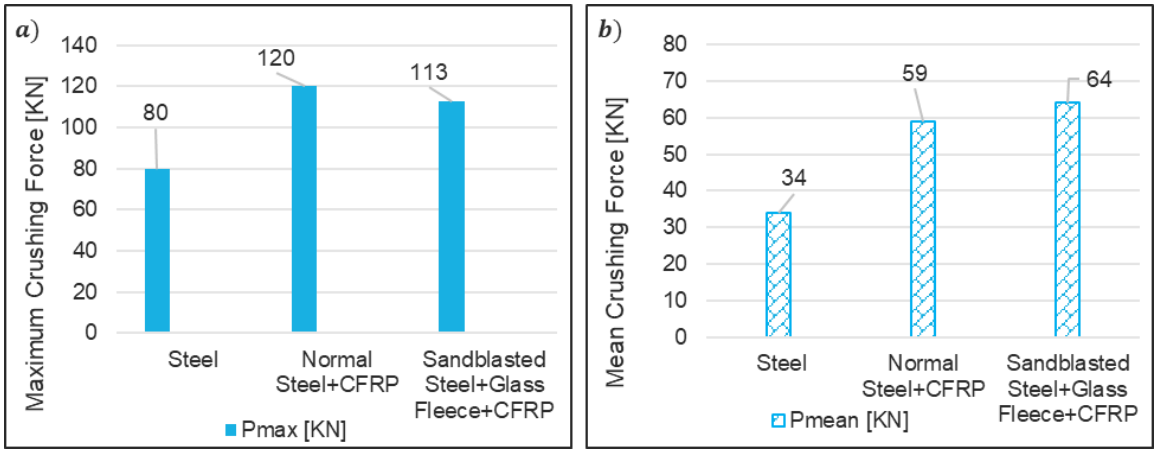

Figure 6-28: Maximum crushing force and mean crushing force of interface samples with respect to steel tube.

The important measurements for compression test are energy absorption and specific energy absorption that were calculated and listed in Figure 6-29. Based on the energy absorption and specific energy absorption values, it can be noted that 8 % higher specific energy and total energy absorption for modified sample when compared with normal sample. However, it was observed that the values of both normal and modified samples are same for some samples, which can be seen in the error bar calculated based on standard deviation. In order to compare these results with the steel tube, specific energy absorption was used as the mass of the steel tube is different from hybrid sample. In comparison with steel tube, the specific energy absorption has an increase of 89 % for hybrid samples. It can be concluded that the interface doesn't have any influence on the specific energy absorption or the total energy absorption. However, the specific energy of the hybrid sample can be increased significantly when compared with the steel tube.

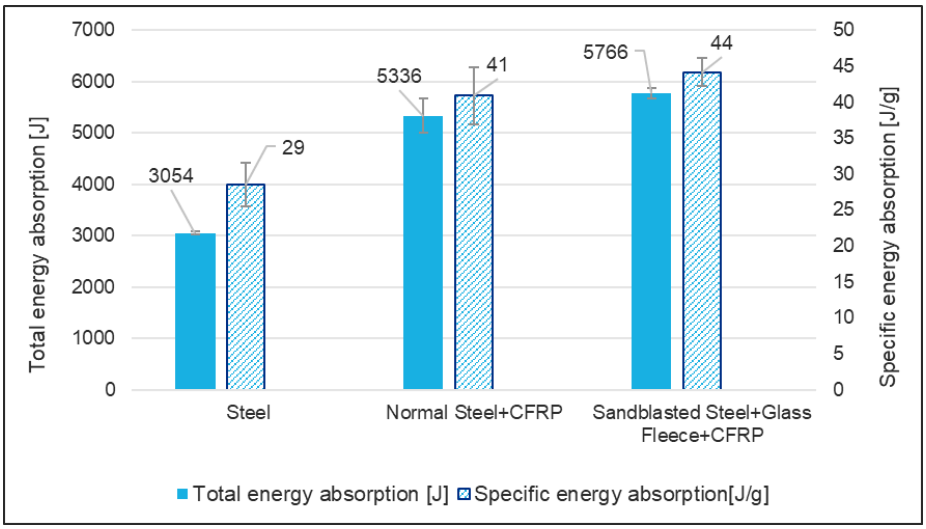

Figure 6-29: Total energy absorption and specific energy absorption of interface samples with respect to steel tube.

6.1.2.2 Torsion Tests

The torsional stiffness of the hybrid sample was determined using torsion setup based on the real load situation. A hydraulic rotary cylinder based on the double vane principle was used to introduce the torsional moment on the test samples. These valves can generate a torque of ±1,000 Nm at a torsion angle of ±50°. The structure of the torsion test setup consists of rotating cylinder equipped with an angle of rotation and torque sensor. The clamps and load introduction are connected to the test specimen by means of a force-fit with the aid of annular springs as shown in Figure 6-30. The left side of the samples are fixed, whereas the right side of the samples is subjected to twist which is controlled by the sensors and the cylindrical values. Quasi-static tests were performed at 5°/min, for both normal and modified sample and data was recorded as shown in Figure 6-31 and Figure 6-32. The points represent the data values recorded and the line represents trend line in Figure 6-31 and Figure 6-32. Torsional stiffness values of both hybrid samples are same with a small deviation of 3% in their value. A reference sample, which is made out of just steel was also used to perform torsion test. The torsion stiffness of the steel tube recorded is 324 Nm/deg, which is 35% less than both hybrid samples. To make sure if the experimental values determined are accurate, the torsional stiffness of the steel tube was

calculated using Equation 11 and Equation 12. Where K is the torsional stifness (Nm/rad); G is shear modulus (Pa); L is Length (m); J is polar moment of inertia (m^4); D is outer diamter (m) and d is inner diameter (m). The torsional stifness calculated for the steel tube was 18488 Nm/rad, which can be equated to 323 Nm/deg. The input values used to calcuate torsional stifness are, polar moment of inertai of 92,440 mm^4; Shear modulus of 70 GPa.

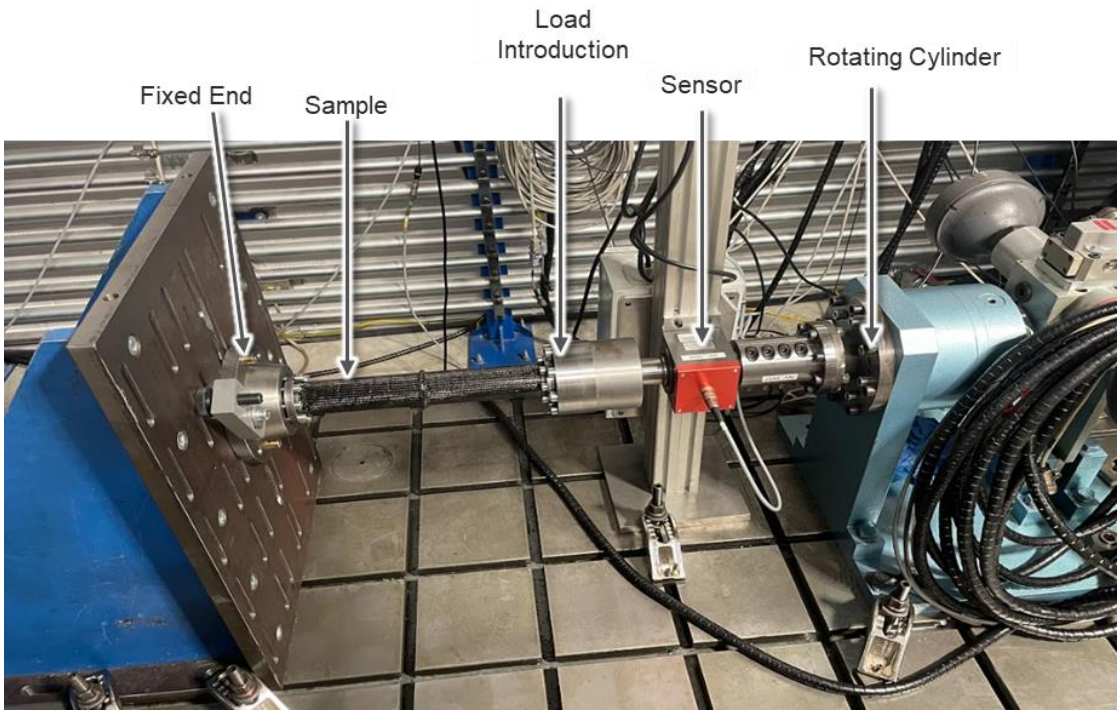

Figure 6-30: Torsion test setup for interface samples.

$$K = \frac{G\,J}{L} \qquad \textbf{Equation 11}$$

$$J = \frac{\pi}{32}(D^4 - d^4) \qquad \textbf{Equation 12}$$

Since there was not much difference between the normal and modified sample torsion stiffness, normal sample was used to perform a fatigue test using a cyclic load. Fatigue tests measure the materials resistance to damage and failure under application of repeated load along with determining the total number of load cycles for complete structural failure. Since the current proposed application is for drive shafts, which are under constant application of loads, characterizing its fatigue test is an important factor. A sinusoidal alternating load of ±700 Nm with a frequency of 10 Hz was applied. The fracture criterion was defined as a 15 % change in the peak values of the angle of rotation. Thus, failure could be detected independent of specimen and stiffness as shown in Figure 6-33. The sample reached the above-mentioned criteria at 17,680 and 18,194 cycles respectively. For both the samples, the failure occurred in the steel part of the hybrid section. Based on torsional stiffness, it can be concluded that change in interface doesn't have any influence on the torsional stiffness. In addition, the torsion stiffness of the hybrid sample has been estimated and compared with the steel shaft.

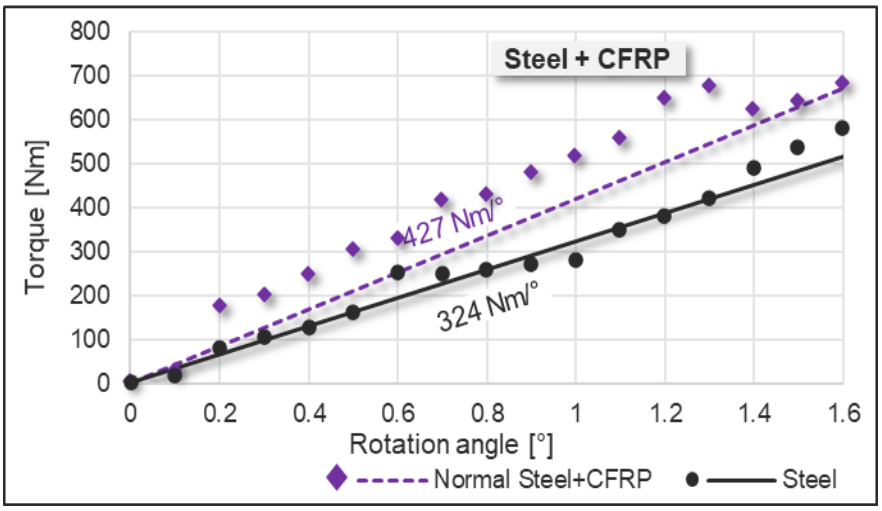

Figure 6-31: Torsion results of Normal sample (Normal steel + CFRP) with respect to steel tube.

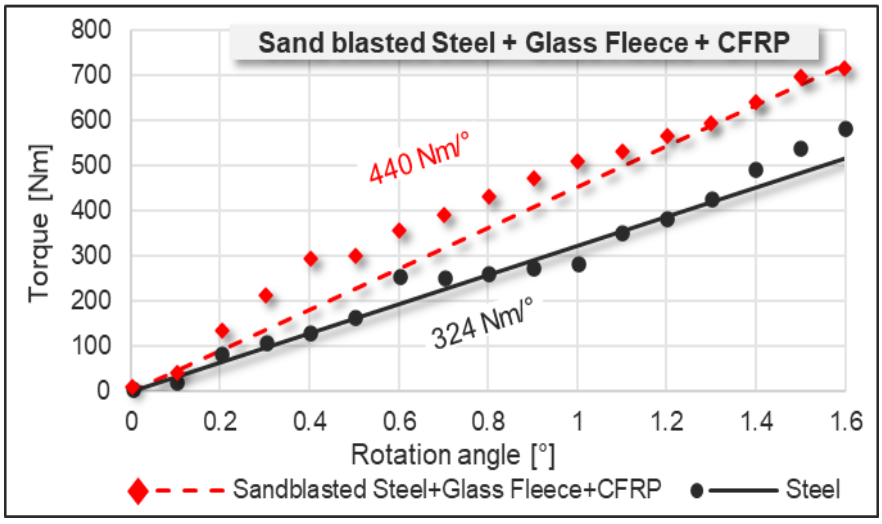

Figure 6-32: Torsion results of modified sample (Sandblasted steel + Glass Fleece + CFRP) with respect to steel tube.

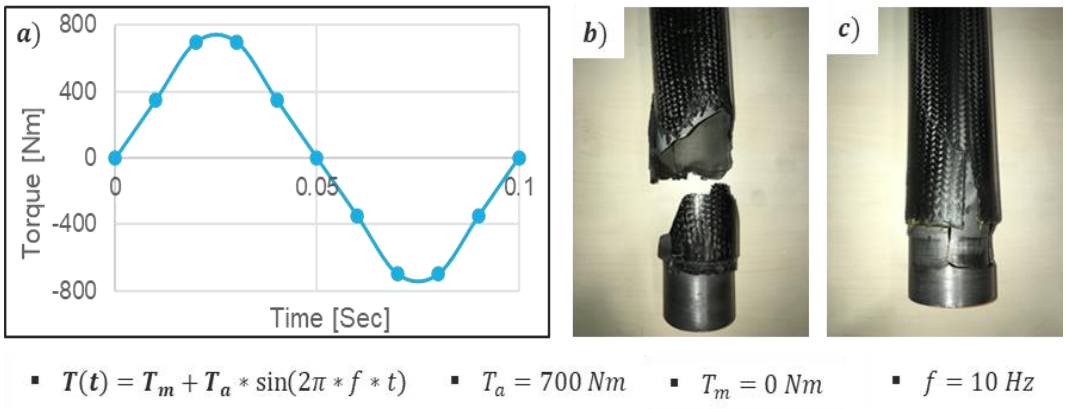

Figure 6-33: Fracture mode of sample based on Fatigue results and test input.

6.2 Self-Sealing Process

The second manufacturing process is based on Self-sealing process and is again divided into two stages. In the first stage, insulation material based Self-sealing process was studied. The objective here is to find the suitable parameters to seal the contour of the mold using the matrix itself. In addition, the influence of catalysts in the Self-sealing process was also investigated. In order to study the Self-sealing process in detail, a small mold (further referred to as 2D-mold) that can produce hybrid structures of 150 x 150 mm was used, which is based on insulation material type. This dimension represents one-half of the cylindrical shaft dimensions. The thickness of the sample was fixed to 3 mm and can be varied if necessary. Once the suitable parameters for the self-sealing process are determined using the 2D-mold, a hybrid shaft was produced with the same parameters using both insulation and cooling channel type based Self-sealing process. The hybrid sample was then tested for ILSS and compared with the sample that is produced via conventional sealing process if the sealing zone has any negative influence.

Two parameters are most critical for ensuring a fast curing in the sealing zone and thus ensure a reliable Self-sealing. These are the temperature in the sealing zone and the gap height. Both parameters determine the amount of energy that can be transferred to the resin in a given time. Combined with the injection pressure or the mass flow rate, the transferred energy per time and volume is given, which in turn determines the degree of curing per time. To quantity the process in an efficient way, a 2D mold was used as stated before that can produce hybrid plates as shown in Figure 6-34.

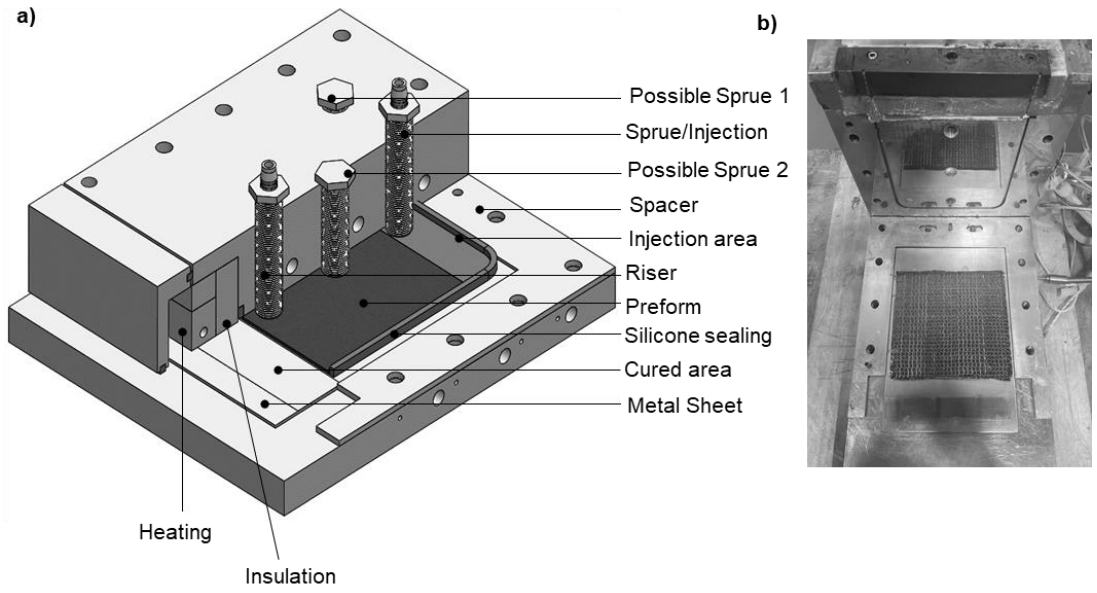

Figure 6-34: a) CAD model showing sectional view of the mold and b) 2D model based on Self-sealing process.

In order to prove that the general process parameters of the intrinsic RTM process can be adopted from the former study to the 2D-mold, a reference hybrid plate sample was produced using conventional sealing (polymer-based sealing) and tested for its ILSS value. The injection pressure was set to 5 bar, mold temperature to 120 °C and initial mass flow rate to 0.15 kg/min.

The sample was produced three times using the same parameters. The 2D-mold was designed so that light RTM can be used, where the resin was injected at one end and the out vent was located at the other end of the mold. Selected dimensions and process parameters thus represent one–half of the hybrid shaft mold. For ILSS tests, the sample was divided into three zones and three specimens are cut at each zone as shown in Figure 6-35. Injection zone is where the resin is injected and sealing zone is the furthest location possible from injection point. The ILSS for flat specimens were tested based on ISO 14130. This standard specifies a procedure for determining the apparent ILSS of fiber-reinforced plastic composites by the short-beam method based on Equation 13. Where, F is the failure or maximum load [N] that is determined by experiments; b is the width [mm] and h is thickness [mm] of the test specimen.

$$\tau = \frac{3}{4} * \frac{F}{b * h}$$ **Equation 13**

Similar to the hybrid shaft, the ILSS value near the injection zone is less when compared with the specimens at the center or at the outlet vent as shown in Figure 6-36. However, it can be noted that the values of center specimens are in the range of both injection and sealing specimens. To compare the ILSS value of the flat sample with the shaft sample, all nine specimens of a sample is averaged with results in a value of 17.8 MPa with a standard deviation of 2.6 MPa. The ILSS value of flat sample is 1.6% less than hybrid sample, which has an ILSS value of 18.1 MPa. This difference can be ignored as the standard deviation value of falt sample ILSS is higher that can offset the difference.

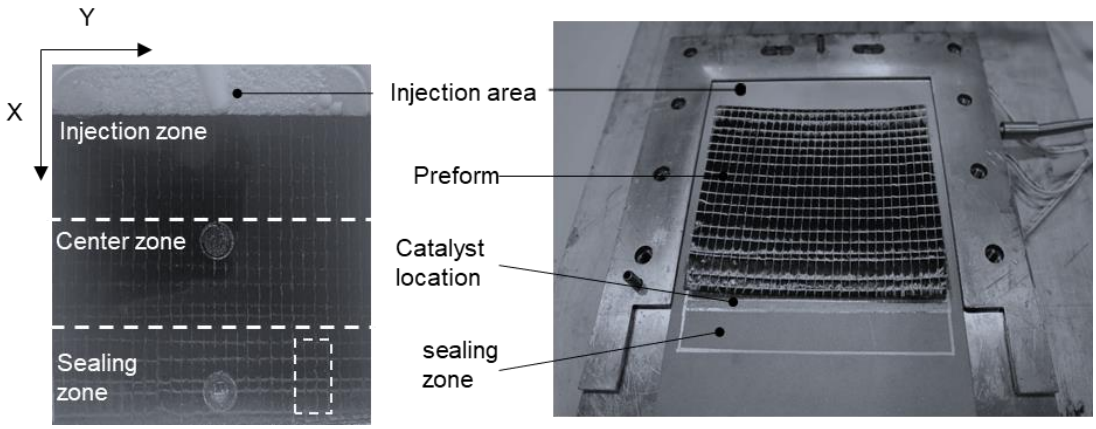

Figure 6-35: Closer view of various zones in mold with respect to sample location

After proving the adopted process parameters are suitable for the FRP production, the mold is modified so that the Self-sealing technique can be validated. Only one of four edges of the mold was modified to work based on Self-sealing technique, whereas other edges are sealed using conventional polymer sealings. The zone selected to equipe with Self-sealing process is opposite end of the injection point, which was referred as sealing zone. A steel component that is equipped by electric heating cartridges achieves a local higher temperature in the sealing zone. This steel component is mounted to the upper mold and allows the adjustment of its height respective to the distance between heating element and metal sheet that controls the gap height. Thermal

insulation is obtained using special material made from glass fleeces (K-Therm® AS 600M. In order to quantify the functionality of leakage, the area of resin flow beneath the gap in the self-sealing zone was measured using ImageJ software. In order to measure this area, the steel section of sample was extended in the direction of self-sealing zone to 220 mm from 150 mm as shown in Figure 6-37. The goal here is to stop the flow of resin within the heating zone of the self-sealing setup as shown in Figure 6-37. Additional 16 mm of resin leakage can be measured past heating zone as steel was further extended that is included within 220 mm as shown in Figure 6-37.

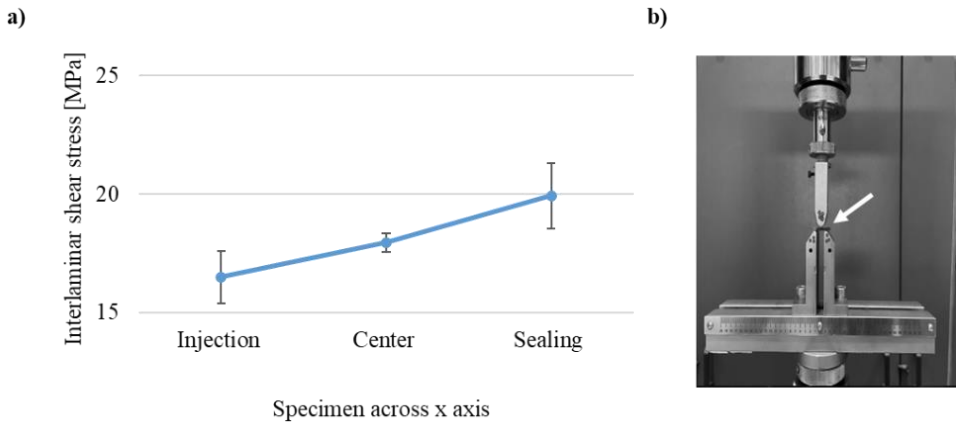

Figure 6-36: a) Standard deviation along with ILSS across X-axis and b) Test fixture with respect to specimen used for present study, the arrow indicates the specimen.

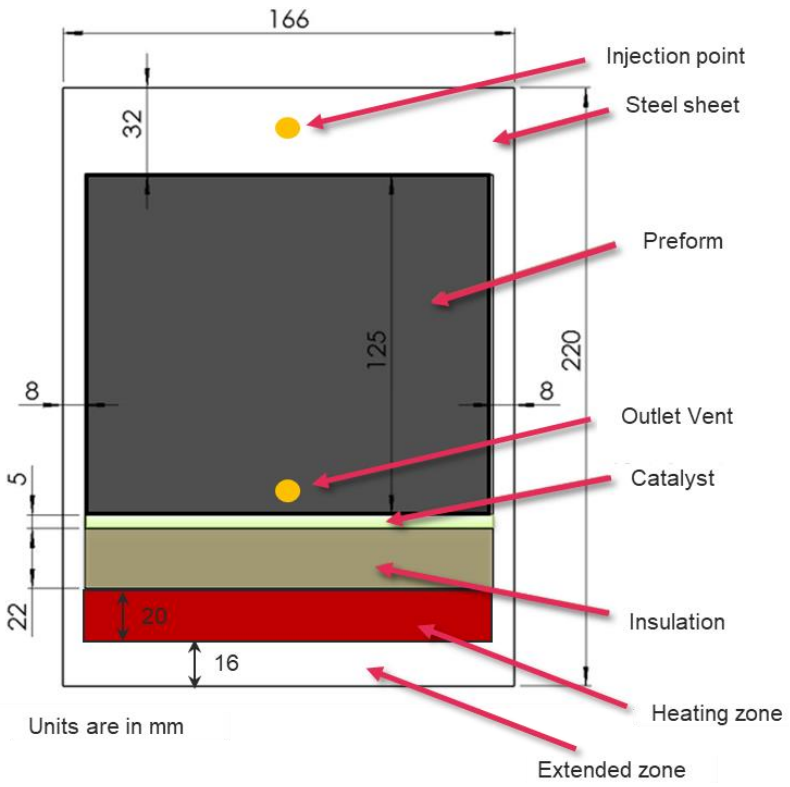

Figure 6-37: Schematic diagram showing various zones on the sample surface with respect to Self-sealing process of 2D mold.

At first, a sample was produced by maintaining the sealing temperature same as production temperature, which is 120 °C and a gap height of 0.1 mm without catalyst. Production parameters are same as the reference sample produced early, which has injection pressure of 5 bar, mold temperature of 120 °C and initial mass flow rate of 0.15 kg/min. The sealing completely failed as the resin covered the entire heating element and insulation materials as shown in Figure 6-38a. In the next step, the sealing temperature was increased to 160 °C. In this case, the flow of resin partly stopped within the extended area, thus showing an increased curing rate compared to the temperature of 120°C. The border to which the resin flows is marked by a red line in Figure 6-38b. Same result was observed when the temperature in sealing zone was increased to 200 °C as shown in Figure 6-38c. However, when the sealing temperature was set to 240 °C, 83% of the area was sealed within 5 mm of the extended zone, which is close to heating zone as shown in Figure 6-38d. For the next step, 5% of DABCO catalyst was added at the sealing zone near the insulation material and better sealing was observed within heating zone as shown in Figure 6-38e. Considerably, 78% of area can be sealed with this parameter in Self-sealing zone. In a further step, the sealing temperature was slightly increased to 250°C without catalyst. In this case, the resin flow was completely stopped beneath the sealing zone, proving the self-sealing process to work as intended as shown in Figure 6-38f. Similar results were observed by adding 5% of DABCO catalyst at sealing temperature of 250 °C, i.e., 100% sealing within heating zone. Likewise, for a sealing temperature of 260 °C, 100% sealing within heating zone was observed in both cases i.e., with and without DABCO catalyst. Finally, the gap height was increased to 0.2 mm, maintaining the sealing temperature of 260°C. In these cases, the resin flows through the heating zone and even the extended zone resulting in a complete failure even with adding of 5% DABCO. This effect can be related using Equation 9, which is influenced by amount of resin cured in the sealing zone. In the case of 0.1 mm of gap height, the amount of energy needed to cure is 68 J, which is doubled in case of 0. 2 mm of gap height that was calculated to be 129 J. However, at the same time flow rate increases, which requires more than 138 J for sealing. These values are calculated by assuming that the entire heating zone is filled with resin system. Table 27 shows summarizes the sealing zone parameters and their % of sealing area.

In order to check if the sealing zone has any influence on the interface of hybrid structures, ILSS was used to evaluate. Figure 6-39 shows the results of the ILSS value measured for samples produced using conventional and Self-sealing process. It can be observed that the ILSS values are not affected by the new self-sealing process as the difference observed was only 2%. This difference can be ignored if the standard deviation is considered, which is 3% for both types of samples.

In conclusion, the self-sealing process was validated using the 2D mold and can be transferred to the mold that produce Hybrid shafts. It can be noted that if the temperature of 240 °C is considered, then catalyst should also be used. In the case of 250 °C as sealing temperature, catalyst influence is negligible. Since applying catalyst in hybrid shaft mold is difficult, the sealing temperature was set to 250 °C.

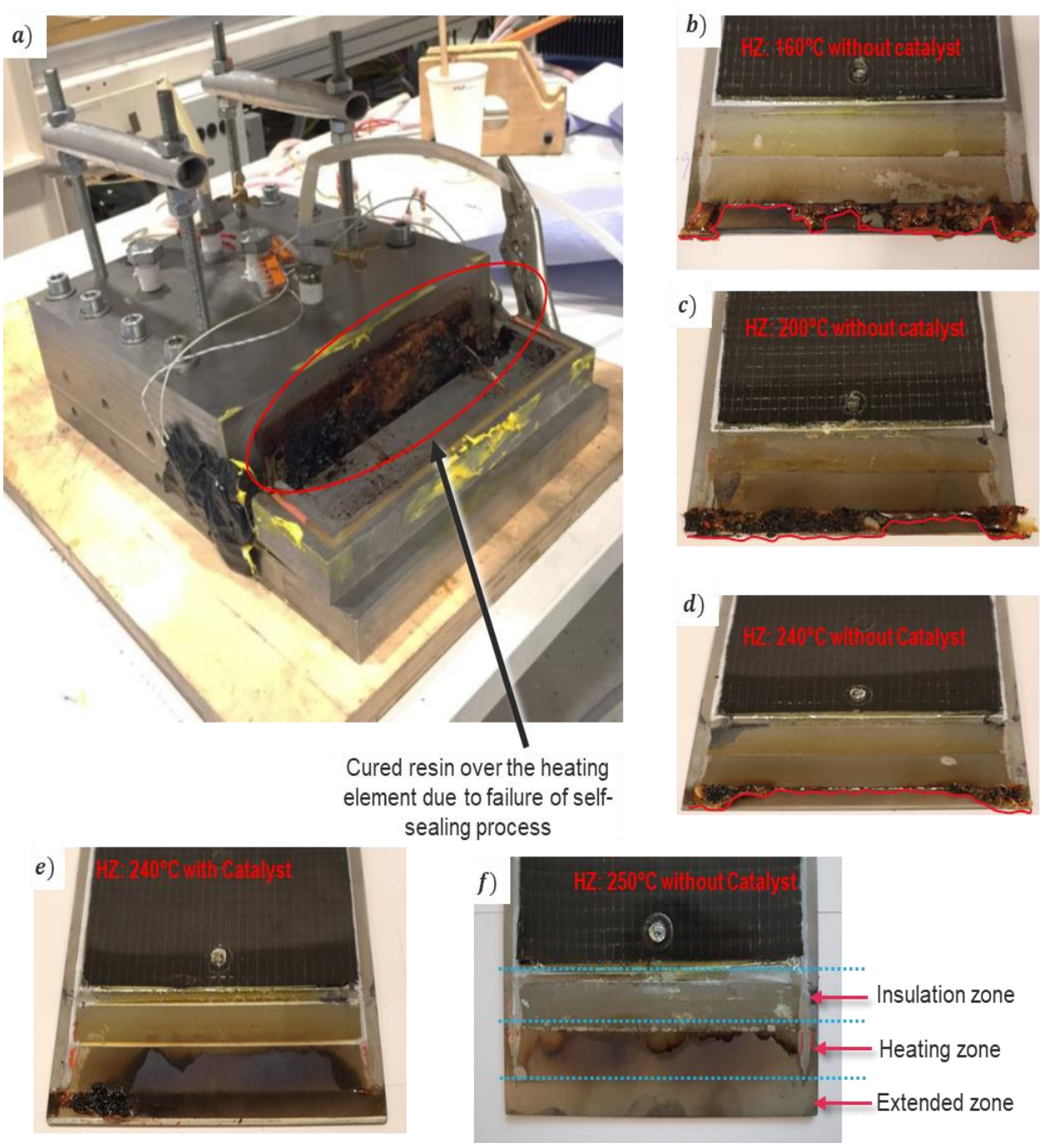

Figure 6-38: 2D mold leakage during self-sealing process along with resin flow area in the self-sealing zone. **Note:** The area marked is done only after 10 min of injection time.

Table 27 : Self-sealing sample's parameters and amount of area sealed in self-sealing zone.

Gap Height / mm	Self-Sealing Temperature / °C	Catalyst / DABCO (5%)	Sealed area
0.1	120	NO	0%
		YES	0%
	160	NO	0%
		YES	0%
	200	NO	0%
		YES	0%
	240	NO	0%
		YES	80%
	250	NO	100%
		YES	100%
	260	NO	100%
		YES	100%
0.2	250	YES	0%
	260	YES	0%

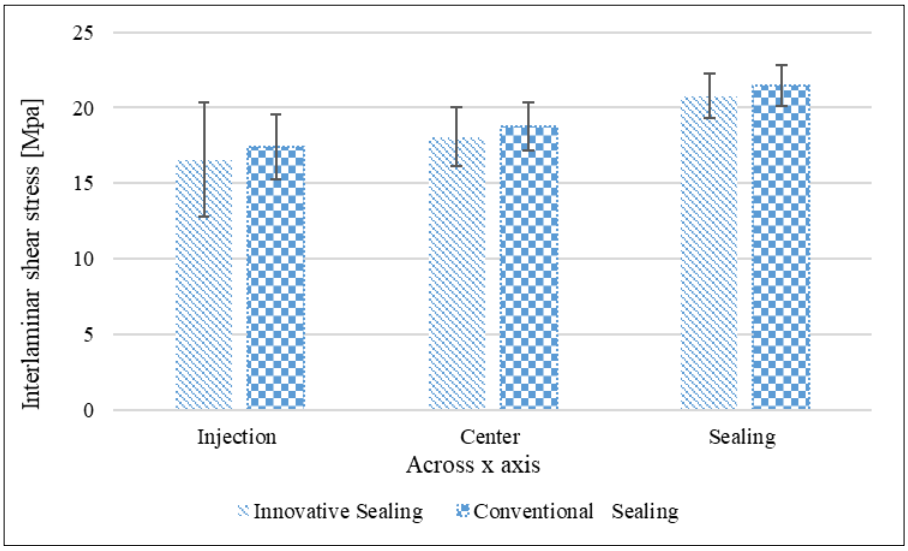

Figure 6-39 Interlaminar shear strength of sample produced via 2D mold using self-sealing and conventional sealing.

6.2.1 Producing Hybrid shaft using Self-sealing based on Insulation

The mold was modified using the second insert to validate the self-sealing functionality on producing hybrid shaft. The modification was done similar to 2D mold such that, three contours of the cavity were sealed with silicone seals, while the fourth contour is equipped with a heating element that works based on the self-sealing process as shown in Figure 6-40. The self-sealing area has a gap height of 0.1 mm that was measured using gauge tapes. The gap height is the zone where the epoxy flows and is cured that seals the mold.

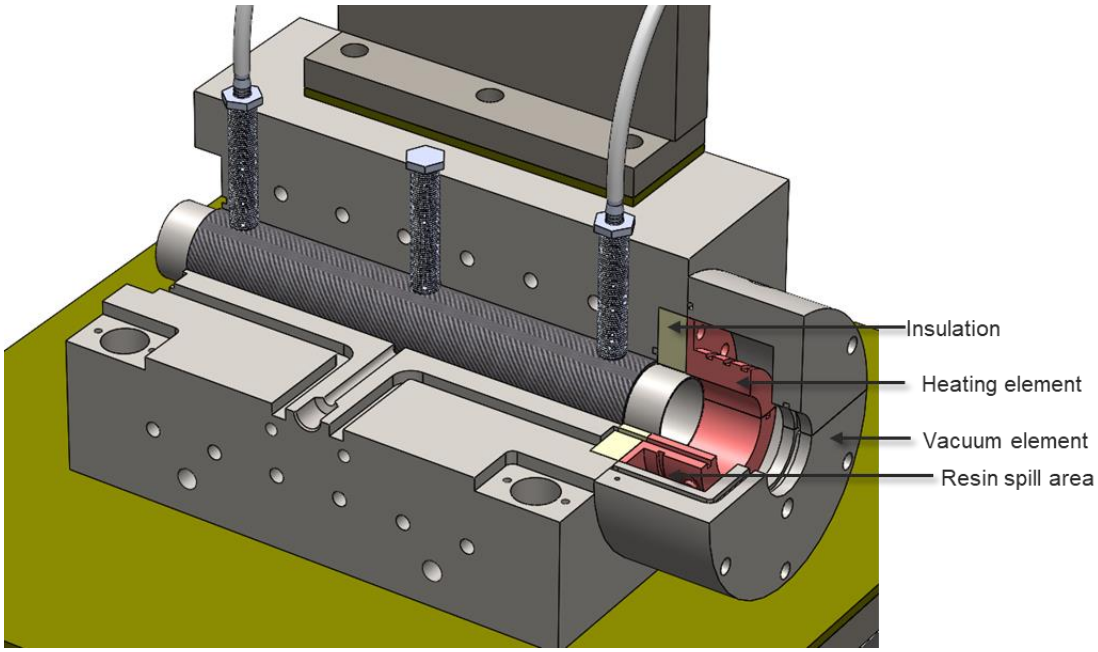

Figure 6-40: Schematic diagram showing self-sealing based on insulation material.

Thermal insulation was installed between the cavity and the heating element to avoid the heat transfer to cavity as it affects the curing process. An additional component was installed over the entire self-sealing zone to obtain the vacuum and it was designed in such a way that it collects the epoxy in case of sealing failure preventing the contamination of surroundings as shown in Figure 6-40. Before production, the mold was tested experimentally for transient state thermal analysis as shown in Figure 6-41. In addition to mold thermocouples, three thermocouples were connected to the outer surface of steel tube sample that are located 120 ° apart from each other at the center of the heating element. The top mold has one measuring point, whereas bottom mold has two measuring points. Figure 6-41b shows the results recorded for three thermocouples. After 38 minutes, a temperature of 250 °C was recorded for all the measuring points. The test was run for an additional 7 min during which the temperature at all three points was homogeneous with a tolerance of ±5 °K.

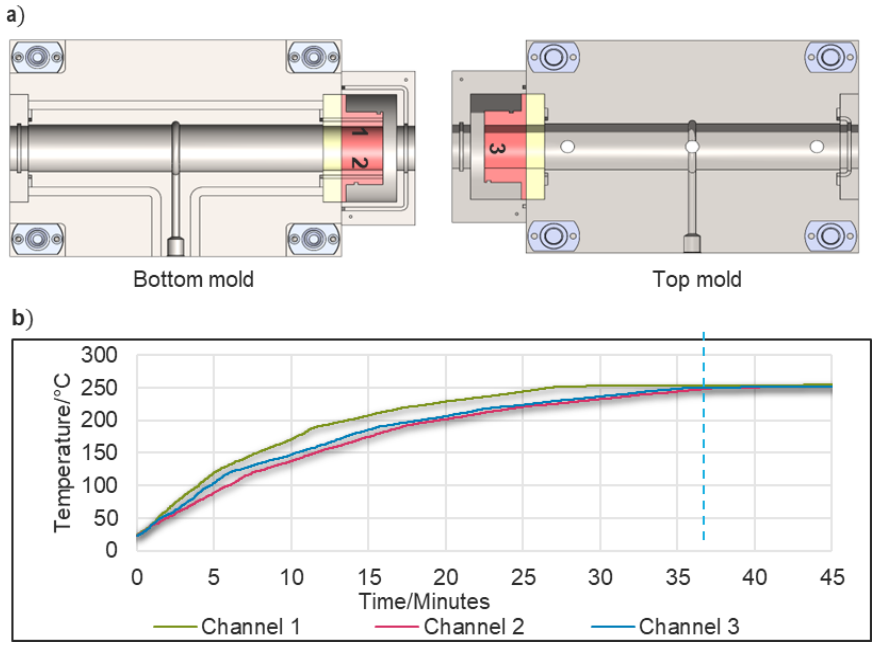

Figure 6-41: Experimental thermal analysis of the insert type 2 with respect to mold a) Thermocouple 1,2 and 3 location on the mold surface and b) Graph of temperature VS time on the surface of the sample.

Similar to flat hybrid parts, the steel part of the hybrid shaft sample has been extended to 410 mm instead of 340 mm. The extension of length is necessary to quantify the efficiency of the self-sealing and compare with similar samples. The amount of resin deposited in the heating zone of Self-sealing is used to express the efficiency of the self-sealing process. The amount of resin was considered based on area rather than volume meaning one of the directions, which is height of resin was ignored for easy study.

Figure 6-42 shows a contour plot, indicating the resin flow length depending on the circumference position. The area of resin flow can be calculated by integrating these curves.

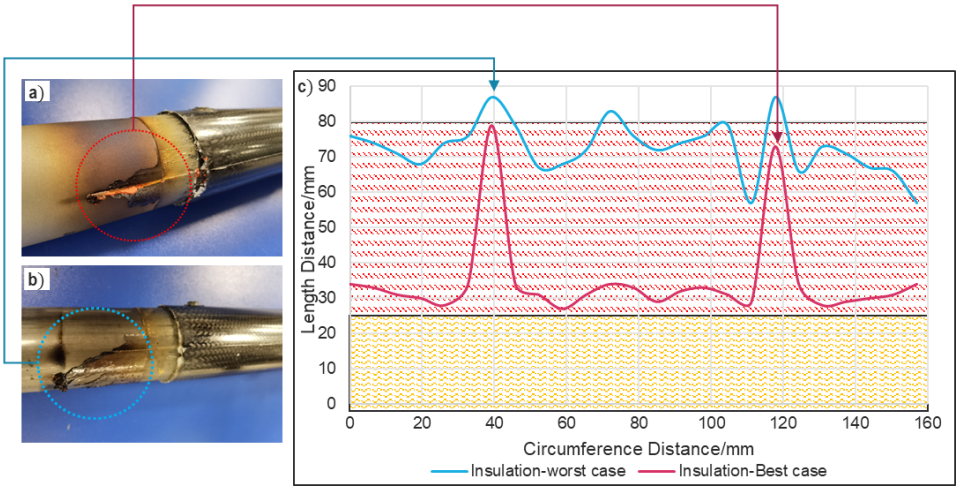

Figure 6-42: Leakage profile near Self-sealing technique a) Best possible sealing b) Worst possible sealing and c) Resin flow along length with respect to circumference distance

A total of nine hybrid samples were produced using Self-sealing via VA-LRTM. The sealing profile of all nine hybrid samples were never the same, even though the production parameters were kept constant as shown in Figure 6-43. The leakage area calculated ranged from 1556 mm^2 to 7527 mm^2 that can be equated to a range of 15% - 71% of total area available at the heating zone. However, for all nine samples, the main leakage was always spotted near the upper and lower mold intersection i.e., near the two halves of the mold. This phenomenon can again be explained using Equation 11, which gives the relationship between amount of epoxy and energy required to cure. At the two halves of the mold, the sealing zone components are also split into two, which provides a secondary path for the resin to flow as shown in Figure 6-44. Due to this, the amount of epoxy at the two halves of mold is more than the rest of the self-sealing zone, which requires more energy to cure. This issue can be addressed by replacing it with a single part heating element of the Self-sealing zone rather than two halves, which is addressed in chapter 6.2.2. Another major defect has been spotted at the insulation zone of the Self-sealing process. Figure 6-45 shows the insulation material before and after eight production cycles. It can be noted that the side facing the mold is highly contaminated due to epoxy filling the highly porous glass fleece affecting its thermal behavior. The epoxy infiltrated ~25 % of the insulation material and reached the bottom end that was not supposed to come in contact with epoxy as shown in Figure 6-45.

Figure 6-43: Leakage profile of the hybrid shaft samples produced via self-sealing process based on insulation. **Note:** The red line indicates the border of resin flow.

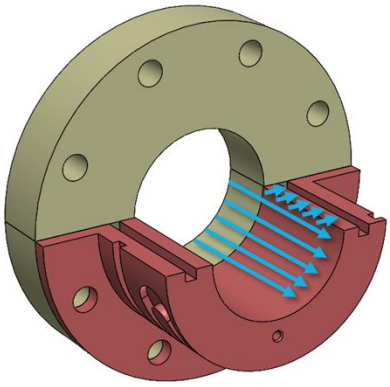

Figure 6-44: Possible flow directions of resin in Self-sealing process based on insulation.

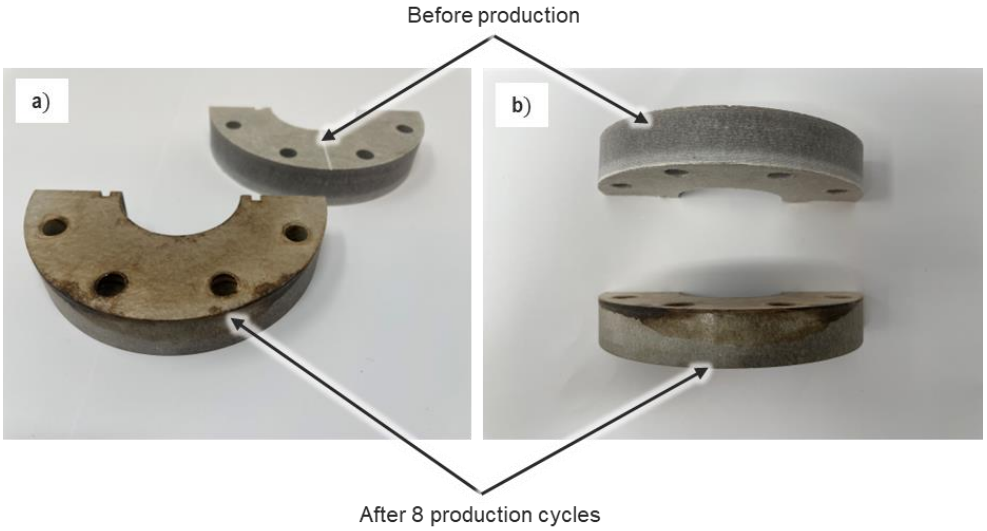

Figure 6-45: a) Side view of the insulation material contamination and b) Bottom view of the insulation material contamination.

ILSS tests were carried out to check the influences of Self-sealing on the mechanical properties of the hybrid shafts. In order to keep all the parameters same, three samples based on interface 4 (sand blasted steel + glass fleece + CFRP) was produced and tested as shown Figure 6-40. Here the left side of the sample represents the conventional sealing, whereas the right side represents the Self-sealing. The sample was cut into 20 specimens, the same as before and tested. Figure 6-46 shows the results of ILSS tests. It can be noticed that there is no significant negative influence on the sample with respect to insulation based Self-sealing and traditional sealing. Therefore, it can be concluded that Self-sealing can be used in manufacturing line, but the above-mentioned issues should be addressed.

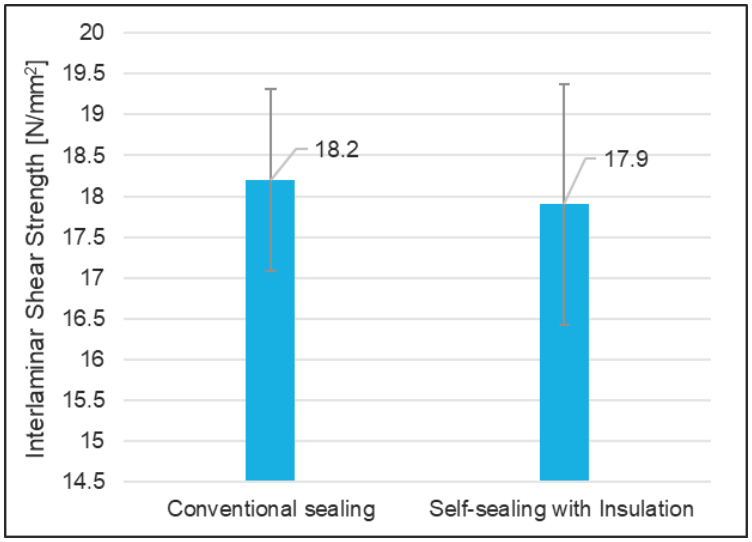

Figure 6-46: ILSS results of hybrid shaft manufactured using conventional and Self-sealing.

6.2.2 Producing Hybrid shaft using Self-sealing based on Cooling Channel

To further optimize the self-sealing and address the issue of insulation material contamination, a new component has been designed and manufactured via AM. Figure 6-47 shows the CAD model of the prototype with integrated cooling channel. As stated before, the entire self-sealing zone is made out of one part rather two halves. With the help of cooling channels, the heated area can be cooled fast, which is not possible with the use of insulation material. The main goal of the new prototype component is to fulfil the functionality of both heat sink and the insulation and a simple integration into the existing VA-LRTM mold without any modification to mold. The functionality of the heat sink is to cure the resin in a defined area with a temperature as high as 250 °C and the cooling channel must prevent the dissipation of the temperature into the mold. The temperature of the mold should not increase more than 120 °C as stated in previous sections. The functionality of heat sink mainly depends on the material´s thermal conductivity and its density. The easiest way to raise the temperature of the material is to use heating cartridge, which is the current selection. The geometry of the prototype is divided into three sections as shown in Figure 5-10, where C represents the cooling channel area, H for adding the heating cartridge and L for the lattice structure. To reduce the heat transfer and increase the efficiency, a lattice structure was designed on other side of the prototype component as shown in Figure 5-10.

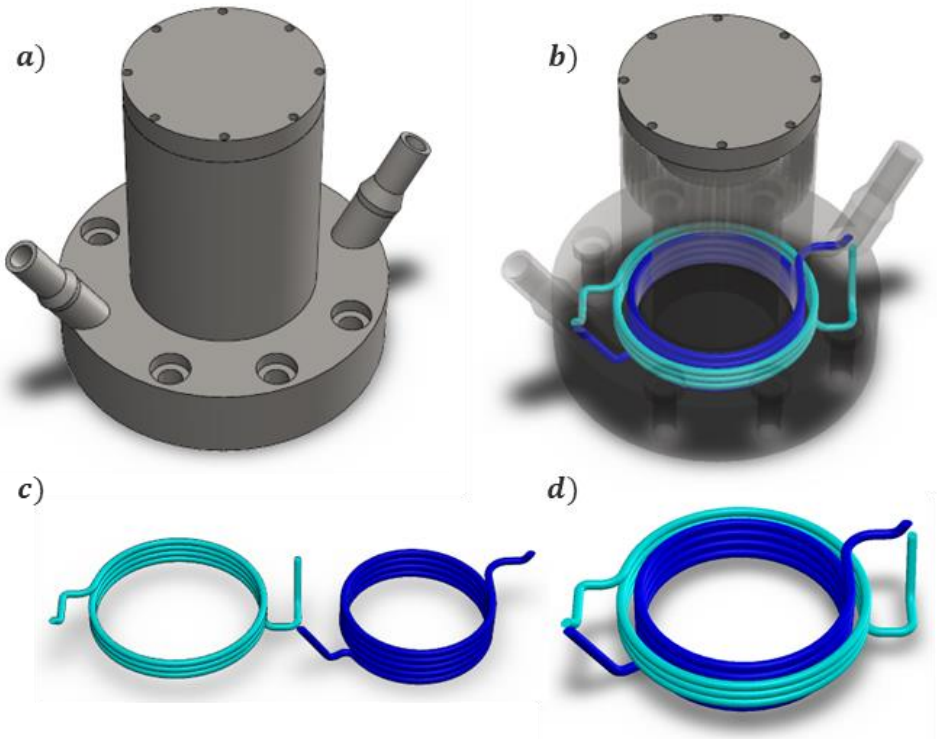

Figure 6-47: a) CAD Model of AM prototype b) Cooling channel location in the AM prototype c) CAD mold showing both cooling channels separately and d) Cooling channels configuration.

Selection of cooling channel dimensions is the first step for validating the functionality and adjusting the design before production. The diameter of cooling channel was fixed to 3 mm as more than 4 mm requires support, which will be challenging for support removal. Supports are

extra structures used in 3D printing process that supports the structures overhanging, which needs to be removed after printing. Improper removal of supports may create rough surface resulting in high resistance that may lead to high backpressure during water flow. Two channels with a length of ~900 mm run in opposite directions to each other in order make the cooling effect homogenous. Theoretical calculations for cooling channel length were carried out with an assumption that the cooling channel can dissipate the entire energy generated by the heating element with a water flow rate of 7.5 L/min using Equation 14. Where α is the heat transfer coefficient, A is the area of heat transfer, and ΔT is the temperature difference from wall to fluid. However, such an approach will result in preventing the heating element to reach 250 °C that can be adjusted by reducing the water flow rate using regulator valve that can change the water flow rate during the experiments. Figure 6-48 shows the CAD model of the mold integrated with cooling channel.

$$L = \frac{\dot{Q}/_4}{\alpha * U_{Halbkreis} * \Delta T}$$ **Equation 14**

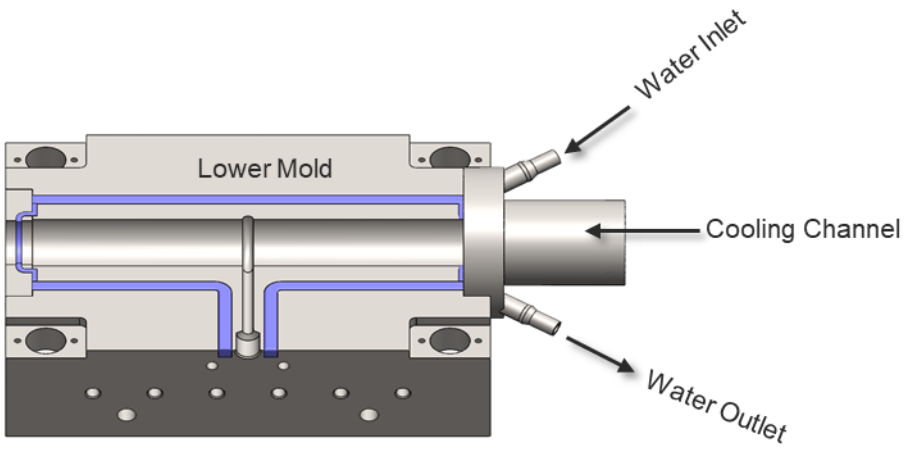

Figure 6-48: CAD model showing the Mold integrated with AM printed prototype based on self-sealing concept at one end and the other end with traditional sealing insert.

Selection of suitable material for printing the prototype is an important step as the prototype should have the same thermal properties as the mold. The material selected for the prototype is Tool Steel 1.2709 that has the thermal conductivity in the range of 15-20 W/m-K whereas the mold thermal conductivity is ~15 W/m-K. This material should fit into mold without any issues related to thermal expansion during a rise in temperature. The manufacturing of the prototype component was successful, and no support was used during the production stage. The produced prototype was milled on the surface that is in contact with the mold to have smooth surface for use of sealing to get vacuum. The integration of the prototype into the mold was achieved as

shown in Figure 6-50. Before producing a hybrid shaft to validate the process, the water flow rate in the cooling channel should be selected. A special valve was used to regulate the water flow into the cooling channels in order to achieve the required temperature. The water flow valve, also known as water flow regulator, can adjust the flow of water from 1 to 8 liters per min. It was concluded experimentally that water flow rate of 2 L/min is optimal for reaching the temperature of 250 °C at sealing zone and 120 °C in the production zone of the mold as shown Figure 6-49. The same technique as before was followed to check the temperature at the heating zone. Four thermal couples were attached to the steel tube and placed under the mold and closed for the thermal trials. The location of thermocouples is at the center of the heating zone and separated by 90 °each. Both water flow and heating were turned on at the same time. For 3.5 L/min, the heating zone didn't reach 250 °C in 60 minutes which is double the time in comparison with insulation based Self-sealing. Later the water flow rate was changed to 2 L/min as that's the minimum flow rate of the building water system. After 50 min, the sealing zone reached 250 °C which is our required condition. The outlet water was measured to be 18 °C in comparison with inlet of 15 °C. However, this is not always the same as the inlet water temperature changes depending on the environment conditions and if the water inlets at other locations are open as this works on central system.

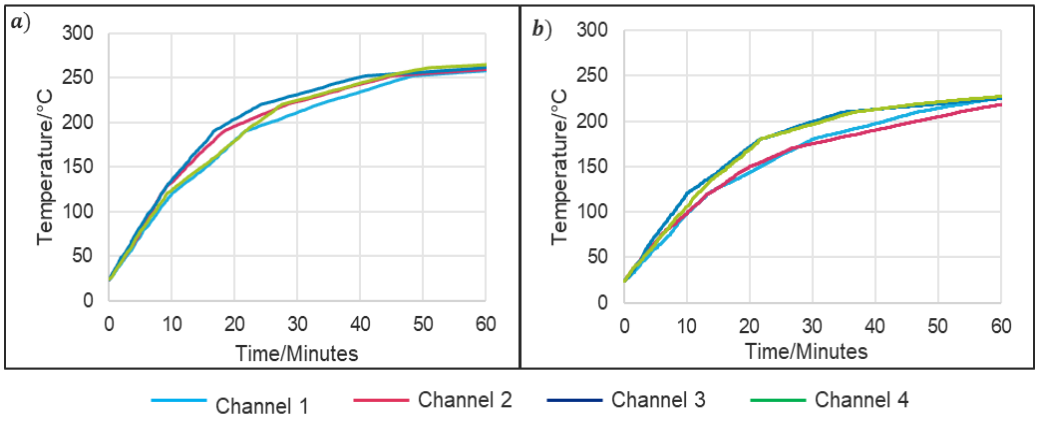

Figure 6-49: Thermal profile of the heating zone for water flow rate at a) 2 L/min and b) 3.5 L/min.

To validate the AM prototype functionality for the self-sealing process, six hybrid shafts were produced. For comparison with existing setup, the AM prototype component was integrated to the left side, whereas the insulation based Self-sealing is equipped on the right side as shown in Figure 6-50. Three more samples were produced with AM prototype on the left side and a traditional sealing on the right side.

The demonstrator planned to validate is based on interface 4 hybrid shaft where steel is sand blasted, and a glass fleece is used between steel and CFRP. For the AM side the resin flows to maximum distance of 6 mm under heating area, whereas on the insulation-based sealing, the resin flows up to 35 mm. Figure 6-51 shows the resin flow front for both cases. To check if the Self-sealing based on AM prototype has any influence on mechanical properties, ILSS test was carried out based on the setup used previously. Figure 6-52 shows the results of the samples for ILSS. It can be noticed that there is no significant negative influence of the AM-prototype component with respect to insulation based Self-sealing and traditional sealing. Therefore, it can

be concluded that the AM prototype component does not have any negative influence on the manufacturing process making it a suitable replacement for the existing sealing material making it cost-effective with achieving a step closer to automatic process.

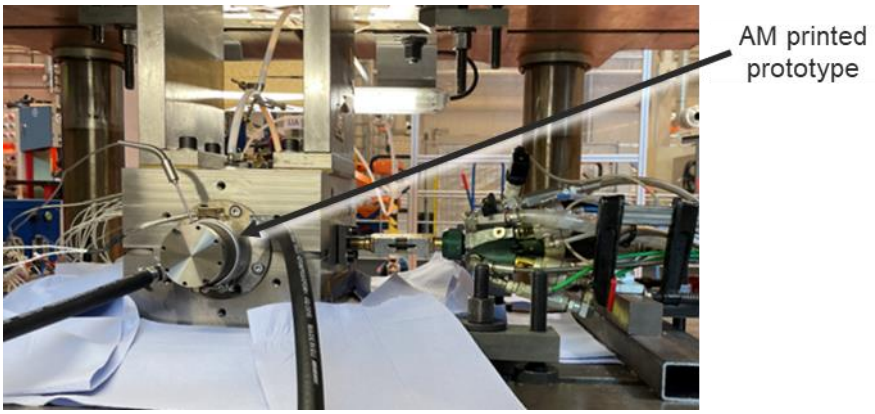

Figure 6-50: Mold setup with prototype component installed into the mold.

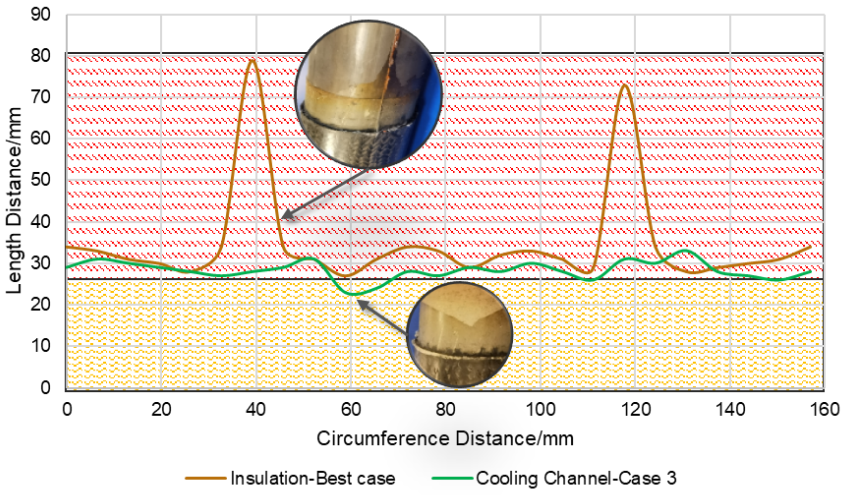

Figure 6-51: Resin profile in the Self-sealing zone for insulation setup and cooling channel setup; Yellow area indicates the insulation/cooling zone; Red area indicates the heating zone.

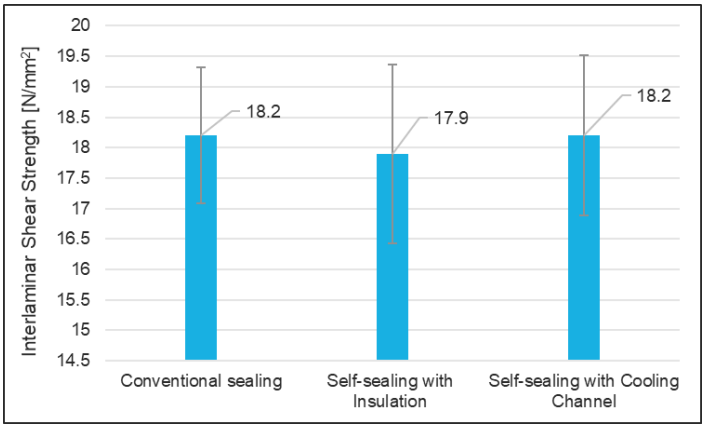

Figure 6-52: ILSS results of hybrid shaft manufactured using various sealing setup.

6.3 In-Mold Cleaning Process

The third process is not a manufacturing process, but it does influence the manufactured sample quality. In the third process, a method to clean the mold at the press itself was carried out. For this process, two different cleaning solutions were used with their respective input parameters. Hybrid samples were produced using the same process parameters before and after each cleaning process and then tested for ILSS to evaluate its influence factor on mechanical properties.

The surface of the mold is highly contaminated after producing parts for the previous studies as shown in Figure 6-53. Mold needs a maintenance procedure that involves cleaning and polishing. In order to evaluate the effect of the cleaning process, besides roughness measurements of the tool surface, also hybrid samples were produced before and after the cleaning process. In the traditional ultrasonic procedure, the entire mold will be moved to the ultrasonic station where electric connections and corrosive elements are removed. The mold is then placed in a tank with cleaning solution and the ultrasonic procedure is initiated for the entire mold. However, in the current concept, the cleaning takes place just for the cavity that is contaminated rather than the entire mold as in traditional method. A few important considerations were drafted as follows.

- Suitable ultrasonic transducer should be selected that fits into the mold cavity without major modification to the mold
- Mold along with the cleaning setup should be sealed so that there won't be any leakage of the cleaning solution as the electric connections are still connected to the mold to activate the cleaning solution using temperature
- Selection of inlets and outlets strategy for pumping cleaning solution and water into the mold

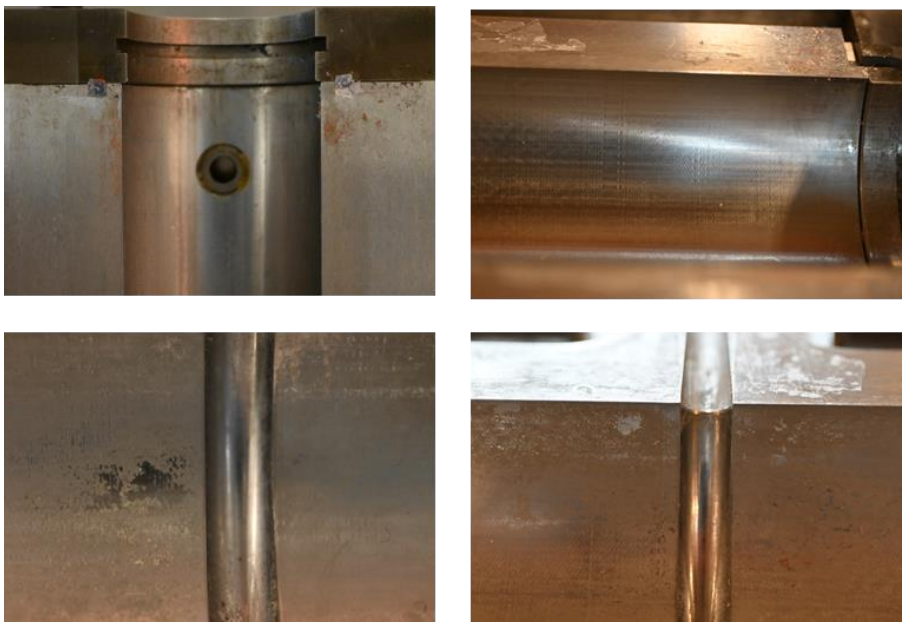

Figure 6-53: Image showing few spots on mold surface with contamination.

As per the first step, few commercially available ultrasonic transducers that can be a potential fit for the existing mold were listed as shown in Table 28. It was recommended to have a minimum distance of 10 mm from ultrasonic transducer and the surface of the mold to avoid damage. The outer diameter of the mold cavity is 54 mm that results in excluding both SP06-30A/30B-HD as it fails to maintain minimum distance. The other three ultrasonic transducers fulfill their minimum distance requirement, but they vary in length. The length of the mold cavity is 427 mm and SP07-40-HD is the closest one with a length of 418 mm, which thus was selected for studying the cleaning process as shown in Figure 6-54.

Table 28: Dimensions of various ultrasonic transducers.

No.	Type	Diameter / mm	Length / mm	Frequency / kHz
1	SP03-40-HD	30	228	40
2	SP05-40-HD	30	292	40
3	SP06-30A-HD	38	298	30
4	SP06-30B-HD	38	381	30
5	SP07-40-HD	30	418	40

The mold setup is modified with insert 4 at the ends. One end has an insert that acts as a clamp to hold the ultrasonic transducer and the other end has an insert equipped with an outlet one way pressure valve for evacuating the cleaning solution and water from the mold after the process. The inlets for cleaning solution and water are connected to the existing connection that are used to evacuate the gases during production stage. Since the mold works based on vacuum, the existing sealings are suitable to prevent the leakage during cleaning stage. To verify the sealing reliability, a test run was performed by filling the entire mold with water under 7 bar pressure and no leakage was observed. The mold has heating cartridges at various locations that can be used to heat up the cleaning solution for better efficiency. After the sealing check, the entire mold was prepared for cleaning process. The mold is closed with transducer placed in the cavity. After the mold is closed, the cleaning solution is injected into the mold.

Two different iterations based on two different cleaning solutions were used with respect to their process parameter. Table 29 shows the parameter used for the first cleaning solution which is based on Citric acid. As per the calculations based on the volume of the cavity when transducer is placed, approximately 0.5 liters of solution can fit that was injected into the mold. The mold is heated to 70 °C and maintained for 30 min for activating the cleaning solution as this increases the ultrasonic step efficiency. After 30 min, the ultrasonic is switched on for another 30 min while maintaining the temperature with a frequency of 40 HZ with a power of 700 watts. The cleaning solution is collected in an empty canister using a vacuum pump with a pressure of 1 bar after the process. The mold is then rinsed with water of pressure 6 bar and the contamination is collected for safe disposal. To evaluate the cleaning method efficiency, the mold surface roughness is measured at various locations.

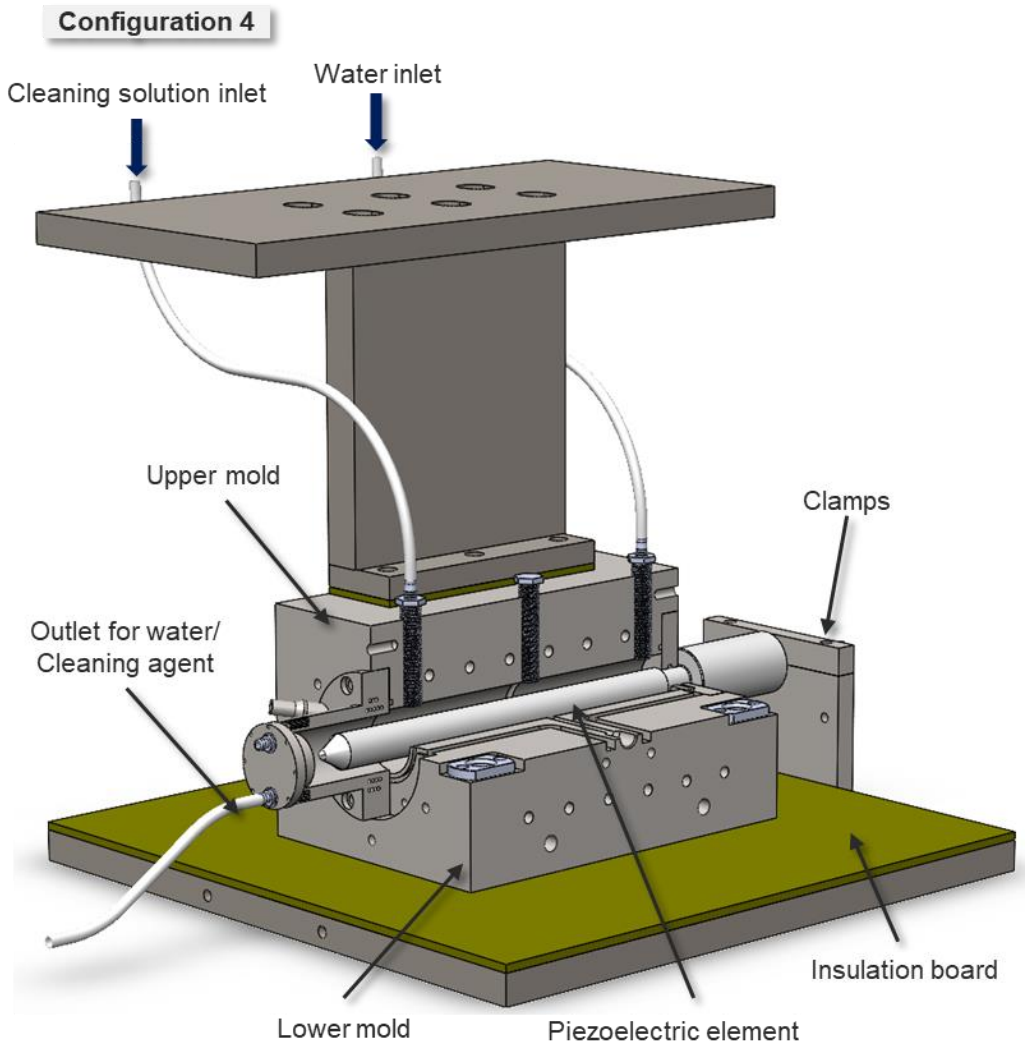

Figure 6-54: CAD model showing the mold integrated with SP07-40-HD ultrasonic transducer (cross-sectional view).

Table 29: Iteration 1 parameters used for cleaning procedure.

No.	Parameter for Iteration 1	Values
1	Cleaning Solution (Citric acid + Acetone)	1 Mol Citrix acid : 2 Mol Acetone
2	Frequency	40 kHz
3	Power	700 Watts
4	Cleaning time (active running time of the ultrasonic unit)	30 Minutes
5	Cleaning temperature	70°C

It was observed that the cavity surface of bottom mold was cleaned completely based on the proposed concept. Meanwhile, the cavity of upper mold is partially cleaned as the cleaning solution is not in contact with the top areas due to evaporation of solution into long inlet hoses caused by preheating as shown in Figure 6-55. To evaluate the cleaning process, the surface roughness of the mold was recorded using a mobile surface roughness testing machine from Mahr GmbH. The values of lower mold after cleaning process are 1.12 µm and 8.55 µm for R_a and R_z respectively. There is an improvement when compared with the values before cleaning, which are 1.82 µm and 12.18 µm for R_a and R_z respectively for the lower mold. For the upper mold the values are 1.89 µm and 10.83 µm for R_a and R_z respectively. The values recorded before cleaning process for upper mold are 2.79 µm and 14.95 µm for R_a and R_z respectively. It should be noted that the reading for upper mold after cleaning was measured at cleaned area but not the uncleaned or the interaction area.

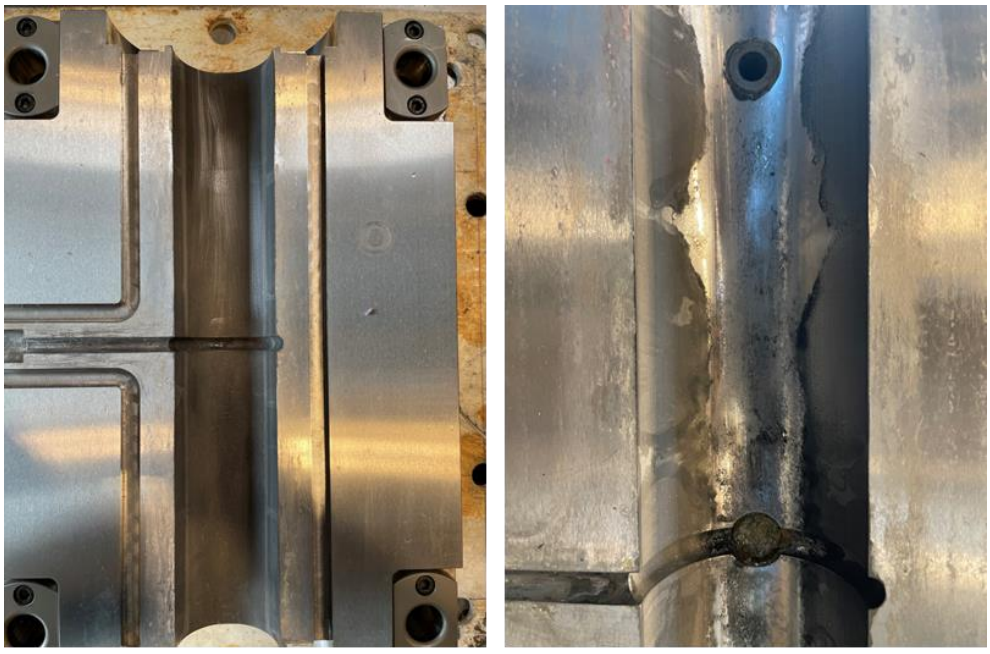

Figure 6-55: Mold surface after first cleaning process.

In order to check the effectiveness of the second cleaning solution, the mold is again prepared for cleaning process by polishing so that the influence of second iteration can be noted without any influence from first iteration. The mold is polished using grit papers such as 80, 200, 500, 1000, 2000 and then diamond polished. The surface roughness of the mold after the polishing stage was 0.32 µm and 1.98 µm for R_a and R_z respectively, which is like the first iteration. Mold was installed back to the press and the contamination was manually applied via hand layup technique. The surface roughness measured after applying contamination was 2.58 µm and 9.69 µm for R_a and R_z respectively, which is comparable to the situation in case of the first iteration. Table 30 shows the parameter used for the second iteration. One of the major differences of second iteration from first iteration is the cleaning solution valve was open throughout the entire process so that it compensates the evaporation effect of the cleaning solution. Also, the cleaning

solution used in second Iteration is more aggressive than the one from first iteration that also has shorter run time of ultrasonic device as shown in Table 30. The power of the ultrasonic was reduced to 50 % as the solution is more aggressive than the solution used in the first iteration. The idea behind this approach is to check if there is possibility to achieve same cleaning result as iteration 1 with a reduced energy by using aggressive cleaning solution. The ultrasonic device did not run continuously in second iteration rather it ran for 1 min, then paused for 10min, and then again for 1 min making a total of 3 min run time of ultrasonic. The cleaning solution was heated to 70 °C prior to ultrasonic process to activate the cleaning solution and maintained it for entire process same as 1st iteration. After the cleaning phase, the entire solution is evacuated using vacuum pump and then rinsed with water. Once the water is evacuated completely, the mold is opened and evaluated.

Table 30: Iteration 2 parameters used for cleaning procedure.

No.	Parameter für Iteration 2	Values
1	Cleaning Solution (Benzyl Alcohol + Water)	1 Mol benzyl Alcohol : 3 Mol Water
2	Frequency	40 kHz
3	Power	350 Watts
4	Cleaning time (active running time of the ultrasonic unit)	1 Minutes – 10 min Pause [3 times]
5	Cleaning temperature	70°C

It can be observed that the cleaning process was as effective as iteration 1 even with lesser power and shorter duration of ultrasonic device. The surface roughness of the mold was tested to be 0.91 µm and 6.31 µm for R_a and R_z respectively. In order to check the necessity of any mold post process after cleaning stage, a hybrid sample was produced without any preprocessing of the mold. The production of sample was successful, but the quality of the sample produced is not perfect and during demolding stage, portion of the sample surface was stuck to the mold that can be seen in Figure 6-56b. The surface of the mold after demolding the sample was measured to be 2.1 µm and 7.18 µm for R_a and R_z respectively. It can be observed that polishing of the mold is important for better demolding for the current mold conditions. Figure 6-57 and Figure 6-58 shows the surface roughness values of upper and lower mold respectively. The values are averaged based on 5 points on upper model and lower mold each. The measure points were kept constant for all stages for better reliability. It was calculated that there is ~33% improvement in first iteration whereas ~65% in second iteration for the upper mold surface quality with respect to contamination. In the case of lower mold, the surface roughness was improved by ~ 39% in first iteration and ~74% in second iteration.

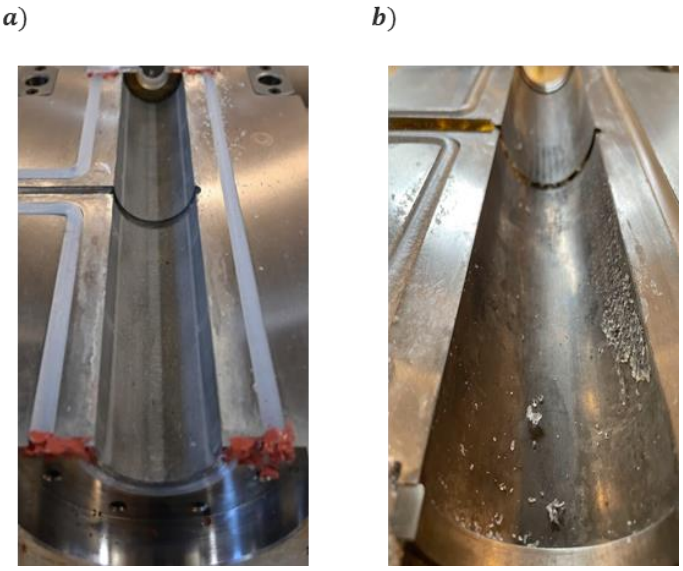

Figure 6-56: Surface of the mold a) before production and after 2nd iteration of cleaning and b) after Hybrid shaft production.

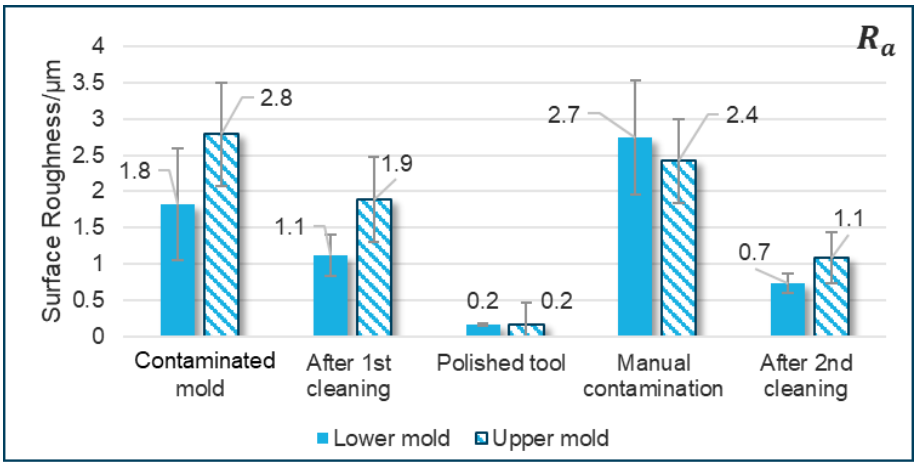

Figure 6-57: Surface roughness (R_a) of the mold through various stages of cleaning process.

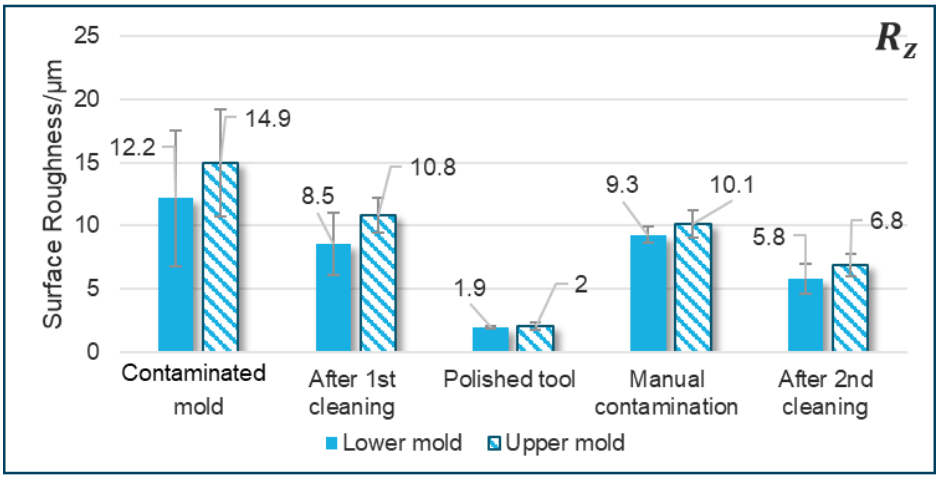

Figure 6-58: Surface roughness (R_Z) of the mold through various stages of cleaning process.

Figure 6-59 shows the mechanical property of the sample produced after second iteration cleaning stage. It is obvious that the ILSS value of the sample is greatly reduced which suggests the necessity for post processing the mold after cleaning stage. The decrease in ILSS can be related to thickness issue. The thickness of the hybrid sample was not the same throughout its length as the portion of sample surface broke during demolding stage. The diameter varied from 54 mm to 53.6 mm. However, during calculating the force, the maximum diameter was used to calculate the ILSS.

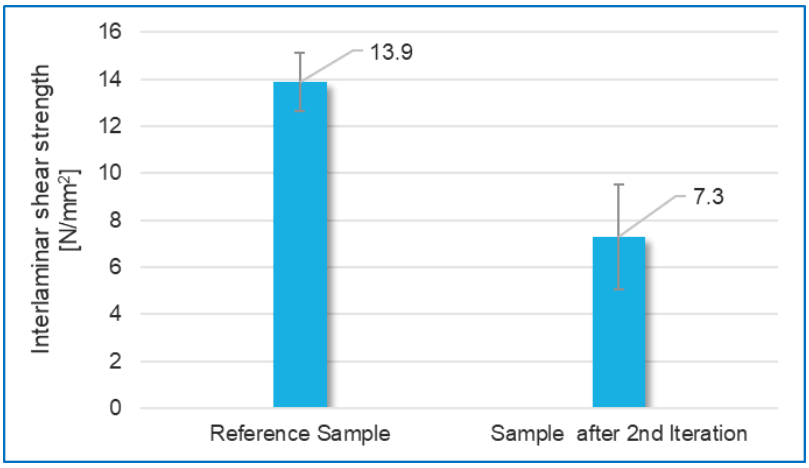

Figure 6-59: ILSS values of hybrid sample produced after second iteration with respect to the sample produced when mold surface is prepared via polishing technique.

7 Conclusion and Outlook

Reduction in mass of the vehicle directly lowers the CO_2 emission, which contributes to lower global warming. A well-balanced design for mass reduction in vehicles is to make use of both FRP and metal. The biggest challenge for using hybrid structures is cost incurred due to various production stages that are labor intense and material cost. In our current work, two alternative techniques were suggested that could potentially lower the manufacturing cost and possibly automate the production process. To validate the concept, VA-LRTM technique was used, which is commonly used in manufacturing process in automotive and aerospace industries.

The first concept introduces a self-sealing technique where the injected matrix system acts as a sealing element at the mold contours due to accelerated curing of matrix system. This process replaces the use of traditional polymer based sealing systems, which are constantly changed because of damage over the production cycle. Generally, the function of sealing system is to prevent the overflow of matrix system and seal the mold for obtaining vacuum. A mold was designed that can produce flat hybrid structures via VA-LRTM process based on Self-sealing concept. Before validating the Self-sealing, the possibility of use of catalyst was studied. After literature research, it was determined that DBTL, UL-28 and DABCO were suitable candidates for amino based matrix system. DSC dynamic tests based on ASTM E 798-06 were performed to study the influence factor of these selected catalyst with respect to epoxy resin system. The results of dynamic DSC measurements showed that DABCO exhibited better effect on the curing of epoxy resin system i.e., the position of the exothermic peak shifted from 108.6 °C to 84.4 °C by using 5 % DABCO. Based on these results, 5% of DABCO was selected as a suitable catalyst for the Self-sealing process. With selection of catalyst, the parameter study for Self-sealing process was carried out. Two different parameters sets were determined for the Self-sealing process. In the first parameter, the Self-sealing needs a temperature of 240 °C with the use of 5% DABCO catalyst. For the second parameter, the use of catalyst can be skipped if the sealing temperature is set to 250 °C. For both the parameters, the gap height should be 0.1 mm. So, it can be concluded that use of catalyst required 10 °C less sealing temperature for current epoxy system. In addition to validating the process, the influence of this process on mechanical properties of the hybrid sample produced was also investigated. Based on ILSS, it was determined that the Self-sealing process doesn't influence the ILSS value of the hybrid sample. These parameters were transferred to a mold that can produce hybrid shafts that resemble the cross section of drive shaft of the automotives and validated successfully for the same Self-sealing parameters. The Self-sealing process was further optimized using the AM printed component that has inbuilt conformal cooling channels in it.

The second concept introduces an In-mold cleaning process that works based on ultrasonic cleaning method where the cleaning takes places at the press itself rather than at a cleaning station. In order to validate this concept, the same mold that produces hybrid shaft was used with two different cleaning solutions. Change of cleaning solution also changes the parameter such as amount of power and run time of ultrasonic device. Both cleaning solutions were successful as visual inspection showed no traces of epoxy on the mold surface after cleaning. However, for a better quantification, surface roughness of the mold was used to evaluate the cleaning process.

Both parameter sets resulted in reduction of surface roughness by a maximum of 58% i.e., 0.12 µm of R_a from 1.82 µm of R_a. However, it was concluded that after the cleaning process, the mold should be polished before producing samples. This conclusion was based on the ILSS value of the hybrid sample that was produced right after cleaning process without any polishing stage.

A parameter study was also conducted in the current study to select the optimized parameters for producing a reference hybrid sample that can be used for comparing hybrid samples produced using the Self-sealing process. The factors studied are injection pressure and mold temperature. Based on experiments, a hybrid sample produced using mold temperature of 120 °C and injection pressure of 5 bar has better mechanical properties than a sample produced using mold temperature of 80 °C and injection pressure of 9 bar. In conclusion, both proposed concepts were validated successfully by producing the hybrid shafts and characterizing their mechanical properties.

8 Abbreviations and Symbols

Abbreviations

- ARALL — Aramid Reinforced Aluminum Laminates
- ABS — Acrylonitrile Butadiene Styrene
- AM — Additive manufacturing
- AHSS — Advanced high-strength steel
- ASTM — American Society for Testing and Materials
- AF — Adhesion failure
- BMC — Bulk Molding Compound
- CAD — Computer aided Design
- CAM — Computer Aided Manufacturing
- CC — Conformal cooling
- CMn — Carbon-manganese
- CO_2 — Carbon dioxide
- CFRP — Carbon Fiber Reinforced Plastic
- CARALL — Carbon Fiber Reinforced Aluminum Laminate
- C-RTM — Compression Resin Transfer Molding
- CT — Classical laminate theory
- CTE — Coefficient of Thermal
- DABCO — 1, 4 - diazabicyclo [2. 2. 2] octane
- DBTL — Dibutyltin dilaurate
- DOE — Design Of Experiments
- DP — Dual Phase
- DSC — Differential scanning calorimetry
- DVB — Double Vacuum Bagging
- EA — Energy Observation
- EMR — Electromagnetic Riveting
- EP — Epoxy
- F-SPR — Friction Self-Piercing Riveting
- FDS — Flow drill screwing Riveting
- FSBR — Friction stir blind Riveting
- FRP — Fiber Reinforced Plastics
- FML — Fiber Metal Laminate
- FSW — Friction Stir Welding
- FST — Flame-Smoke-Toxicity
- GFRP — Glass Fiber Reinforced Plastic
- GLARE — Glass Reinforced Aluminum Laminates
- GMT — Glass Mat Reinforced Thermoplastic
- HP-RTM — High Pressure Resin Transfer Molding
- HSS — High-Strength Steel
- HSLA — High-Strength Low-Alloy

- LCM Liquid Composite Molding
- ILSS Inter Laminar Sheer Strength
- IMA In Mold Assembly
- L-RTM Light Resin Transfer Molding
- LM Life Module
- MTCI Metal Thermoplastic Composite interface
- MWCNT Multiwalled carbon nanotubes
- NVH Noise, Vibration and Harshness
- PA Polyamide
- PCF Peak Crushing Force
- PE Polyethylene
- PDA Polydopamine
- PMA Post Mold Assembly
- PH-SPR Pre-Holed Self-Piercing Riveting
- PC-SPR Post-Curing Self-Piercing Riveting
- PEEK Poly ether ether ketone
- PP Polypropylene
- PPS Poly Phenylene Sulfide
- PC Polycarbonate
- PU Polyurethane
- PET Poly ether terephthalate
- PPS Poly phenylene sulfide
- PBT Polybutylene terephthalate
- PEI Poly ether imide
- PES Poly ether sulphone
- RTM Resin Transfer Molding
- SBS Short Beam shear test
- SEA Specific Energy Absorption
- SMC Sheet Molding Compound
- SPR Self-Piercing Riveting
- SRCL Self-Reactive Coupling Layer
- SMC Sheet Molding compounds
- SVB Single Vacuum Bagging
- TEDA Triethylenediamine
- TiGrL Titanium-graphite laminates
- T-FML Thermoplastic fiber Metal Laminate
- UHMWPE Ultrahigh Molecular Weight Polyethylene Fiber
- UV Ultraviolet
- UL-28 Dimethyltin carboxylate
- VA-RTM Vacuum Assisted Resin Transfer Molding
- VA-LRTM Vacuum Assisted Light Resin Transfer Molding
- VE Vinyl Ester

Symbols

Symbol	Unit	Description
m	kg	Mass
l	m	length
w	m	Width
h	m	Height
d	m	Depth
r	m	radius
d	m	Diameter
A	m^2	Area
V	m^3	Volume
I	m^4	Moment of Inertia
T	°	Temperature
T	s	Time
E	J	Energy
F	N	Force
P	Pa	Pressure
ρ	kgm^{-3}	Density
τ	Pa	Shear Stress
v	ms^{-1}	Velocity
a	ms^{-2}	Acceleration
P	W	Power
W	J	Work
τ	N m	Torque
E	Pa	Youngs modulus
σ	Pa	Stress
ε	m/m	Strain

9 References

[1] B. Johannes, K. Anton, K. Manuel, E. Richard, W. Thomas und T. Torbjörn, „Total CO2-equivalent life-cycle emissions from commercially available passenger cars," *Renewable and Sustainable Energy Reviews,* Bd. 159, 2022.

[2] P. Martin, „www.statista.com," Statista, 8 April 2022. [Online]. Available: https://www.statista.com/statistics/268739/production-of-passenger-cars-worldwide/.

[3] C. Robert, O. Sebastian und R. Renato, „Tightening EU ETS targets in line with the European Green Deal: Impacts on the decarbonization of the EU power sector," *Applied Energy,* Bd. 293, 2021.

[4] R. Silvia, U. Ruben, B. Paolo und T. Christian, „Towards the EU Green Deal: Local key factors to achieve ambitious 2030 climate targets," *Journal of Cleaner Production,* Bd. 320, 2021.

[5] Marco Cavazzuti, Andrea Baldini, Enrico Bertocchi, Dario Costi, Enrico Torricelli und Patrizio Moruzzi , „High performance automotive chassis design: a topology optimization based approach," *Struct Multidisc Optim,* pp. 44-56, 2011.

[6] P. Ragnarsson, „Lightweighting: a solution to low carbon mobility, Making every gram CO2 saving count," European Aluminium, Belgium, 2018.

[7] A. C. Serrenho, J. B. Norman und J. M. Allwood, „The impact of reducing car weight on global emissions: The future fleet in Great Britain," *Philosophical Transactions of The Royal Society A Mathematical Physical and Engineering Sciences ,* 2017.

[8] M. Kleiner, S. Chatti und A. Klaus, „Metal forming techniques for lightweight construction," *Journal of Materials Processing Technology,* Bd. 177, Nr. 1-3, pp. 2-7, 2006.

[9] Feraboli Paolo, Masini Attilio und Bonfatti Andrea, „Advanced composites for the body and chassis of a production high performance car," *International Journal of Vehicle Design,* Bd. 44, pp. 233-246, 2007.

[10] Z. Guohua, L. Jiapeng , S. Guangyong und L. Qing, „Comparative study on metal/CFRP hybrid structures under static and dynamic loading," *International Journal of Impact Engineering,* Bd. 141, 2020.

[11] M. Bambach, „Experiments and crushing mechanism analysis of hybrid square metal tubes with filament wound CFRP," *Composites Part C: Open Access,* Bd. 6, 2021.

[12] Zheng Wang, Christian Lauter, Meike Frantz, Thomas Tröster und Bamned Sanitther, „Intrinsic Manufacturing of Metal-FRP-Hybrid Structural Automotive Components by Resin Transfer Moulding," in *18th International Conference on Composite Structures*, Lissabon, 2015.

[13] A.Pramanik, A.K.Basak, Y.Dong, P.K.Sarker, M.S.Uddind, G.Littlefair, A.R.Dixit und S.Chattopadhyaya, „Joining of carbon fibre reinforced polymer (CFRP) composites and aluminium alloys – A review," *Composites Part A: Applied Science and Manufacturing,* Bd. 101, pp. 1-29, 2017.

[14] Jing Zhang und Shanglu Yang, „Self-piercing riveting of aluminum alloy and thermoplastic composites," *Journal of Composite Materials ,* Bd. 49, pp. 1493-1502, 2015.

[15] Xun Liu, Yong Chae Lim, Yongbing Li, Wei Tang, Yunwu Ma, Zhili Feng und Jun Ni, „Effects of process parameters on friction self-piercing riveting of dissimilar materials," *Journal of Materials Processing Technology,* Bd. 237, pp. 19-30, 2016.

[16] Alexander Streitferdt, Natalie Rudolph und Iman Tah, „Co-Curing of CFRP-Steel Hybrid Joints Using the Vacuum Assisted Resin Infusion Process," *Applied Composite Materials,* Bd. 24, pp. 1137-1149, 2017.

[17] Michael Vistein, Dominik Deden, Roland Glück und Stefan Schneye, „Automated Production of Large Fibre Metal Laminate Aircraft Structure Parts," *Procedia Manufacturing,* Bd. 38, pp. 1300-1307, 2019.

[18] J. Min, J. Hu, C. Sun, H. Wan, P. Liao, H. Teng und J. Lin, „Fabrication processes of metal-fiber reinforced polymer hybrid components: a review," *Advanced Composites and Hybrid Materials,* 2021.

[19] J. Chung und K. Lee, „A framework of collaborative design environment for injection molding," *Computers in Industry,* Bd. 47, Nr. 3, pp. 319-337, 2002.

[20] I. Ribeiro, P. Pecas und E. Henriques, „Incorporating tool design into a comprehensive life cycle cost framework using the case of injection molding," *Journal of Cleaner Production,* Bd. 53, pp. 297-309, 2013.

[21] D. F. Heaney, Handbook of metal injection molding, USA: Woodhead Publishing, 2012.

[22] D. O. Kazmer, Injection Mold Design Engineering, Carl Hanser Verlag GmbH & Company KG, 2016.

[23] Y.-M. Chen und J.-J. Liu, „Cost-effective design for injection molding," *Robotics and Computer-Integrated Manufacturing,* Bd. 15, Nr. 1, pp. 1-21, 1999.

[24] N. Loh, S. Tor und K. A. Khor, „Production of metal matrix composite part by powder injection molding," *Journal of Materials Processing Technology,* Bd. 108, Nr. 3, pp. 398-407, 2001.

[25] H.-P. Heim, Specialized Injection Molding Techniques, Technology & Engineering , 2015.

[26] A. E. Haroun, S. O. Duffuaa, M. Ben-Daya, S. O. Duffuaa, A. Raouf, J. Knezevic und D. Ait-Kadi, Handbook of Maintenance Management and Engineering, Springer, 2009.

[27] C. S. Wong, F. T. S. Chan und S. H. Chung, „Injection Mold Maintenance Scheduling with Mold-Lifting Crane Consideration," in *23rd International Conference on Flexible Automation & Intelligent Manufacturing*, 2013.

[28] H. Chu, Z. Liu, C. Zhang, Z. Liu, Y. Zhao und C. Yang, „Decision-making for structural parameters of injection mold gating system based on agent model and intelligent algorithm," *The International Journal of Advanced Manufacturing Technology,* pp. 7599-7614, 2022.

[29] M. R. Khosravani, S. Nasiri und T. Reinicke, „Intelligent knowledge-based system to improve injection molding process," *Journal of Industrial Information Integration,* Bd. 25, 2022.

[30] D. Nimawat und B. Gidwani, „An overview of Industry 4.0 in manufacturing industries," *International Journal of Industrial and Systems Engineering,* Bd. 40, Nr. 4, pp. 425 - 454, 2022.

[31] T. M. Kruckenberg und R. Paton, Resin Transfer Moulding for Aerospace Structures, Springer Science, 1998.

[32] K. Potter, Resin Transfer moulding, Chapman and Hall, 1997.

[33] C.-W. Su, W.-J. Su, F.-J. Cheng, G.-Y. Liou, S.-J. Hwang, H.-S. Peng und H.-Y. Chu, „Optimization process parameters and adaptive quality monitoring injection molding process for materials with different viscosity," *Polymer Testing,* Bd. 109, 2022.

[34] J. Luo, Z. Liang, C. Zhanga und B. Wanga, „Optimum tooling design for resin transfer molding with virtual manufacturing and arti®cial intelligence," *Composites: Part A,* pp. 877-888, 2001.

[35] S. Caba und M. Kich, „Analysis of the resin transfer molding (RTM) process for FRP and its process simulation fundamentals," in *AIP Conference Proceedings*, 2015.

[36] J. Hausmann, P. Naghipour und K. Schulze, „Analytical and numerical residual stress models for fiber metal laminates – comparison and application," *Procedia Materials Science 2,* pp. 68 - 73, 2013.

[37] J. Michael und R. Gunther, „Knowledge-based approach in the field of non-destructive inspection of CFRP metal hybrid components via optical lock-in thermography," *NDT and E International,* 2020.

[38] M. E. Messiry, „Theoretical analysis of natural fiber volume fraction of reinforced composites," *Alexandria Engineering Journal,* pp. 301 - 306 , 2013.

[39] Dong Chensong, "Development of a process model for the vacuum assisted resin transfer molding simulation by the response surface method," *Composites Part A: Applied Science and Manufacturing,* vol. 37, pp. 1316-1324, 2006.

[40] Ryosuke Matsuzaki, Seiji Kobayashi, Akira Todoroki und Yoshihiro Mizutani, „Flow control by progressive forecasting using numerical simulation during vacuum-assisted resin transfer molding," *Composites Part A: Applied Science and Manufacturing,* Bd. 45, pp. 79-87, 2013.

[41] T. S. Lundström und B. R. Gebart, „Influence from process parameters on void formation in resin transfer molding," *Polymer Composites,* Bd. 15, pp. 25 - 33, 1994.

[42] P. Bhat, J. Merotte, P. Simacek und S. G.Advani, „Process analysis of compression resin transfer molding," *Composites Part A: Applied Science and Manufacturing,* Bd. 40, pp. 431 - 441, 2009.

[43] V. Buchinger und Z. S. Khodaei, „Vacuum assisted resin transfer moulding process monitoring by means of distributed fibre-optic sensors: a numerical and experimental study," *Advanced Composite Materials ,* Bd. 31, pp. 467 - 484, 2022.

[44] C. Schillfahrt, E. Fauster und R. Schledjewski, „Influence of process pressures on filling behavior of tubular fabrics in bladder-assisted resin transfer molding," *Advanced Manufacturing: Polymer & Composites Science ,* Bd. 3, pp. 148 - 158, 2017.

[45] T. Sinmazçelik, E. Avcu, M. Ö. Bora und O. Çoban, „A review: Fibre metal laminates, background, bonding types and applied test methods," *Materials & Design,* Bd. 32, pp. 3671 - 3685, 2011.

[46] D. Rouison, M. Sain und M.Couturier, „Resin transfer molding of hemp fiber composites: optimization of the process and mechanical properties of the materials," *Composites Science and Technology,* Bd. 66, pp. 895 - 906, 2006.

[47] F. Ge, Y. Lin, F. Zhang, Z. Zhang und M. Wang, „Crushing Characteristics Comparison between Aluminum/CFRP and Aluminum/CFRP/Aluminum Hybrid Tubes," *Polymers,* 2022.

[48] G. R. Villanueva und W. J. Cantwell, „The high velocity impact response of composite and FML-reinforced sandwich structures," *Composites Science and Technology,* Bd. 64, pp. 35 - 54, 2004.

[49] S.U.Khan, R.C.Alderliesten und R.Benedictus, „Post-stretching induced stress redistribution in Fibre Metal Laminates for increased fatigue crack growth resistance," *Composites Science and Technology,* Bd. 69, pp. 396 - 405, 2009.

[50] R. Alderliesten, „On the Development of Hybrid Material Concepts for Aircraft Structures," *Recent Patents on Engineering,* Bd. 3, pp. 25 - 38, 2009.

[51] G. Wu und J.-M. Yang, „The Mechanical Behavior of GLARE Laminates for Aircraft Structures," *Failure in Structural Materials,* 2005.

[52] H. Li, Y. Hu, C. Liu, X. Zheng, H. Liu und J. Tao, „The effect of thermal fatigue on the mechanical properties of the novel fiber metal laminates based on aluminum–lithium alloy," *Composites Part A: Applied Science and Manufacturing,* Bd. 84, pp. 36 - 42, 2016.

[53] R. J. H. Wanhill, „Carbon Fibre Polymer Matrix Structural Composites," in *Aerospace Materials and Material Technologies*, 2017.

[54] A. Böttcher, „Series-production Adhesive Process for Hybrid Components," *Lightweight Design worldwide,* pp. 48 -52, 2019.

[55] R. Drössler, R. Waffler, M. Krahl und D. Haider, „Tool Technology for Lightweight Structures in 3-D Hybrid Designs," *Lightweight Design worldwide,* Bd. 11, pp. 42 - 47, 2018.

[56] N. DeMattia, „https://www.bmwblog.com/," BMW, 1 September 2015. [Online]. Available: https://www.bmwblog.com/2015/09/01/bmw-7-series-carbon-core-more-important-that-you-might-think/.

[57] G. Zhu, G. Sun, Q. Liu, G. Li und Q. Li, „On crushing characteristics of different configurations of metal-composites hybrid tubes," *Composite Structures,* Bd. 175, pp. 58 - 69, 2017.

[58] D. G. Lee, H. S. Kim, J. W. Kim und J. K. Kim, „Design and manufacture of an automotive hybrid aluminum/composite drive shaft," *Composite Structures,* Bd. 63, pp. 87-99, 2004.

[59] C. Zheng und S. Lei, „Mechanical Analysis and Optimal Design for Carbon Fiber Resin Composite Wound Hydrogen Storage Vessel With Aluminum Alloy Liner," *J. Pressure Vessel Technol.,* Bd. 131, 2008.

[60] Y. Liu, B. Zwingmann und M. Schlaich, „Carbon Fiber Reinforced Polymer for Cable Structures—A Review," *Polymers,* 2015.

[61] U. K. Vaidya und K. K. Chawla, „Processing of fibre reinforced thermoplastic composites," *International Materials Reviews,* 2008.

[62] M. N. Norizan, N. Abdullah, H. M. H. M.M., H. A. Aisyah, K. Abdan, L. c. hao und S. A. Rafiqah, „The Challenges and Future Perspective of Woven Kenaf Reinforcement in Thermoset Polymer Composites in Malaysia: A Review," *Polymers,* 2021.

[63] A. Shau und P. Ray, „ASPECTS OF POLYMERS AND POLYMERIC COMPOSITES IN CHEMICAL PROCESS INDUSTRIES," in *Polymer and Composites as Material of Construction for Chemical Process Industies*, 2012.

[64] T. Vidil, F. Tournilhac, S. Musso, A. Robisson und L. Leibler, „Control of reactions and network structures of epoxy thermosets," *Progress in Polymer Science,* Bd. 62, pp. 126 - 179, 2016.

[65] E. Gudonis, E. Timinskas, E. Timinskas und V. G. V. V. Tamulėnas, „FRP reinforcement for concrete structures: State-of-the-art review of application and design," *Engineering Structures and Technologies ,* 2013.

[66] B. N. Cox und G. Flanagan, Handbook of Analytical Methods for Textile, 1997.

[67] V. GOODSHIP, „Plastic Recycling," *Science Progress,* pp. 245 - 268, 2007.

[68] R. G. Weatherhead, „Catalysts, Accelerators and Inhibitors for Unsaturated Polyester Resins," in *FRP Technology* , Applied science publisher, pp. 204 - 239.

[69] „Composite One," [Online]. Available: https://www.compositesone.com/product/initiators-catalysts/. [Zugriff am 07 02 2023].

[70] [Online]. Available: https://www.surfacesciencewestern.com/analytical-services/differential-scanning-calorimetry-dsc/. [Zugriff am 06 06 2023].

[71] Metallica, „Carbon Steel pipes & Stainless Steel Seamless Pipes," [Online]. Available: https://www.steelpipesfactory.com/material-grades-standards/en-10305-1-e235/. [Zugriff am 18 05 2023].

[72] „mysteel24," [Online]. Available: https://mysteel24.com/en/shop/item/7375. [Zugriff am 18 05 2023].

[73] H. S. Steel, 03 2022. [Online]. Available: https://www.round-bars.com/cold-drawn-steel-introduction/. [Zugriff am 18 05 2023].

[74] K. Ramaswamy, R. M.O'Higgins, A. K. Kadiyala, M. A.McCarthy und C. T.McCarthy, „Evaluation of grit-blasting as a pre-treatment for carbon-fibre thermoplastic composite to aluminium bonded joints tested at static and dynamic loading rates," *Composites Part B: Engineering,* Bd. 185, 2020.

[75] V. S. Balakrishnan, A. Obrosov, F. Kuke, H. Seidlitz und S. Weiß, „Influence of metal surface preparation on the flexural strength and impact damage behaviour of thermoplastic FRP reinforced metal laminate made by press forming," *Composites Part B: Engineering,* Bd. 173, 2019.

[76] A. Heckert und M. F.Zaeh, „Laser Surface Pre-treatment of Aluminium for Hybrid Joints with Glass Fibre Reinforced Thermoplastics," *Physics Procedia,* Bd. 56, pp. 1171 - 1181, 2014.

[77] L. U. ,. B. P. U. K. C. Department of Chemical Engineering, D. H. Berry, J. E. Seebergh, J. H. Osborne und K. Y. Blohowiak, „Effect of surface morphology on crack growth at a sol–gel reinforced epoxy/aluminium interface," *Journal if adhesives,* pp. 477 - 516, 2006.

[78] B. Bernd-Arno, H. Sven, G. Nenad, M.-C. Moritz, W. Tim und A. Neumann, „Forming and Joining of Carbon-Fiber-Reinforced Thermoplastics and Sheet Metal in One Step," *Procedia Engineering,* Bd. 183, pp. 227 - 232, 2017.

[79] Y. Guo, C. Zhai, F. Li, X. Zhu, F. Xu und X. Wu, „Formability, defects and strengthening effect of steel/CFRP structures fabricated by using the differential temperature forming process," *Composite Structures,* Bd. 216, pp. 32 - 38, 2019.

[80] M. Zhou, X. Xiong, D. Drummer und B. Jiang, „Interfacial interaction and joining property of direct injection-molded polymer-metal hybrid structures: A molecular dynamics simulation study," *Applied Surface Science,* Bd. 478, pp. 680-689, 2019.

[81] Z. Zhang und R. Kovacevic, „Laser cladding of iron-based erosion resistant metal matrix composites," *Journal of Manufacturing Processes,* Bd. 38, pp. 63 - 75, 2019.

[82] L. Guo, J. Liu, H. Xia, X. Li, X. Zhang und H. Yang, „Effects of surface treatment and adhesive thickness on the shear strength of precision bonded joints," *Polymer Testing,* Bd. 94, 2021.

[83] H. Wan, J. Min, J. Lin, B. E. Carlson, S. Maddela und C. Sun, „Effect of laser spot overlap ratio on surface characteristics and adhesive bonding strength of an Al alloy processed by nanosecond pulsed laser," *Journal of Manufacturing Processes,* Bd. 62, pp. 555 - 565, 2021.

[84] M. Povol, J. Tabucol, T. M. Brugo und A. Zucchelli, „Electrical Resistance Curing Method for Hybrid Metal-CFRP Tubes," *Applied Composite Materials,* Bd. 27, pp. 375 - 389, 2020.

[85] X. Zhou, Y. Zhao, X. Chen, Z. Liu, J. Li und Y. Fan, „Fabrication and mechanical properties of novel CFRP/Mg alloy hybrid laminates with enhanced interface adhesion," *Materials & Design,* Bd. 197, 2021.

[86] F. Hirsch, S. Müller, M. Machens, R. Staschko, N. Fuchs und M. Kästner, „Simulation of self-piercing rivetting processes in fibre reinforced polymers: Material modelling and parameter identification," *Journal of Materials Processing Technology,* Bd. 241, pp. 164 - 177 , 2017.

[87] X. Zhang, X. He, B. Xing, W. Wei und J. Lu, „Pre-holed self-piercing riveting of carbon fibre reinforced polymer laminates and commercially pure titanium sheets," *Journal of Materials Processing Technology,* Bd. 279, 2020.

[88] J. Wang, G. Zhang, X. Zheng, J. Li, X. Lia, W. Zhu und J. Yanagimoto, „A self-piercing riveting method for joining of continuous carbon fiber reinforced composite and aluminum alloy sheets," *Composite Structures,* Bd. 259, 2021.

[89] X. Liu, Y. C. Lim, Y. Li, W. Tang, Y. Ma, Z. Feng und J. Nia, „Effects of process parameters on friction self-piercing riveting of dissimilar materials," *Journal of Materials Processing Technology,* Bd. 237 , pp. 19 - 30 , 2016.

[90] Z. Cao und M.Cardew-Hall, „Interference-fit riveting technique in fiber composite laminates," *Aerospace Science and Technology,* Bd. 10, Nr. 4, pp. 327 - 330, 2006.

[91] H. Jiang, T. Luo, G. Li, X. Zhang und J. Cui, „atigue life assessment of electromagnetic riveted carbon fiber reinforce plastic/aluminum alloy lap joints using Weibull distribution," *International Journal of Fatigue,* Bd. 105, pp. 180 - 189, 2017.

[92] L. Shengwang, Z. Weifang, W. Yufeng und C. Yu, „The Damage Investigation of Wedge-Shaped Electromagnetic Riveting Structure of CFRP/Aluminium Alloy," *Journal Test Evaluation ,* Bd. 41, Nr. 2, 2013.

[93] P. Nagel und G. Meschut, „Flow drill screwing of fibre-reinforced plastic-metal composites without a pilot hole," *Welding in the World,* Bd. 61, pp. 1057 - 1067, 2017.

[94] J. Min, Y. Li, J. Li, B. E. Carlson und J. Lin, „Friction stir blind riveting of carbon fiber-reinforced polymer composite and aluminum alloy sheets," *The International Journal of Advanced Manufacturing Technology,* Bd. 76, pp. 1403 - 1410, 2015.

[95] H. A. Khan, W.-M. Wang, K. Wang, S. Li, S. Miller und J. Li, „Investigation of mechanical behavior of dissimilar material FSBR joints exposed to a marine environment," *Journal of Manufacturing Processes,* Bd. 37, pp. 376 - 385, 2019.

[96] J. Min, Y. Li, B. E.Carlson, S. J. Hu, J. Li und J. Lin, „A new single-sided blind riveting method for joining dissimilar materials," *CIRP Annals,* Bd. 64, Nr. 1, pp. 13 - 16 , 2015.

[97] K. Nagatsuka, B. Xiao, L. Wu, K. Natata, S. Saeki, Y. Kitamoto und Y. Iwamoto, „Dissimilar materials joining of metal/carbon fibre reinforced plastic by resistance spot welding," *Welding International ,* pp. 505 - 512, 2018.

[98] F. Lionetto, F. Balle und A. Maffezzoli, „Hybrid ultrasonic spot welding of aluminum to carbon fiber reinforced epoxy composites," *Journal of Materials Processing Technology,* Bd. 247, pp. 289 - 295, 2017.

[99] Y. Ma, D. Bridges, Y. Yu, J. Han, H. Li und A. Hu, „Joining of Carbon Fiber Reinforced Plastic to Aluminum Alloy by Reactive Multilayer Films and Low Power Semiconductor Laser Heating," *Applied science,* Bd. 9, Nr. 2, 2019.

[100] X. Tan, J. Zhang, J. Shan, S. Yang und J. Ren, „Characteristics and formation mechanism of porosities in CFRP during laser joining of CFRP and steel," *Composites Part B: Engineering,* Bd. 70, pp. 35 - 43, 2015.

[101] S.M.Goushegir, J. Santos und S.T.Amancio-Filho, „Friction Spot Joining of aluminum AA2024/carbon-fiber reinforced poly(phenylene sulfide) composite single lap joints: Microstructure and mechanical performance," *Materials & Design,* Bd. 54, pp. 196 - 206, 2014.

[102] R.-W. Kim, C.-M. Kim, K.-H. Hwang und S.-R. Kim, „Embedded Based Real-Time Monitoring in the High-Pressure Resin Transfer Molding Process for CFRP," *Applied science ,* 2019.

[103] V. Gutowski, W. Yang, S. Li, K. Dean und X. Zhang, „Lightweight Nanocomposite Materials," in *Lightweight and Sustainable Materials for Automotive Applications*, 2017.

[104] Y. Hamidi und C. Altan, „Process-Induced Defects in Resin Transfer Molded Composites," *In Comprehensive Composite Materials II,* p. 95–106, 2018.

[105] C. Rudd, A. Long, K. Kendall und C. Mangin, „Liquid Moulding Technologies," Cambridge, UK, Woodhead Publishing: Cambridge, 1997.

[106] K. Vallons, I. Duque, S. Lomov und I. Verpoest, „Loading direction dependence of the tensile stiffness, strength and fatigue life of biaxial carbon/epoxy NCF composites," *Composites Part A: Applied Science and Manufacturing,* Bd. 42, Nr. 1, pp. 16 - 21, 2011.

[107] Y. Li, B. Stier, B. Bednarcyk, J.-W. Simon und S. Reese, „The effect of fiber misalignment on the homogenized properties of unidirectional fiber reinforced composites," *Mechanics of Materials,* Bd. 92, pp. 261 - 274, 2016.

[108] M. Shah und V. Chaudhary, „Flow modeling and simulation study of vacuum assisted resin transfer molding (VARTM) process: A review," in *IOP Conference Series: Materials Science and Engineering*, 2020.

[109] J. Vilà, C. González und J. LLorca, „A level set approach for the analysis of flow and compaction during resin infusion in composite materials," *Composites Part A: Applied Science and Manufacturing,* Bd. 67, pp. 299 - 307, 2014.

[110] MOMENTIVE, *Preform binder systems for mass production of Automotive composite parts.*

[111] M. Kang, W. Lee und H. Hahn, „Analysis of vacuum bag resin transfer molding process," *Composites Part A: Applied Science and Manufacturing,* Bd. 32, Nr. 11, pp. 1553 - 1560, 2011.

[112] S. G. Advani und K.-T. Hsiao, „Vacuum assisted resin transfer molding (VARTM)," in *Manufacturing techniques for polymer matrix composites*, Woodhead Publishing, 2012, p. Delaware.

[113] K.-T. Hsiao, R. Mathur, S. G. Advani, J. W. Gillespie, Jr. und B. K. Fink, „A Closed Form Solution for Flow During the Vacuum Assisted Resin Transfer Molding Process," *Journal of Manufacturing Science and Engineering ,* 2000.

[114] J. Merotte, P. Simacek und S. G. Advani, „Resin flow analysis with fiber preform deformation in through thickness direction during Compression Resin Transfer Molding," *Composites Part A: Applied Science and Manufacturing,* Bd. 41, Nr. 7, pp. 881 - 887, 2010.

[115] J. Merotte, P. Simacek und S. G. Advani, „Flow analysis during compression of partially impregnated fiber preform under controlled force," *Composites Science and Technology,* Bd. 70, Nr. 5, pp. 725 - 733, 2010.

[116] P. Simacek, S. G. Advani und a. S. A. Iobst, „Modeling Flow in Compression Resin Transfer Molding for Manufacturing of Complex Lightweight High-Performance Automotive Parts," *Journal of Composite Materials,* Bd. 42, Nr. 23, 2008.

[117] T. Mennecart, L. Hiegemann und N. B. Khalifa, „Analysis of the forming behaviour of in-situ drawn sandwich sheets," *Procedia Engineering,* Bd. 207, pp. 890 - 895, 2017.

[118] H. Li, J. Tian, W. Fei, Z. Han, G. Tao, Y. Xu, X. Xu und J. Tao, „Spring-back and failure characteristics of roll bending of GLARE laminates," *Materials Research Express,* Bd. 6, Nr. 8, 2019.

[119] L. Shahid und F. Janabi-Sharifi, „A neural network-based method for coverage measurement of shot-peened panels," *Neural Computing and Applications,* 2018.

[120] H. Li, W. Zhang, W. Jiang, X. Hua, X. Guo, X. Fu und J. Tao, „The feasibility research on shot-peen forming of the novel fiber metal laminates based on aluminum-lithium alloy," *The International Journal of Advanced Manufacturing Technology,* pp. 587 - 596, 2018.

[121] C. Russig, M. Bambach, G. Hirt und N. Holtmann, „Shot peen forming of fiber metal laminates on the example of GLARE," *International Journal of Material Forming,* Bd. 7, pp. 425 - 438, 2014.

[122] C. J.Yocom, X. Zhang und Y. Liao, „Research and development status of laser peen forming: A review," *Optics & Laser Technology,* Bd. 108, pp. 32 - 45, 2018.

[123] A. Gisario und M. Barletta, „Laser forming of glass laminate aluminium reinforced epoxy (GLARE): On the role of mechanical, physical and chemical interactions in the multi-layers materia," *Optics and Lasers in Engineering,* Bd. 110, pp. 364 - 376, 2018.

[124] D. D. W. Howell und S. Fukumoto, „Compression molding of long chopped fiber thermoplastic composite".

[125] T. Stallmeister und T. Tröster, „In-Mold-Assembly of hybrid bending structures by compression molding," in *25th International Conference on Material Forming*, Portugal, 2022.

[126] S. AB., „ Plastics: materials and processing," Perason Education Inc, 2006.

[127] R. A. Tatara, „Compression Molding," in *Applied Plastics Engineering Handbook*, DeKalb, IL, United States, Elsevier, p. 290.

[128] K. Sravani, K. Mythili und G. V. Ratnam, „Strengthening of RC Beams using FRP Sheet," *International Journal of Research and Innovation,* 2016.

[129] H. W und J. Z, „Design and Manufacturing of Fiber-Reinforced Composites," in *In Advanced Strutured Materials*, Switzerland, Springer International Publishing, 2021.

[130] Y. Mujahid, N. Sallih und M. Z. Abdullah, „A Comparison of Single-Vacuum-Bag and Double-Vacuum-Bag Methods for Manufacturing High-Quality Laminated Composites," *Advances in Manufacturing Engineering ,* p. 457–467, 2020.

[131] O. A. Ekuase, N. Anjum, V. O. Eze und O. I. Okoli, „A Review on the Out-of-Autoclave Process for Composite Manufacturing," *Journal of Composites Scirence ,* 2022.

[132] H. N. Dhakal und S. O. Ismail, „Design, manufacturing processes and their effects on bio-composite properties," in *Sustainable Composites for Lightweight Applications*, Woodhead Publishing Series in Composites Science and Engineering, 2021, pp. 121 -177.

[133] V.M.KARBHARI, „Fabrication, quality and service-life issues for composites in civil engineering," in *Durability of Composites for Civil Structural Applications*, Woodhead Publishing Series in Civil and Structural Engineering, 2007, pp. 13 - 20.

[134] N. A. Peppiatt, „Reciprocating Lip Seals," in *Encyclopedia of Tribology* , Springer Reference , p. 2752–2758.

[135] Z. Wang, C. Lauter, C. Lauter, B. Sanitther und T. Tröster, „Intrinsic Manufacturing of Metal-FRP-Hybrid Structural Automotive Components by Resin Transfer Moulding," in *18th International Conference on Composite Structures*, Lissabon, 2015.

[136] „INSTRON," [Online]. Available: https://www.instron.com/en/resources/test-types/torsion-test. [Zugriff am 11 02 2023].

[137] [Online]. Available: https://www.illiehsill.top/ProductDetail.aspx?iid=241136267&pr=73.88. [Zugriff am 27 12 2022].

[138] M. B. Roller, „Characterization of the Time-Temperature-Viscosity Behavior of Curing B-Staged Epoxy resin," *Polymer Enginerring and Sciecne ,* Bd. 15, Nr. 6, 1975.

[139] T. GmbH, *Data sheet of Flowstop,* Michelstadt : Tartler GmbH, 2014.

[140] AGK, *Data sheet of Insulation materials,* AGK Hochlleistungswerkstoffe GmbH.

[141] S. Feng, A. M. Kamat und Y. Pei, „Design and fabrication of conformal cooling channels in molds: Review and progress updates," *International Journal of Heat and Mass Transfer,* 2021.

[142] O. Tuteski und A. Kočov, „Conformal cooling channels in injection molding tools – design considerations," *Mach. Technol. Mater,* Bd. 12, pp. 445-448, 2018.

[143] Y. Wang, K.-M. Yu, C. C. Wang und Y. Zhang, „Automatic design of conformal cooling circuits for rapid tooling," *Computer-Aided Design,* Bd. 43, Nr. 8, pp. 1001 - 1010, 2011.

[144] N. Williams, „Metal AM," 2018. [Online]. Available: https://www.metal-am.com/articles/how-3d-printing-is-increasing-efficiency-and-quality-in-the-injection-moulding-industry/. [Zugriff am 13 02 2023].

[145] J. Spoerre, C. Zhang, B. Wang und R. Parnas, „Integrated Product and Process Design for Resin Transfer Molded Parts," *Journal of Composite Materials,* Bd. 32, Nr. 13, 1998.

[146] C. Kaynak und Y. O. Kas, „Effects of Injection Pressure in Resin Transfer Moulding (RTM) of Woven Carbon Fibre/Epoxy Composites," *Polymers & Polymer Composites,* Bd. 14, Nr. 1, 2006.

[147] C. Lee und K. Wei, „Resin Transfer Moulding (RTM) Process of a High Performance Epoxy Resin. II: Effects of Process Variables on the Physical, Static and Dynamic Mechanical Behaviour," *Polymer Engineering and Science,* Bd. 40, Nr. 4, pp. 935 - 943, 2000.

[148] MOMENTIVE, *Technical Data Sheet,* 2012.

[149] [Online]. Available: https://www.r-g.de/art/202106. [Zugriff am 07 05 2021].

[150] G.-L. Song, C. Zhang, X. Chen und D. Zheng, „Galvanic activity of carbon fiber reinforced polymers and electrochemical behavior of carbon fiber," *Corrosion Communications,* Bd. 1, pp. 26-39, 2021.

[151] Pavel Simacek, Ömer Eksik, Dirk Heider, John W.Gillespie Jr. und Suresh Advani, „Experimental validation of post-filling flow in vacuum assisted resin transfer molding processes," *Composites Part A: Applied Science and Manufacturing,* Bd. 43, pp. 370-380, 2012.

[152] N. A.Patil, S. S.Mulik, K. S.Wangikar und A. P.Kulkarni, „Characterization of Glass Laminate Aluminium Reinforced Epoxy- A Review," *Procedia Manufacturing,* p. 20, 2018.

[153] S. Hovik, „Experimental and numerical methods for characterization of impact damage in titanium-graphite laminates," University of Washington, Washington, 2019.

[154] Y. Chen, Y. Wang und H. Wang, „Research Progress on Interlaminar Failure Behavior of Fiber Metal Laminates," *Advances in Polymer Technology,* 2019.

[155] J. Ni, J. Min, H. Wan, J. Lin, S. W. und Q. Wan, „Effect of adhesive type on mechanical properties of galvanized steel/SMC adhesive-bonded joints," *International Journal of Adhesion and Adhesives,* Bd. 97, 2020.

[156] C. Carey, W. J. Cantwell, G. Dearden, K. R. Edwards, S. P. Edwardson und K. G. Watkins, „Towards a rapid, non-contact shaping method for fibre metal laminates using a laser source," *The International Journal of Advanced Manufacturing Technology,* Bd. 47, pp. 557 - 565, 2010.

[157] L. Shanmugam, M.E.Kazemi, Z. Rao, L. Yang und J. Yang, „On the metal thermoplastic composite interface of Ti alloy/UHMWPE-Elium® laminates," *Composites Part B: Engineering,* Bd. 181, 2020.

[158] C. Zinn, M. Bobbert, C. Dammann, Z. Wang, T. Tröster, R. Mahnken, G. Meschut und M. Schaper, „Shear strength and failure behaviour of laser nano-structured and conventionally pre-treated interfaces in intrinsically manufactured CFRP-steel hybrids," *Composites Part B: Engineering,* Bd. 151, pp. 173 - 185, 2018.

[159] T. Mennecart, H. Werner, N. B. Khalifa und K. A. Weidenmann, „Developments and Analyses of Alternative Processes for the Manufacturing of Fiber Metal Laminates," *International m,anufacturing Science and Engineering Conference,* 2018.

[160] O. Agboola, R. Sadiku, T. Mokrani, I. Amer und O. Imoru, „Polyolefins and the environment," in *Polyolefin Fibres*, Woodhead Publiushing , 2017, pp. 89 - 133.

[161] J. Hodgkin, „Thermosets: Epoxies and Polyesters," in *Encyclopedia of Materials: Science and Technology*, 2001.

[162] W. Ferdous, A. Manalo, C. Salih, P. Yu, R. Abousnina, T. Heyer und P. Schubel, „Behaviour of Polymer Filled Composites for Novel Polymer Railway Sleepers," *Polymers ,* 2021.

[163] „wohlersassociates," wohlersassociates, 2021. [Online]. Available: https://wohlersassociates.com/press-releases/new-wohlers-report-2021-finds-7-5-growth-in-additive/. [Zugriff am 13 02 2023].

[164] M. M. Shokrieh, in *Residual Stresses in Composite Materials*, A volume in Woodhead Publishing Series in Composites Science and Engineering, 2021.